Abstracts 10,316-10,616

SOLID STATE ABSTRACTS

an abstract journal devoted to the theory, production and use of solid state materials and devices

VOLUME 2 NUMBER 2

PHYSICS

METALLURGY

ELECTRONICS

SEMICONDUCTORS

PHOSPHORS

MAGNETICS

DIELECTRICS

SUPERCONDUCTORS

METALS

SOLID STATE ABSTRACTS

VOLUME 2, NUMBER 2

May 1961

Abstracts 10,316–10,616

TABLE OF CONTENTS

Abstracts of the Solid State Literature

Metallurgy and Chemistry of Solids

Thermodynamic Properties of Elements and Alloys 53
Crystal Structure . . . 53
Crystal Growth . . . 57
Crystal Surfaces . . . 60
Radiation Effects . . . 60

Solid State Physics

Crystal Physics (including Energy Band Structure) . 61
Dielectric Properties . . . 62
Carrier . . . 64
Conductivity . . . 65
Breakdown . . . 67
Magnetoelectric (Galvanomagnetic) . . . 67
Other Electrical Properties . . . 68
Magnetic Properties . . . 69
Optical Properties . . . 73
Thermal Properties . . . 76
Mechanical Properties . . . 77

Solid State Devices

Diodes . . . 78
Transistors . . . 79
Magnetoelectric Devices . . . 80
Cryogenic Devices . . . 80
Photodevices . . . 80
Other Photodevices . . . 81
Ferrite Devices . . . 81
Masers and Lasers . . . 82
Other . . . 83

Basic Solid State Device Circuits

Theory and Design of Circuits . . . 84
Amplifiers . . . 86
Oscillators . . . 88
Switching Circuits . . . 88
Signal Converters . . . 89
Filters . . . 89

Applications of Solid State Devices

Scientific, Medical, and Commercial . . . 90
Aeronautical and Space . . . 90
Television . . . 91
Telemetry . . . 91
Microwaves and Ultramicrowaves . . . 91
Digital Computers . . . 91
Analog Computers . . . 94
Power . . . 95
Control . . . 95
Instrumentation . . . 95

New Products . . . 97

Subject Index . . . 99

Author Index . . . 105

Calendar of Conferences — See page 106

Editor: GEOFFREY KNIGHT, JR., Ph.D.

Assistant Editor: JOHN A. MURPHY

PUBLISHED MONTHLY BY

Cambridge Communications Corporation, 238 Main Street, Cambridge 42, Massachusetts, Tel. 491-0710

Subscription Rate: $25.00 per year. Single Copies and Back Issues: $2.50. Advertising Rates on Request.

Cambridge Communications Corp. is not prepared to furnish copies of the articles abstracted. However, there are many libraries throughout the country which maintain photocopying services.

SYMBOLS USED IN THE ABSTRACTS

L: Letter to the Editor. A: Only an abstract is given in the reference. R: Only a review is given in the reference. E: Erratum.

The reference numbers in the indices are the abstract numbers, not the page numbers.

Copyright 1961 by Cambridge Communications Corp. Printed in the U.S.A. by the University Press, Inc.

ABSTRACTS OF THE SOLID STATE LITERATURE

METALLURGY AND CHEMISTRY OF SOLIDS

THERMODYNAMIC PROPERTIES OF ELEMENTS AND ALLOYS

Partial Phase Diagram of the $Fe_2O_3-Y_2O_3-H_2O-Na_2CO_3$ System - See 10,356

10,316 ANISOTROPIC SEGREGATION IN InSb by W. P. Allred and R. T. Bate (Battelle Mem. Inst.); J. Electrochem. Soc., Vol. 108, p. 258, Mar. 1961

A study of the anisotropic segregation of Se in InSb using radioactive Se as a tracer element is reported. A core consisting of a high concentration of Se has been found in the center of crystals pulled in the [111] direction. This phenomenon is thought to result from an extremely rapid lateral growth occurring on the (111) facet. Well-defined striations have also been observed. Crystals grown from seeds oriented in directions other than the [111] are found to have high concentrations of Se in the (111) facets near the edge of the crystal. Removal of the edges leaves the major portion of the crystal relatively homogeneous and with lower impurity content.

Anomalous Segregation at Crystal Facets - See 10,340

10,317 THE KINETICS OF PRECIPITATION FROM SUPERSATURATED SOLID SOLUTIONS by I. M. Lifshitz and V. V. Slyozov (Phys.-Tech. Inst., Kharkov); J. Phys. Chem. Solids, Vol. 19, pp. 35-50, Apr. 1961

The process whereby diffusion effects can cause the precipitation of grains of a second phase in a supersaturated solid solution is analyzed. The kinetics of this type of grain growth are examined in detail. Some grains grow, only to be dissolved later; some increase in size and incorporate others in so doing. This latter phenomenon of coalescence is discussed in a new "kinetic" approximation. Formulae are given for the asymptotic grain size distribution, for the number of grains per unit volume and for the supersaturation as a function of time. The effects of anisotropy, strain, crystalline order and the finite size of the specimen are considered. For a material said to be "supersaturated with vacancies", the vacancies are treated as solute "atoms" which cluster together to form internal cavities. The practical case of a real, finite crystal is important because the vacancies can, in general, also escape to the surface. A special analysis is made of this example, and the results are applied to the theory of sintering.

CRYSTAL STRUCTURE

10,318 LATTICE PARAMETERS AND STRUCTURAL CHANGES IN THE PSEUDO-BINARY ALLOY GeTe-SnTe by J. N. Bierly (Franklin Inst. Labs.), L. Muldawer (Temple U.), and O. Beckman (U. Uppsala, Sweden); Bull. Am. Phys. Soc., Ser. II, Vol. 6, p. 76 (A), Feb. 1, 1961

Measurements of the room temperature lattice constants of the pseudo-binary alloy GeTe-SnTe were reported. They show a continuous transformation from a face-centered rhombohedral structure at GeTe to a NaCl type structure starting at 30% GeTe to 70% SnTe and continuing to SnTe. Determinations of the structure above and below room temperature reveal a continuous variation in structure as a function of composition and temperature. GeTe is rhombohedral at room temperature and generally transforms to a NaCl type structure, $T_c = 390^{\circ}C$. As the percentage of SnTe is increased, the temperature at which the rhombohedral structure transforms to a NaCl structure is decreased, and beyond 70% SnTe the transformation occurs below room temperature. SnTe retains a NaCl structure at least to $77^{\circ}C$. Metallographic examination of the alloys reveals a banded structure in alloys which were rhombohedral at room temperature. These are interpreted as being twin bands, thought to arise from the strain at the cubic-rhombohedral interface.

10,319 X-RAY INDUCED DEFECTS IN LiF CRYSTALS PLASTICALLY DEFORMED AT LOW TEMPERATURES by D. A. Wiegand (Carnegie Inst. Tech.) and R. Smoluchowski (Princeton U.); Bull. Am. Phys. Soc., Ser. II, Vol. 6, pp. 113-114(A), Mar. 20 1961

The deformation of LiF crystals in compression at the temperature of liquid-nitrogen, followed by x-ray irradiation without intermediate warming was discussed. Both the F band and a band in the vicinity of 3400 A are enhanced as a result of the deformation, and the fractional increase in the F band is proportional to the fractional increase of the 3400 A band. While the F band continues to grow throughout the period of irradiation, Δn_f due to deformation saturates in a manner similar to that of the band at 3400 A. These results can be interpreted very simply in terms of vacancy generation during deformation, the negative ion vacancies being readily converted to F centers during irradiation. The saturation of Δn_f suggests that the rate of formation of negative ion vacancies during irradiation is insensitive to this plastic deformation as reported earlier for crystals deformed at room temperature.

Paramagnetic Resonance Measurement of F Centers in LiF - See 10,437

10,320 TRANSIENT PRODUCTION OF F CENTERS IN SODIUM CHLORIDE SINGLE CRYSTALS by V. R. Honnold and J. P. Nolta (Hughes Aircraft); Bull. Am. Phys. Soc., Ser. II, Vol. 6, p. 114(A), Mar. 20, 1961

Transient production of F centers in sodium chloride using a pulsed, bare critical reactor facility was discussed. It has been possible to observe the generation and decay rates of the F centers produced by this high-flux (10^{16} fissions per pulse), short-duration (100 μsec wide at half-peak) pulse of gammas and neutrons because of the fast rise time (~20 μsec) of this pulse. The color center density generated in the crystal is detected by monitoring the change in optical transmission through the crystal using a cadmium sulfide photoresistor. The observed data, together with rate equations first proposed by Mador et al., seems to support two possible models: either indirect production by a modified Varley mechanism or indirect production from a positive and negative ion vacancy pair. Correlating data for this transient production of F centers in sodium chloride was obtained using gammas produced by a 1-Mev electron beam generator. Here again the same rate equations yield satisfactory results.

Neutron Irradiation Produced F Centers in LiH - See 10,338

10,321 STAGES IN THE ANNEALING OF RADIATION INDUCED COLOR CENTERS AND DEFECTS IN Al_2O_3 by W. Levy (Brookhaven Natl. Lab.); Bull. Am. Phys. Soc., Ser. II, Vol. 6, p. 114(A), Mar. 20, 1961

The annealing characteristics of the absorption bands at 6.02, 5.35, and 4.85 ev in reactor-irradiated Al_2O_3 were discussed. These characteristics may be determined by heating crystals for a fixed period, at a series of temperatures differing by a fixed increment, starting at the irradiation temperature and continuing until all color is removed, usually at 700° to 800°C. After each anneal optical absorption measurements are made at room temperature. Also, crystals are irradiated with gamma-ray doses sufficient to produce equilibrium coloring, which shows that most of the color removed during each anneal is due to an electronic process. In crystals irradiated at 65°C and heated for 40 min at each temperature, the defect annealing occurs in three principal stages, for the 6.02-ev band at 100° to 340°, 340° to 500°, and 500° to 730°C. The stages for the 5.35- and 4.85-ev bands are 100° to 370°, 370° to 490°, and 490° to 730°C. Crystals irradiated at 200°C show little annealing in the first two stages. Gamma-ray irradiation restores the 6.02 band in all three stages but diminishes the 5.35 and 4.85 bands only during the second stage. In addition to the principal stages, there is evidence of fine structure in the annealing.

Vacancy Clusters in Solid Solutions - See 10,317

10,322 KINETICS OF DONOR REACTIONS IN OXYGEN-DOPED GERMANIUM by C. S. Fuller (Bell Labs.); J. Phys. Chem. Solids, Vol. 19, pp. 18-28, Apr. 1961

An investigation by means of resistivity and Hall effect measurements of the reaction kinetics leading to the formation of donors in oxygen-doped Ge is reported. Reaction rates have been measured for oxygen concentrations ranging from 0.9 to 12.0×10^{17} cm^{-3} oxygen over the temperature range, 300° - 550°C. The apparent order of reaction is shown to increase with both temperature and oxygen concentration and to approac a limiting value of four. Although the reactions are complex ir the kinetic sense, and consist of series as well as parallel reac- tions, both the forward and reverse reactions are shown to follo approximate first order rates over limited temperature ranges. The reaction of oxygen in the presence of copper is shown to result in the production of a neutral or paired conformation of the Cu and O atoms. The activation energy for donor generation in Cu-doped Ge is 47 kcal (2.0 ev), in excellent agreemer with the activation energy for oxygen diffusion.

10,323 A SPECTROCHEMICAL METHOD FOR THE DETERMINATION OF TRACE IMPURITIES IN INDIUM by J. F. Duke (Natl. Phys. Lab., Teddington); Conf. Ultrapurification Semicon. Mat., Apr. 1961

A spectrographic method for determining trace elements in high purity indium after a preliminary chemical concentration was described. The impurities are separated from the matrix and converted into an aqueous solution of their chlorides. The solution is evaporated to a low bulk before being transferred to a flat, undercut, graphite electrode. The electrode is dried and excited by a 15 amp dc arc in an oxygen-argon atmosphere. The spectra are recorded with a 3.4 metre Ebert grating spectrograph. Copper is used as an internal standard and calibration is by comparison with a solution standard. Satisfactory recovery from synthetic solutions has been demonstrated for thirty to forty elements. The sensitivity of detection of the spectrographic procedure is below 1 microgram for over 25 elements and in several cases as low as 0.01 microgram.

10,324 DETERMINATION OF ULTRATRACE IMPURITIES IN SEMICONDUCTOR MATERIALS by G. H. Morrison (Genl. Tel. and Electronics Labs.); Conf. Ultrapurification Semicon. Mat., Apr. 1961

The role of trace analysis in the evaluation of semiconductor raw materials, purified materials, single crystals, and device material was discussed and recent results in the microanalysis of very small samples using such techniques as activation analysis, emission spectroscopy, and mass spectrometry were reported. The sensitivity of these techniques is of the order of one part per million.

10,325 SPECIFIC DETECTABILITIES BY SEVERAL SPECTROGRAPHIC PROCEDURES by W. C. Myers (Battelle Mem. Inst.); Conf. Ultrapurification Semicon. Mat., Apr. 1961

Measurements of the spectrographic detection limits which can be attained for some 70 elements were reported. The methods used included a dc arc excitation in air, in a 70 per cent argon — 30 per cent oxygen mixture and, in both of these atmospheres a modified cathode-layer technique. Charts of these sensitivities were presented together with comments regarding their use.

10,326 ELECTRON GUN TYPE EXCITATION SOURCE FOR SPECTROGRAPHIC DETERMINATION OF O_2, N_2, H_2, P, S, AND HALOGENS IN GaAs by D. Andrychuk and C. E. Jones (Texas Instr.); Conf. Ultrapurification Semicon. Mat., Apr. 1961

Use of a discharge between a heated filament cathode and a sample-containing anode to volatilize a GaAs sample and to excite the spectra of its constituents was described. The excitation can be altered without changing the volatilization rates.

The excitation energies from a 10-amp current are sufficient to excite the visible region spectra of the elements mentioned in the title. The sensitivity attained is 0.05 per cent for most of these elements. The source was described and the characteristics were discussed.

10,327 THE HALL EFFECT AS AN ANALYTICAL TOOL IN ULTRAPURE SILICON AND GERMANIUM by C. A. Klein (Raytheon); Conf. Ultrapurification Semicon. Mat., Apr. 1961

The intricacy of analyzing electrically active trace impurities in high-resistivity silicon and germanium was discussed. Hall-effect measurements are often used to determine impurity concentrations below the detection limit of classical methods. Their interpretation requires an accurate knowledge of the Hall-coefficient factor $r = \mu_H/\mu$; that is, of the ratio of Hall and drift mobilities. The ratio is not only a function of temperature, but also of the applied magnetic field, and to some extent of the impurity concentration. Some recent work performed with the aim of arriving at a better appreciation of the Hall-coefficient factor in p-type silicon and germanium was evaluated. In both cases the factor was obtained by means of an investigation of carefully taken 1/Re data in the light of theoretical considerations on the free carrier density variation with temperature. It is believed that this approach leads to correct determinations of the net and total impurity concentrations in homogeneous specimens.

10,328 THE DETERMINATION OF TRACE IMPURITIES IN HIGH-PURITY SELENIUM by A. I. Williams (Natl. Phys. Lab.); Analyst, Vol. 86, pp. 172-177, Mar. 1961

Neutron-activation methods developed for the determination of trace amounts of cadmium, copper, nickel, tellurium, and zinc in high-purity selenium are discussed. The methods have sensitivities much greater than those of other analytical procedures. The lower limits of determination are 0.005 ppm of cadmium, 0.001 ppm of copper, 0.05 ppm of nickel, and 0.01 ppm of tellurium and zinc.

10,329 A DIFFERENTIAL ABSORPTION SPECTROMETER FOR THE INFRA-RED by M. D. Sturge (RRE); J. Sci. Instr., Vol. 38, pp. 96-98, Mar. 1961

A method of measuring the small change in absorption coefficient due to the introduction of an impurity into a semiconductor is described. A chopped monochromatic beam of infrared radiation is passed alternately through the doped and undoped halves of a compound specimen and the resulting modulation is measured. A change of less than $10^{-3}\,cm^{-1}$ can be observed in the presence of substantial background absorption. The method is illustrated by a measurement on oxygen-doped germanium.

Impurity Studies In Compound Semiconductors by Electron Spin Resonance - See 10,445

10,330 THE DEVELOPMENT OF A METHOD FOR THE REMOVAL OF BORON FROM SILICON TETRAIODIDE BY ZONE MELTING by J. T. Buford and R. J. Starks (The Eagle-Picher Res. Labs.); Conf. Ultrapurification Semicon. Mat., Apr. 1961

The preparation, primary purification by distillation, zone melting and thermal dissociation processes for silicon tetraiodide were discussed. Emphasis was given to the development of a continuous zone melting process which utilizes the void-zoning technique for material transport. The boron concentration in the silicon produced from silicon tetraiodide from various stages of the process was reported and the observed purification factor was compared with the theoretical purification. Possible reasons for the significant deviations from the theoretical were discussed.

10,331 DIFFUSION PATHS AND ACTIVATION ENERGIES IN AgI AND ZnO CRYSTALS by L. V. Azároff (Ill. Inst. Tech.); Bull. Am. Phys. Soc., Ser. II, Vol. 6, p. 23(A), Feb. 1, 1961

The diffusion paths in hexagonal closest packed structures consist of successive octahedral voids and in cubic closest packed structures of alternating octahedral and tetrahedral voids. The saddle points encountered in both paths are the same since two adjacent voids share a triangular face composed for three closest packed atoms. The activation energy for diffusion is primarily composed of the saddle-point energies because other terms tend to cancel. The existence of continuous paths in the zincblende and wurtzite structures eliminates the need for vacancies, and it can be shown that the activation energy in β AgI is twice that in γ AgI because two saddle points must be crossed in the wurtzite structure as opposed to one only in zincblende. Similarly, it can be shown that the different activation energies for diffusion of Zn in ZnO measured by electrical and by tracer methods can be explained when actual diffusion paths are considered.

10,332 EXPERIMENTAL STUDY OF INTERMETALLIC DIFFUSION IN LARGE TEMPERATURE GRADIENTS by C. J. Meechan (NA Aviation); J. Appl. Phys., Vol. 32, pp. 945-950, May 1961

Results of imposing temperature gradients in the range $2000^{\circ}C/cm - 3000^{\circ}C/cm$ across the interface of binary diffusion couples fabricated from fcc metals are reported. The systems investigated were Au-Ni, Cu-Ni, γFe-Ni, γFe-Pd, and Ni-Pd. It was found that chemical diffusion in these systems was influenced in varying degrees by the temperature gradient. The manner in which the temperature gradient may affect the various contributions to chemical diffusion is discussed.

10,333 DIFFUSION OF ARSENIC IN GERMANIUM FROM THE VAPOUR PHASE by W. Albers (N. V. Philips); Solid-State Electronics, Vol. 2, Nos. 2/3, pp. 85-95, Mar. 1961

Measurements of the diffusion of As in Ge are reported. The diffusion constants and the concentrations of As at the surface in equilibrium with gaseous As of a certain pressure have been determined at different temperatures. From the temperature dependence, the activation energy of diffusion and the pre-exponential constant have been calculated. It is found that, if the diffusion is carried out via the vapour phase and if the diffusion vessel contains zones of different temperatures, the surface concentration of the As depends on the geometry of the vessel, when working in the absence of an inert gas. This effect is caused by the fact that the degree of dissociation of the gaseous As molecules above the Ge sample depends on the geometry of the vessel. A method for eliminating thermal conversion is described.

10,334 GASEOUS DIFFUSION OF ARSENIC AND PHOSPHORUS INTO GERMANIUM by K. Lehovec and C. Pihl (Sprague Elect.); J. Electrochem. Soc., Vol. 108, pp. 552-560, June 1961

An investigation of the diffusion of arsenic and phosphorus from a gaseous ambient into germanium, using capacitance and breakdown measurements of diodes produced by plating indium into indentations of various depths is reported. The diffusion constants found for arsenic in germanium agree well with those published by Bosenberg. On the other hand, the diffusion constant of phosphorus in germanium at 780°C was found to be $5.5 \times 10^{-13} cm^2/sec$, which differs considerably from data by Dunlop. The surface concentration of arsenic in germanium appears to increase in proportion to the fourth root of the arsenic vapor pressure at 725°, 750°, and 800°C, with no significant differences among these temperatures. In the case of phosphorus a fourth root dependence was found also at 780°C, the only temperature investigated. Presence of germanium arsenide was found at the germanium surface, particularly at arsenic surface concentrations exceeding 10^{19}at./cc, using electron diffraction techniques. Thermal conversion of the interior of the germanium wafers (which were 15 ohm-cm n-type) to p-type could be suppressed by arsenic surface concentrations exceeding 5×10^{18}at./cc. This elimination of thermal conversion depends on the surface to volume ratio of the wafer. It is proposed that the thermal conversion level in the bulk of the indiffused material depends on the electric field which arises during diffusion if the impurity concentration exceeds the intrinsic carrier concentration.

10,335 DIFFUSION OF TIN IN GALLIUM ARSENIDE by H. P. Keller and B. Goldstein (RCA Labs.); Bull. Am. Phys. Soc., Ser. II, Vol. 6, p. 17(A), Feb. 1, 1961

Measurements of the diffusion of radioactive tin-113 in GaAs from an evaporated layer in the temperature range from 1069° to 1215°C were reported. The diffusions were carried out in evacuated quartz ampoules which contained an amount of arsenic sufficient to prevent dissociation of the GaAs. Penetration profiles were determined by the use of standard lapping and end-window Geiger counting techniques. These penetration profiles were found to follow the solution to the diffusion equation appropriate to the experimental conditions. The diffusion coefficients of tin can be described by the customary equation $D = D_0 \exp(-E/kT)$ where E, the activation energy, is 2.5 ev and D_0 is $6 \times 10^{-4} cm^2/sec$. Initial tin concentrations are of the order of 10^{19} atoms/cm^3. The fact that tin acts as a donor in GaAs indicates that it replaces gallium. Since zinc and cadmium act as acceptors, this indicates that they, too, replace gallium. Thus, the fact that the activation energy for tin diffusion is, within experimental error, the same as that reported for the diffusion of cadmium and zinc supports the suggestion of sublattice diffusion in compound semiconductors made in earlier work.

10,336 THE DIFFUSION CONSTANTS OF THALLOUS (Tl^+) AND LEAD (Pb^{++}) IONS IN POTASSIUM CHLORIDE by A. Glasner and R. Reisfeld (The Hebrew U.); J. Phys. Chem. Solids, Vol. 18, No. 4, pp. 345-355, Mar. 1961

Measurements of the diffusion constants of monovalent thallium and divalent lead into potassium chloride in the low temperature range of the latter are reported. The activation energy, Q, of thallium ions, was found to be somewhat greater than that of lead ions, the latter being about equal to the activation energy of the self-diffusion of the potassium ions. It is suggested that the comparatively small pre-exponential factor, D_0, for lead is due to its complexation with cation vacancies. The results obtained on heating the pressed disks differed widely from those with the mixed powders. The difference is accounted for by assuming a prevalence of "grain boundary diffusion" in the pressed disks, while "volume diffusion" is deactivated by the high pressure previously applied. The energy of activation with pressed disks is found to be about 10 per cent larger than the latent heat of fusion of the salts employed, namely thallium chloride and thallium sulphate.

10,337 DEVIATIONS FROM STOICHIOMETRY IN MnO AND FeO by D. M. Smyth (Sprague Elect.); J. Phys. Chem. Solids, Vol. 19, pp. 167-169, Apr. 1961

Deviations from stoichiometry in divalent oxides containing cation vacancies such as MnO and FeO are treated according to a simple mass action approximation which predicts that the composition should vary with the sixth root of the oxygen pressure for large deviations from stoichiometry and with the square root of the oxygen pressure close to the stoichiometric composition. Published data for MnO and FeO are in excellent agreement with the predictions.

10,338 CHARACTERISTIC IMPERFECTIONS IN FLUX-GROWN CRYSTALS OF YTTRIUM IRON GARNET by R. A. Lefever, A. B. Chase, and J. W. Torpy (Hughes); J. Am. Ceram. Soc., Vol. 44, pp. 141-144, Mar. 1961

Crystals of yttrium iron garnet grown from lead oxide and lead oxide-lead fluoride flux systems are discussed. The crystals are inhomogeneous and contain characteristic imperfections that may be significant in the evaluation of physical properties. A petrographic study of single crystal sections has revealed dendritic nuclei, oriented layers of submicroscopic foreign material located in the outer regions of the crystals, and oriented occlusions in intermediate positions. Changes in the appearance of thin sections resulting from the use of an oxygen atmosphere during synthesis combined with other observations indicate that divalent iron contributes to inhomogeneities and imperfections present in yttrium iron garnet crystals. Growth mechanisms involving an initial dendritic stage with <100> and <111> fast-growth directions followed by layered growth parallel to major crystal planes, normally {110} and {211}, can be deduced from the appearance and location of crystal imperfections.

Structure of Ferrite Thin Films - See 10,359 and 10,360

10,339 ELECTRON INTERFEROMETER STUDIES OF IRON WHISKERS by H. A. Fowler, L. Marton, J. A. Simpson, and J. A. Suddeth (NBS); J. Appl. Phys., Vol. 32, pp. 1153-1155, June 1961

Electron interference patterns obtained by using an iron whisker as the electrostatic fiber of a Möllenstedt interferometer are described. The tilted fringes in the shadow pattern resemble those observed by Chambers, and show the relationship between flux leakage and geometrical shape of the whisker. Chambers' general model of the flux configuration is confirmed.

Structural Changes in GeTe-SnTe - See 10,318

CRYSTAL GROWTH

10,340 A POSSIBLE MECHANISM OF CRYSTAL GROWTH FROM THE MELT AND ITS APPLICATION TO THE PROBLEM OF ANOMALOUS SEGREGATION AT CRYSTAL FACETS by A. Trainor and B. E. Bartlett (Mullard Southampton Works); Solid-State Electronics, Vol. 2, Nos. 2/3, pp. 106-114, Mar. 1961

A possible mechanism of crystal growth from the melt by which stable facets are assumed to grow by nucleation at the point of critical supercooling, followed by rapid sheet growth across the facet, is described. The velocity of this sheet growth would be independent of the rate of advance of the solid-liquid interface. The mechanism forms the basis of a mathematical treatment of impurity segregation at a facet, taking into account the adsorption of impurity at the solid-liquid interface. An equation is derived which relates the apparent segregation coefficient at a facet to the velocity of sheet growth and the degree of impurity adsorption. It is shown that, for velocities in the expected range, the value of the segregation coefficient tends to a limiting value which may be greater than 1. The application of the theory to the related problem of dendrite growth is suggested.

10,341 SINTERING CRYSTALLINE SOLIDS. I. INTERMEDIATE AND FINAL STATE DIFFUSION MODELS by R. L. Coble (GE Res. Lab.); J. Appl. Phys., Vol. 32, pp. 787-792, May 1961

Photomicrographs of pore and grain boundary structures in sintered powder compacts are presented to provide the basis for a qualitative description of the important phases of the course of densification. From this guide, appropriate grain shapes and pore shapes and locations are selected for the formulation of diffusion sintering models. The principle models presented are for bulk diffusion transport with the grain boundaries as vacancy sinks when the pore phase is continuous and coincident with three grain edges, and also when the pore phase is discontinuous and located at four-grain corners. These models predict that the rate density change is constant when the diffusion coefficient and grain size are constant. The need for simultaneous isothermal densification and grain growth data is indicated. The explicit change in densification rate with discontinuous grain growth is predicted in terms of pore spacing and grain size.

10,342 SINTERING CRYSTALLINE SOLIDS. II. EXPERIMENTAL TEST OF DIFFUSION MODELS IN POWDER COMPACTS by R. L. Coble (GE Res. Lab.); J. Appl. Phys., Vol. 32, pp. 793-799, May 1961

During sintering in alumina powder compacts, the density has been found to increase linearly with the logarithm of time, and the grain size to increase with the one-third power of time. Incorporation of the time dependence of grain size increase into late-stage bulk diffusion sintering models [see abstract 10,341] leads to corrected models by which a semilogarithmic behavior is predicted. The presence of density gradients in normally fabricated pellets makes it impossible to deduce whether theoretical density will be achieved from the early stages of the course of densification. Diffusion coefficients calculated from the intermediate and later stages of sintering bear order-of-magnitude agreement with those calculated from the initial-stage sintering measurements in alumina. All diffusion coefficients from sintering data are higher than Kingery's measured diffusion coefficients for oxygen. It is hypothesized that the sintering process must be controlled by bulk diffusion of aluminum ions while the oxygen transport takes place along the grain boundaries. In controlling the sinterability of alumina to theoretical density, it appears that magnesia does not "inhibit" discontinuous grain growth, but instead increases the sintering rate such that discontinuous growth nuclei do not have time to form.

Vacancy Clusters in Sintering Theory - See 10,317

Anisotropic Segregation in the Growth of InSb Crystals - See 10,316

10,343 STABILITY OF PRESSURE-SUPPORTED MOLTEN ZONES IN HORIZONTAL SHEETS by H. P. Kramer, B. P. Bogert, and D. W. Hagelbarger (Bell Labs.); J. Appl. Phys., Vol. 32, pp.764-768, May 1961

The relationship of the stability limit for pressurized horizontal floating zones to the eigenvalues of a membrane of the same shape is discussed. In particular, a rectangle of length a and width b is stable if $\pi^2(4/a^2+1/b^2) \geq \rho g/\gamma$, and a circle of radius R is stable if $(\beta_{11}/R)^2 \geq \rho g/\gamma$, where ρ is the density, g is the acceleration of gravity, γ is the surface tension constant, and $\beta_{11} = 3.8317$ is the first root of the Bessel function $J_1(x)$. This latter case checks with experiments on melted circular zones of tin.

10,344 EXPERIMENTS ON FLOATING ZONE SILICON by A. J. Goss (Marconi Wireless); Conf. Ultrapurification Semicon. Mat., Apr., 1961

An experimental study of silicon crystal growth in a floating zone furnace with RF heating was described, with special consideration given to the problem of silicon deposition on the coil. Measurements of temperature gradients and interface shapes made in order to improve growth conditions by modifications in technique were reported and results of the crystal growing experiments were given in dislocation patterns. Properties of floating zone crystals were compared with those of pulled silicon crystals by electrical measurements, including diode characteristics.

10,345 THE PREPARATION AND FLOATING ZONE PROCESSING OF GALLIUM PHOSPHIDE by C. J. Frosch and L. Derick (Bell Labs.); J. Electrochem. Soc., Vol. 108, p. 251, Mar. 1961

A procedure for producing large solid multicrystalline ingots of gallium phosphide is described. Bars cut from these ingots are being employed in the investigation of the floating zone technique for growing single crystals under controlled conditions. Methods for producing stable melted zones in GaP bars which demonstrate the feasibility of growing large single crystals are discussed. GaP crystallites grow from the vapor on the bar surfaces above the melted zone during the floating zone processing. These are shown by x-ray analysis to be continuous with and oriented with respect to the underlying bar crystals.

10,346 RADIO-FREQUENCY ZONE MELTING OF CdS, ZnS, ZnSe, and ZnTe by A. G. Fischer (RCA Labs.); Bull. Am. Phys. Soc., Ser. II, Vol. 6, p. 17(A), Feb. 1, 1961

Preparation of crystals of CdS, ZnS, ZnSe, and ZnTe by RF

zone melting in graphite boats was described. Despite the high melting points and corresponding high decomposition pressures, the zone melting was carried out in sealed, standard wall quartz tubing, without enclosing the ampoule in an autoclave or in a block of graphite. The major initial difficulty was the occurrence of explosions. This could be traced to pressure increase due to the cracking of either S_8 or Se_6 molecules in the hot zone to lower species, with a delayed recombination. In the case of the sulfides, a second explosion hazard is caused by the formation of carbon sulfides by direct reaction of sulfur with graphite. These hazards were minimized by increasing the recombination rate of cracked molecules and by increasing the thermal decomposition of the carbon sulfides. Contrary to group III impurities, group IV impurities can be removed by zone refining. Insulating, n- and p-type crystals can be prepared.

10,347 GROWTH OF GRAPHITE SINGLE CRYSTALS AND ALUMINUM OXIDE WHISKERS by P. J. Brant and S. L. Levy (Midwest Res. Inst.); Bull. Am. Phys. Soc., Ser. II, Vol. 6, p. 279(A), Apr. 24, 1961

The design and construction of a 2500°C furnace with unusual temperature stability for the production of graphite single crystals were discussed. By the combined use of carbonized cotton for electrical insulation and lamp black for thermal insulation, a temperature of 2500°C was achieved with an input power of less than 1.5kw. The low thermal loss feature contributes to the high temperature stability. During the production of graphite single crystals by the thermal decomposition of aluminum carbide, graphite crystals also grew by deposition from a vapor phase, and α-phase aluminum oxide whiskers were deposited. These whiskers grew to a length of 4cm while maintaining a uniform cross section of less than 10μ.

10,348 VACUUM RADIATION FURNACE WITH PRECISE CONTROL OF TEMPERATURE GRADIENTS FOR CRYSTAL GROWTH BY SUBLIMATION by A. C. Prior (RRE); J. Sci. Instr., Vol. 38, pp. 198-201, May 1961

A furnace designed for the growth of lead selenide single crystals at 775°C is described. It provides an inherently high degree of temperature uniformity and, without the use of a servo control system, the gradients can be adjusted and maintained to less than 1/10°C/cm and 1/4°C in 10cm. A changed gradient can be established in 5 minutes. In heating from cold a steady temperature is attained in 75 minutes, and the furnace can be cooled in a few minutes. This performance is achieved by minimizing the total mass of the heated material and by the use of highly reflecting water-cooled silvered surfaces for the walls. The regulating system for controlling the absolute temperature to 0.1°C is described. Evaporation of the alloy heater element limits the maximum temperature to about 940°C. This can be raised by the use of other elements.

10,349 VAPOR PHASE PREPARATION OF GALLIUM PHOSPHIDE CRYSTALS by M. Gersherzon and R. M. Mikulyak (Bell Labs.); J. Electrochem. Soc., Vol. 108, pp. 548-551, June 1961

A method for the preparation of single crystals of GaP by the vapor phase reaction of gallium suboxide with phosphorus is described. Several crystal habits are distinguished including that of a filamentary form which appears to be a precursor of the other types. The crystals are strong and relatively free of strains. Electrical measurements indicate carrier densities and total donor and acceptor concentrations that are significantly less than those corresponding to crystals prepared by other methods. Low resistivity crystals of either n- or p-type can be prepared by doping during growth.

10,350 INTERFERENCE METHOD FOR MEASURING THE THICKNESS OF EPITAXIALLY GROWN FILMS by W. G. Spitzer and M. Tanenbaum (Bell Labs.); J. Appl. Phys., Vol. 32, pp. 744-745(L), Apr. 1961

A method of determining the thickness of thin lightly doped epitaxial layers deposited on heavily doped substrates of the same semiconductor by observing the interference fringes produced by infrared radiation reflected from the surface of the epitaxial layer and from the interface between the layer and the substrate is described. The interference method can be used because at sufficiently large carrier concentrations the dielectric constant of semiconductors in the infrared is a function of the carrier concentration. Measurements made on layers deposited on p-type silicon and germanium are discussed. For silicon the interference method gave a thickness of 7.6 ± 0.3μ while the lapping and staining method gave a value of 7.3μ. H_0 comparative measurements were made in the germanium sample since the staining technique could not clearly delineate the junction. The lower limit on the layer thickness which can be measured by the interference technique depends on the particular semiconductor.

10,351 GROWTH STEPS ON GERMANIUM DENDRITES by G. R. Booker (Westinghouse); J. Electrochem. Soc., Vol. 108 pp. 564-568, June 1961

Detailed examinations of the two main faces of a number of germanium dendrites by optical, interference, and electron microscopy are reported. Regular growth steps up to approximately 5000A in height were observed. The steps were not single, low-index crystallographic planes, nor were they steeply inclined, the gradients h/v ranging from 4 to more than 15. A number of irregular types of growth steps were also observed; their formation is discussed. The regions between observable growth steps have been shown to contain additional steps too small to be detected individually. The evidence suggests that small steps of this type are also frequently present on well-grown dendrites not possessing observable growth steps.

10,352 A STUDY OF GROWTH PROCESSES IN GERMANIUM DENDRITES USING PULSE ELECTROPLATING TECHNIQUES by R. C. Smith (Westinghouse Res. Labs.); J. Electrochem. Soc. Vol. 108, p. 238, Mar. 1961

Pulse electroplating is shown to reveal resistivity variations in germanium dendrites. The evolution of the edges of the dendrites is deduced from the configuration of the resistivity variations. The results suggest that dendritic growth involves at least two processes.

10,353 LEAD- AND MANGANESE-ACTIVATED CALCIUM CADMIUM SILICATE PHOSPHORS by Y. Uehara, Y. Kobuke, I. Masuda and T. Kushida (Tokyo Shibaura Elec.); J. Electrochem. Soc., Vol. 108, p. 235, Mar. 1961

The preparation and properties of (Pb + Mn)-activated calcium

cadmium silicate phosphors with various mole ratios of Cd to Ca are described. All phosphors produce a main, broad and variable emission band in the orange, and three minor, narrow and invariant bands at about 6880, 6950, and 7050 A. The phosphors show a complicated shift of the main emission band with increasing Cd content, despite a linear relationship between Cd content and lattice spacings. The introduction of sulfate ions into the phosphor base changes the emission characteristics. With half of the Ca introduced as sulfate, the peak emission shifts from 6100 to 6200 A. The results are discussed in the light of several assumptions.

10,354 THE GROWING OF ELECTROLUMINESCENT AND PHOTOCONDUCTIVE SINGLE CRYSTALS OF ZINC SULPHIDE by F. Karel; Czech. J. Phys., Vol. B11, p. 292(A), 1961

The preparation of ZnS single crystals for physical research is described. The conditions for the preparation of luminescent and pure single crystals and the method of activation with copper and manganese are given.

Preparation of Thin Tin Films by Vacuum Evaporation - See 10,405

10,355 USE OF HELIUM FLUSH IN THE VACUUM DEPOSITION OF THIN FILMS by G. N. Srivastava and G. D. Scott (U. Toronto); Brit. J. Appl. Phys., Vol. 12, pp. 255-256, May 1961

Observations that silver films deposited in a vacuum chamber previously flushed with helium exhibit less aggregation (as shown in electron micrographs) and reduced aging (as determined from electrical conductivity) compared with films produced under the usual high vacuum procedures are reported. It is concluded that, in general, flushing the vacuum chamber with helium is of value in producing stable, compact and pure evaporated films.

10,356 THE HYDROTHERMAL CRYSTALLIZATION OF YTTRIUM IRON GARNET AND YTTRIUM GALLIUM GARNET AND A PART OF THE CRYSTALLIZATION DIAGRAM Y_2O_3-Fe_2O_3-H_2O-Na_2CO_3 by R. A. Laudise, J. H. Crocket and A. A. Ballman (Bell Labs.); J. Phys. Chem., Vol. 65, pp. 359-361, Feb. 1961

The crystallization under hydrothermal conditions of yttrium iron garnet, $Y_3Fe_2(FeO_4)_3$ and yttrium gallium garnet, $Y_3Ga_2(GaO_4)_3$ is discussed. Yttrium gallium garnet was observed to transport in a temperature gradient and crystallized on a seed in 1M Na_2CO_3 at 1500 atm and 360°C when the starting materials were Ga_2O_3 and Y_2O_3. The system Fe_2O_3-Y_2O_3-H_2O-Na_2CO_3 was investigated and yttrium iron garnet was found to form in optimum yields in from one to six days between 685° and 765°C at 1330 atm in approximately 3M Na_2CO_3. Slow decompositions of both garnet and Fe_2O_3 to Fe_3O_4 were observed to decrease the yields at longer times and a mechanism for this effect is proposed. Yttrium iron garnet was found to be congruently saturating and parts of the crystallization diagram were determined. Garnets as large as 2 mm were prepared.

10,357 INDUCTION HEATED PRESSURE VESSEL FOR GROWING OXIDE SINGLE CRYSTALS by A. Ferretti, D. G. Wickham, and A. Wold (Lincoln Lab.); Rev. Sci. Instr., Vol. 32, pp. 566-568, May 1961

An induction-heated oxygen-pressure vessel for growing ferrite crystals under sufficient oxygen pressure to minimize their decomposition is described. The furnace is capable of operation at 1600°C and 75 atm pressure.

10,358 GROWTH OF BARIUM FERRITE SINGLE CRYSTALS by R. J. Gambino and F. Leonhard (USASRDL); J. Am. Ceram. Soc., Vol. 44, pp. 221-224, May 1961

The growth of barium ferrite single crystals weighing up to 5.6 gm from a sodium carbonate flux by cooling melts slowly from about 1250°C is described. The phase diagram of the system BaO - Na_2O - Fe_2O_3 has been studied in the region of the $BaFe_{12}O_{19}$ composition. The effects of variations in batch composition, heating cycle, and seeding from the point of view of crystal yield and quality are reported.

PbO and PbF_2 Flux Grown YI6 Crystals - See 10,338

10,359 PREPARATION AND PROPERTIES OF THIN FERRITE FILMS by E. Banks, N. H. Riederman, H. W. Schleuning, and L. M. Silber (Brooklyn Polytech. Inst.); J. Appl. Phys., Suppl. to Vol. 32, pp. 44S-45S, March 1961

The preparation of ferrite films, approximately 1000 A thick, by vacuum evaporation of the metals and subsequent high-temperature oxidation is discussed. Films of iron, nickel, cobalt, magnesium, and copper ferrites, mixed ferrites, and mixed ferrite-aluminates, as well as yttrium iron garnet, have been prepared. X-ray powder diffractometry indicates that the ferrite films are single-phase spinels, while the garnet shows the garnet structure. In many respects, the properties of the films are the same as those of bulk ferrites of similar composition. The resistivity of the films can be controlled by proper oxidizing procedures. X-band magnetic resonance measurements indicate that the saturation magnetizations of the films are comparable to those of the corresponding bulk ferrites, though the films show larger resonance linewidths. It has been possible to prepare magnesium ferrite films with magnetizations from 2200 gauss to less than 500 gauss by proper annealing and quenching. The possible advantages of thin films are that they allow optical studies of the material by transmission, and should permit determination of magnetic exchange constants through observation of spin wave resonances.

10,360 FERRITE THIN FILMS by H. P. Lemaire and W. J. Croft (RCA); J. Appl. Phys., Suppl. to Vol. 32, pp. 46S-47S, March 1961

Two methods of preparing ferrite thin films of various compositions by spraying hot suspensions of hydroxides onto a heated substrate are described. The ferrite films are formed essentially through a coprecipitation mechanism. X-ray diffraction has shown that the films have a cubic spinel structure. Various compositions have been attained; magnetite, nickel ferrous ferrite, a magnetite-zinc ferrite series, and other mixed ferrites. Coercive force measurements were made from hysteresis loops obtained on a 1000-cycle loop tracer. The films are magnetically isotropic and have a high squareness ratio. Film thicknesses have been varied from a few hundred A to about 1μ. Relative film thicknesses were estimated by using a spectrophotometric technique. For a fixed composition, coercive

force decreases with increasing thickness. Magnetite films had coercive forces varying from 170 to 300 oe depending on thickness. A nickel ferrous ferrite series had coercive forces varying from 225 oe for thick films to 400 oe for a very thin one. Coercive force measurements are related to composition variations in a series of zinc ferrous ferrite films.

10,361 REACTION KINETICS OF POLYCRYSTALLINE YTTRIUM IRON GARNET by W. R. Holmquist, C. F. Kool, and R. W. Moss (Lockheed); J. Am. Ceram. Soc., Vol. 44, pp. 194-196, Apr. 1961

A study of the formation of yttrium iron garnet, $Y_3Fe_2(FeO_4)_3$, starting with (1) Fe_2O_3 and Y_2O_3 and (2) Fe_3O_4 and Y_2O_3, as a function of temperature and time by means of magnetic moment and X-ray measurements is discussed. The reaction began at 600°C and was completed at 1200°C. The perovskite phase appeared only between 600° and 800°C. Above 1200°C only the garnet phase was present. The microwave line width and g-factor at 9303 Mc have also been measured and related to the preparation variables.

10,362 ON THE GROWTH OF SAPPHIRE MICROCRYSTALS by C. M. Hargreaves (N.V. Philips); J. Appl. Phys., Vol. 32, pp. 936-938, May 1961

Thermodynamical considerations on the vapor-phase growth of whisker and platelet crystals of α-Al_2O_3 by the oxidation of aluminum which indicate that the vapor-phase mass transport is probably due to the suboxide Al_2O, and not AlO as previously suggested, are reported. Electron microscope observations confirm the optical evidence that spiral growth steps do not occur on the (0001) surfaces of Al_2O_3 crystals grown in this way.

CRYSTAL SURFACES

10,363 THE OXIDE FILMS FORMED ON COPPER SINGLE CRYSTAL SURFACES IN WATER-II. RATE OF GROWTH AT ROOM TEMPERATURE by J. Kruger (NBS); J. Electrochem. Soc., Vol. 108, pp. 503-509, June 1961

Measurements of the increase in film thickness with time on {100}, {110}, {111}, and {311} surfaces of a copper single crystal immersed in water in equilibrium with atmospheres containing either oxygen or oxygen-helium mixtures containing 1, 10, or 20% oxygen are reported. With the 1% oxygen atmosphere, a Cu_2O film rapidly reached a limiting thickness that remained constant for 1.5 to 2 hr; thereafter the formation of CuO was observed. Stirring delayed the formation of CuO. Similar behavior was observed for 10% and 20% oxygen atmospheres; the limiting film thickness of Cu_2O and the time required to observe the formation of CuO increased with decreasing oxygen content in the atmosphere. When a 1% oxygen atmosphere was used, parabolic film growth was observed. In all cases the {111} plane exhibited the lowest growth rate.

10,364 KINETICS OF THE OXIDATION OF PLATINUM by G. C. Fryburg and H. M. Petrus (NASA); J. Electrochem. Soc., Vol. 108, pp. 496-503, June 1961

The oxidation of platinum ribbons at temperatures from 900° to 1500°C and at pressures from 15μ to 1 atm is discussed. An energy of activation of 42.5 kcal $mole^{-1}$ was obtained from the temperature-dependence of the rate. An unusual pressure-dependence was found to result from the back-reflection of the volatile PtO_2 by the surrounding gas molecules: At 1 atm pressure only a fraction of a per cent of the PtO_2 formed escapes from the platinum.

10,365 ACID CUTTING AND ACID POLISHING OF COPPER CRYSTALS by F. W. Young, Jr., and T. R. Wilson (Oak Ridge Natl. Lab.); Rev. Sci. Instr., Vol. 32, pp. 559-562, May 1961

An acid saw and an acid polisher for cutting and polishing copper crystals are described. Evidence that the cutting and polishing do not introduce dislocations into the crystals is presented. Using these techniques, copper crystals with a dislocation density of $5 \times 10^3/cm^2$ have been prepared.

10,366 SATURATION CURRENTS AT N-TYPE SILICON AND GERMANIUM ELECTRODES IN CHEMICAL ETCHING SOLUTIONS by D. R. Turner (Bell Labs.); J. Electrochem. Soc., Vol. 108, pp. 561-563, June 1961

The anodic saturation current density of an n-type Si or Ge electrode is considerably larger in chemical etching than in nonetching solutions because the chemical etching process produces excess holes at the surface of the semiconductor. Measurements showing that the rate at which these excess holes become available to the electrolytic anodic dissolution reaction is proportional to the chemical etching rate, the surface recombination velocity, and the anodic multiplication factor are reported. Three practical applications of the experiment are indicated: (a) a monitor for chemically etching semiconductors; (b) a tool to study the process of chemical etching; and (c) a simple method for fluoride ion analysis.

Micromasking for Chemical Etching of Semiconductors - See 10,483

RADIATION EFFECTS

10,367 THERMOLUMINESCENCE OF SODIUM CHLORIDE IRRADIATED WITH 40-Mev ALPHA PARTICLES by C. Giamati, G. Allen, and M. Hacskaylo; Bull. Am. Phys. Soc., Ser. II, Vol. 6, p. 30(A), Feb. 1, 1961

An investigation of the effect of 40-Mev alpha particles on NaCl crystals by means of post-irradiated thermoluminescence measurements was reported. A possible mechanism was suggested to account for the results. The suggested interpretation of the results allows a partial separation of the effects of atomic displacement from the effects of ionization. The explanation appears to be consistent with diverse other investigations of alkali halides.

Transient Production of Color Centers in NaCl Single Crystals - See 10,320

X-Ray Induced Color Centers in Plastically Deformed LiF Crystals - See 10,319

Neutron Irradiation of LiH - See 10,438

10,368 EFFECT OF FISSION SPECTRUM NEUTRONS ON N-TYPE GERMANIUM by D. Binder (Hughes Aircraft); Phys. Rev., Vol. 122, pp. 1147-1148, May 15, 1961

It is reported that the electron removal rate for n-type germanium irradiated with fission spectrum neutrons is 8 ± 1 per neutron at room temperature. This value is compared with the results of monoenergetic neutron irradiations from 2 to 5 Mev. The fact that the removal rate is roughly constant is explained by the constancy of the energy dissipated in elastic collisions.

Annealing of Radiation Induced Color Centers and Defects in Al_2O_3 - See 10,321

10,369 ELECTRON SCATTERING BY THIN FOILS FOR ENERGIES BELOW 10 KEV by H. Kanter (Westinghouse Res. Labs.); Phys. Rev., Vol. 121, pp. 461-471, Jan. 15, 1961

Measurements of the transmission (η_T) of electrons through thin films of C, Al_2O_3, Al, Ni, Ag, and Au, together with their distribution in angle and energy, in a spherical retarding-potential analyzer are reported. The distributions are characterized by average and most probable scattering angle, average and most probable fractional energy loss, etc. The dependence of these variables on initial energy (E_p), film thickness, and material has been investigated. For sufficient film thickness, the transmitted energies, the scattering angles and η_T can be represented as universal functions of the reduced energy, E_p/E_c, where E_c is the critical E_p for the onset of transmission. Direct relations exist between η_T, scattering angles, and energy losses for the complete range of scattering from small-angle scattering to total diffusion. The dependence of η_T and average fractional energy loss on Z is consistent with published results on backscattering coefficient and energy loss for thick layers. An estimate of the mean free path for inelastic collisions proves to be in good agreement with the predictions of the Bohr-Bethe theory. Range-energy relations are almost independent of Z when the range is measured in mass per unit area.

Characteristic Electron Energy Losses by Scattering in Ge - See 10,460

10,370 ANGULAR DISTRIBUTION OF ELECTRONS SUFFERING CHARACTERISTIC ENERGY LOSS IN PASSAGE THROUGH METAL FILMS by H. Watanabe (Hitachi Central Res. Lab.); J. Phys. Soc. Japan, Vol. 16, pp. 912-916, May 1961

The distribution in energy and angle of 20 - 25 kv electrons scattered by Al, Ag and Au evaporated films was measured with an electron velocity analyzer of Möllenstedt type. The energy resolution is about 5×10^{-5}, and the angular resolution better than 5×10^{-4} radian. The angular distribution of the characteristic energy loss was compared with Ferrell's calculation. Comparison shows that the experimental result is consistent with a simple Bohm-Pines approach provided that a correction is made for finite resolution of both energy and angle.

SOLID STATE PHYSICS

CRYSTAL PHYSICS
(Including Energy Band Structure)

10,371 ON THE SOLUTION OF THE HARTREE-FOCK EQUATION IN TERMS OF LOCALIZED ORBITALS by W. H. Adams (U. Chicago); J. Chem. Phys., Vol. 34, pp. 89-102, Jan. 1961

The Hartree-Fock method is discussed with emphasis on the transformation properties of the Hartree-Fock equation. This equation may be solved in terms of non-orthogonal one-electron functions, and in some cases it may be more convenient to choose such solutions. Equations which define the localized one-electron functions are developed and it is shown how these equations may be solved. For a system of closed shell atoms or ions, it is suggested that the localized orbitals of each atom or ion can be expanded in terms of functions centered on its nucleus. This suggestion is based on the success of the ionic theory of crystals. Due to the symmetry of a crystal, it is suggested that use of the localized orbitals could lead to expressions for the first order Hartree-Fock density matrix and the Hartree-Fock energy of a crystal, i.e., one could obtain the solution of the Hartree-Fock equation for a crystal.

10,372 SOME PROPERTIES OF ALKALI HALIDE CRYSTALS by E. A. Braun (AEI Res. Lab.); Am. J. Phys., Vol. 29, pp. 182-186, Mar. 1961

The cohesive energy of alkali halide crystals is approximated by treating it as arising from purely polar interactions. An attractive Coulomb potential and a repulsive overlap potential are the only terms that need to be considered. The phenomenon of coloration of alkali halides is described with particular emphasis on the mechanisms involved. As an example of luminescence, the luminescent process in thallium activated alkali halides is discussed.

10,373 DISTORTION CORRECTION TO THE SURFACE ENERGY OF THE {110} FACE OF ALKALI HALIDE CRYSTALS by G. C. Benson, E. Dempsey, and P. Balk (Natl. Res. Counc., Ottawa); J. Chem. Phys., Vol. 34, pp. 157-162, Jan. 1961

Formulas for the contribution of surface distortion to the surface energy of the {100} and {110} faces of the NaCl-type lattice and of the {110} face of the CsCl-type lattice are obtained by a generalization of a treatment described previously for the {100} face of the NaCl structure. Numerical values of the distortion correction to the surface energy of the {110} faces of all of the alkali halides are presented. These results are discussed in relation to the values calculated previously for the {100} face and to the limited experimental information available.

Measurements of Band Structure in Solids Using Magnetoplasma Effects - See 10,416

Effect of Magnetic Fields on Energy Band Structure - See 10,447

10,374 INTERBAND MAGNETO-REFLECTION IN InSb by G. B. Wright and B. Lax (Lincoln Lab.); Bull. Am. Phys. Soc., Ser. II, Vol. 6, p. 18(A), Feb. 1, 1961

A study of interband magneto-reflection from InSb at 80°K in the region from 0.225 to 0.340 ev was reported. Ten lines have been observed in addition to four previously reported from room temperature data. Six lines with inverse effective cyclotron

masses of 21, 45, 83, 101, 142, and 158 have been interpreted as heavy-hole electron transitions to the n = 0, 1, and 2, spin up and spin down, electron bands. The energy gap determined from the zero field intercept of these lines is 0.228ev. The electron g factor, determined from the splitting of the first two lines, is 48. Unresolved structure in the first two lines, and lines with slopes of 112 and 128, are attributed to "light-hole" electron transitions. The shape of the lines has been matched qualitatively by assuming a complex index of refraction proportional to $1/E_{(\log E)^2}$, which seems to indicate the importance of Coulomb attraction between electron and hole.

10,375 BAND STRUCTURE OF HEAVILY DOPED GERMANIUM by H. Schlosser (Genl. Tel. and Electronics Labs.); Bull. Am. Phys. Soc., Ser. II, Vol. 6, p. 27(A), Feb. 1, 1961

Changes in the band structure of Ge upon the addition of column III and V impurities were calculated using perturbation theory and the simple model of the band structure Energy versus wave vector (k) and density of states versus k curves have been obtained for a number of impurity concentrations in the range $10^{18}/cm^3$ to $5 \times 10^{20}/cm^3$. It is found that, relative to the pure material, the band edge shifts and the density of states and energy curves change in shape. In the density-of-states and energy curves for the perturbed crystal, tails are found at the band edges that correspond to a much lower effective mass than is characteristic of the unperturbed crystal. At impurity concentrations appreciably lower than $10^{18}/cm^3$, a discrete impurity level exists, and the perturbation theory diverges. These results have been applied to a calculation of the elastic tunneling current in Esaki diodes.

10,376 AN LCAO THEORY OF THE k = 0, 0, 0 VALENCE BAND SPLITTINGS IN ZINC BLENDE AND WURTZITE STRUCTURES by S. Adler and J. L. Birman (Genl. Tel. and Electronics Labs.); Bull. Am. Phys. Soc., Ser. II, Vol. 6, p. 22(A), Feb. 1, 1961

Bloch sums of localized functions having the transformation properties of angular momentum eigenfunctions with $J^2 = \frac{3}{2}$ and $\frac{1}{2}$ (s and p orbital parts) were used to set up the Hamiltonian matrices at k = 0, 0, 0 for zincblende and wurtzite structures. By means of perturbation theory, accurate expressions have been obtained for the valence band eigenenergy splittings in each structure, in terms of appropriate crystal potential matrix elements. A series of approximations, probably valid for ZnS in both crystal structures, can then be made: First order; first neighbor; two center; neglect of Zn 4p — S3p mixings; band gaps greater than any valence band splittings and greater than the matrix elements of the difference between zincblende and wurtzite potentials. All valence band splittings (one in zincblende and two in wurtzite) can then be expressed in terms of two parameters: δ (spin orbit) and α (uniaxial field), which can be estimated theoretically from an assumed crystal potential. Experimentally, for ZnS one finds from reflection measurements, made on pure zincblende and wurtzite crystals, δ = 0.068ev and α = −0.023ev at 77°K. The theory may be applied to CdS (zincblende structure) and predicts a valence band splitting of 0.065 ev at 77°K in this material.

Valence Band Conduction Phenomenon in Te - See 10,410

Energy Gap of $CdSnAs_2$ - See 10,420

Theory of Impurity States in Si - See 10,435

Impurity Levels in Semiconducting Diamonds - See 10,456

Bulk and Surface Deviations from Intrinsic Fermi Energy Values See 10,412

10,377 THE FERMI SURFACE AREAS OF MAGNESIUM, ZINC AND CADMIUM by E. Fawcett (RRE); J. Phys. Chem. Solids, Vol. 18, pp. 320-328, Mar. 1961

Measurements of the surface conductance of polycrystalline samples of the hexagonal divalent metals magnesium, zinc and cadmium under anomalous skin effect conditions are reported and used to determine the Fermi surface areas of these crystals. The results for zinc and cadmium are in good agreement with the theoretical values, which are estimated in the nearly-free electron approximation for recently proposed models of their Fermi surfaces. For magnesium the Fermi energy is regarded as a variable parameter, and the experimental value for the area provides a sensitive measure of its position relative to the calculated energy levels at points of high symmetry in the Brillouin zone. The area for each metal, when combined with the dc conductivity and the electronic specific heat, also yields average values of the mean free path and Fermi velocity.

10,378 INTERACTION OF ELECTRONS AND HOLES WITH ACOUSTIC WAVES IN INTRINSIC SEMICONDUCTORS by N. Mikoshiba (Electrotech. Lab., Tokyo); J. Phys. Soc. Japan Vol. 16, pp. 895-905, May 1961

A self-consistent semiclassical theory of the interaction of electrons and holes with acoustic waves in intrinsic semiconductors is given. The ultrasonic absorption coefficient can be written as $\Lambda = \Lambda_R + \Lambda_K$, where Λ_R is due to the change of the deformation potential energies of electrons and holes by their recombination, Λ_K is due to the change of the kinetic energy caused by the intraband transition. The formula of Λ_R is identical with that used by Southgate in the analysis of his experiments, if the frequency at which $\omega\tau = 1$ satisfies the inequality $(ql)^2 < 3(\tau_0/\tau)$, where ω, q are the angular frequency and the wave number of acoustic waves, and l, τ_0, τ are the mean free path, the intraband relaxation time, and the lifetime of electrons or holes, respectively. When the frequency $\omega = 1/\tau$ satisfies $(ql)^2 > 3(\tau_0/\tau)$, no absorption peak can be expected, contrary to the simple phenomenological treatment; Λ_R becomes smaller than the value of Southgate's formula and is obscured by Λ_K. Altogether, the characteristics of the interaction are very similar to those in many-valley semiconductors. The acousto-electromotive force is too small to be detectable in experiments.

DIELECTRIC PROPERTIES

10,379 AUTOEMISSION FROM THIN DIELECTRIC LAYERS by L. Eckertová; Czech. J. Phys., Vol. 11B, p. 297(A), 1961

The mechanism of autoemission from thin dielectric layers and methods of experimentally obtaining and investigating this emission are discussed. The connection between this phenom-

enon and the creation of a discharge in high vacuum is pointed out. The characteristics of emitters created by producing a strong electric field in thin layers of mica by introducing a voltage between the metallic base and the metallic grid pressed onto the surface are given. The results of the measurements are discussed.

Measurement of Dielectric Constant in Solids Using Magneto-Plasma Effects - See 10,416

10,380 EFFECTS OF OXYGEN VACANCIES ON THE DIELECTRIC PROPERTIES OF RUTILE (TiO_2) by P. L. Castro and L. E. Hollander, Jr. (Lockheed Missiles and Space Div.); Bull. Am. Phys. Soc., Ser. II, Vol. 6, p. 23(A), Feb. 1, 1961

Measurements of some of the properties of nonstoichiometric single crystals of TiO_2 in which the oxygen content varied over a range corresponding to specific resistivity from 10^4 to 10^{12} ohm cm were reported. The dielectric constant and the loss tangent have been determined for both the "a" and "c" crystallographic directions for frequencies between 60 cps and 300 kc. Measurements of capacitance made with crystals which were systematically decreased in thickness showed a linear dependence of capacitance with inverse thickness. No rectification was observed with asymmetrical electrodes. These results indicate a strictly bulk dielectric effect. A direct correlation between dielectric constant and oxygen vacancy density was shown. The nonstoichiometric compositions exhibit an increase in dielectric constant and dielectric loss at low frequencies. Loss measurements in the "c" direction have a minimum at 200 - 300 cps and a peak at 10^4 cps; these maxima and minima are not observed in the "a" direction. The results of this study suggest that the dielectric behavior of rutile may be explained on the basis of an artificial dielectric theory which considers regions of conductors embedded in an insulating matrix.

10,381 DIFFUSION THEORY APPROACH TO ELECTRICAL BREAKDOWN IN ALKALI HALIDES by E. Offenbacher and S. W. Spaulding (Temple U.); Bull. Am. Phys. Soc., Ser. II, Vol. 6, p. 22(A), Feb. 1, 1961

The problem of electrical breakdown in alkali-halide crystals was discussed using a diffusion equation. The conduction electrons are assumed to diffuse in energy space under the influence of phonon collisions and the applied field. The average first transit time required for an electron to gain a significant energy has been calculated as a function of applied field. The significant energy for any given field is taken to be that above which the electrons on the average gain energy more rapidly than they lose energy to the lattice. The average first transit time is a parameter which can be compared to the recombination time of electrons excited to the conduction band by impact ionization. When the transit time becomes less than the recombination time, the number of electrons excited to the conduction band increases rapidly, and electrical breakdown is said to occur. Approximate knowledge of such recombination times permits approximate definition of the breakdown field strength.

10,382 STUDY OF ELECTRIC BREAKDOWN OF LIQUID DIELECTRICS USING SCHLIEREN OPTICAL TECHNIQUES by B. Farazmand (U. Birmingham); Brit. J. Appl. Phys., Vol. 12, pp. 251-254, May 1961

The mechanism of electric breakdown in liquid dielectrics is considered. The liquid dielectric chosen throughout the experiments was n-hexane, because an extensive literature exists on the breakdown of this material. The applied voltage was a rectangular pulse of variable duration supplied from a 125 kv impulse generator. A novel rotary multiple electrode containing eight pairs of electrodes was incorporated in a simple and efficient fractionation-filtration unit. A protection circuit incorporating an inverter and a trigatron limited the duration of breakdown current. A series of photographs of the state of n-hexane under the applied electric field was taken by the Schlieren technique, using a spark light-source and a still camera. A statistical survey of the results shows the formation of a region of very low refractive index at the cathode. It is suggested that this is due to streamers with a very large number of branches, which propagate towards the earthed electrode. The rate of growth increases with voltage and above a certain voltage, if enough time is allowed, the stepped streamers bridge the electrode gap and breakdown of the liquid results.

10,383 INVESTIGATION OF RARE-EARTH DOPED BARIUM TITANATE by V. J. Tennery and R. L. Cook (U. Illinois); J. Am. Ceram. Soc., Vol. 44, pp. 187-193, Apr. 1961

The effect of additions of 0.0015 to 0.0030 mole fraction of rare earth oxides on the dc resistivity of sintered barium titanate is discussed. The substitution may be represented by $(X_2O_3)_m(BaTiO_3)_{1-m}$, where X is the rare earth. The rare earths samarium, gadolinium and holmium were introduced singly into the titanate and the resistivity was measured as a function of temperature from $-170^\circ C$ to $+330^\circ C$. An anomalous increase, which in some cases amounted to an increase in the resistivity of 4000 times the value in the tetragonal phase, occurred near the tetragonal cubic transition temperature at $120^\circ C$. The thermoelectric power of the material changed sign at the Curie temperature. The tetragonal phase exhibited n-type behavior whereas the cubic phase was p-type. The rhombohedral and orthorhombic phases exhibited conduction activation energies of the order of 0.2 ev whereas the activation energy was approximately 0.1 ev in the tetragonal phase.

10,384 INTERPRETATION OF MICROWAVE ABSORPTION MEASUREMENTS IN CRYSTALLINE STRONTIUM TITANATE by B. D. Silverman (Raytheon); Bull. Am. Phys. Soc., Ser. II, Vol. 6, p. 12(A), Feb. 1, 1961

An investigation of the microwave loss tangent of crystalline strontium titanate above the transition temperature using a linear chain model of a ferroelectric was reported. The model consists of oxygen and titanium ions coupled along chains in the [1, 0, 0], [0, 1, 0], and [0, 0, 1] directions on the unit cell. The microwave radiation field excites the transverse mode of uniform polarization which decays by transferring energy to lattice thermal modes. The temperature dependence of the loss tangent due to damping of the polarization mode by an n^{th} order anharmonicity is found to be $T^{n-2}/(T-T_c)$. Impurity damping yields a dependence of the form $1/(T-T_c)$, where T_c is the transition temperature. These results were compared with experiment. The behavior of the loss tangent for a sample subjected to a biasing field was also discussed.

10,385 MICROWAVE LOSSES IN STRONTIUM TITANATE by R. O. Bell and G. Rupprecht (Raytheon); Bull. Am. Phys.

Soc., Ser. II, Vol. 6, p. 12(A), Feb. 1, 1961

Measurements of the microwave loss of single crystal $SrTiO_3$ from 3 kMc/sec to 37kMc/sec over a temperature range from 80°K to 475°K were reported. The temperature dependence of the loss tangent shows a minimum at 140°K or about 60° above the Curie temperature. At temperatures below the minimum the losses show an appreciable increase, while above the minimum the increase is more gentle. The loss tangent at the minimum was found to be proportional to the frequency with a value of 1.0×10^{-3} at 20kMc/sec. With a dc electric field applied parallel to the microwave field, the loss tangent shows an increase. The field-dependent part of the loss tangent, tan δ_F (up to 7kMc/sec), is proportional to the square of the electric field, to the frequency of the microwave field, and to ϵ^n where n lies between 4 and 5.

Anisotropic Dielectrics - See 10,509

Electron Spin Resonance of Ferroelectric Tri-Glycine-Sulfate - See 10,439

Electron Spin Resonance of Ferroelectric KH_2PO_4 and KD_2PO_4 - See 10,440

10,386 DIELECTRIC PROPERTIES OF FINELY DISPERSED BARIUM TITANATE by A. L. Khodakov (Rostov-on-Don State U.); Soviet Phys.-Solid State, Vol. 2, pp. 1904-1907, Mar. 1961

Preparation of specimens of barium titanate in which the particle size range of each consisted of a small interval between 1μ and 20μ and evaluation of the dependence of dielectric properties on particle size are reported. Permittivity is plotted as a function of particle size, and both, in turn, are plotted as functions of frequency and electric field intensity. Permittivity decreases with decreasing particle size and, for specimens having particles up to 5μ diameter, decreases with increasing frequency. Two theoretical explanations of the results are presented.

10,387 RATIO OF DIELECTRIC CONSTANT ACROSS A SHOCK FRONT IN BARIUM TITANATE by P. S. Brody and R. H. Wittekindt (Diamond Ord. Fuze Labs.); Bull. Am. Phys. Soc., Ser. II, Vol. 6, p. 42(A), Feb. 1, 1961

Experimental values of the ratio of the dielectric constants across a shock front in polarized elements of barium titanate ceramic inferred from oscillographic records of voltage were reported. The elements were right cylinders polarized in the axial direction with fired silver electrodes on the cylinder ends. The shock front produced by a high-velocity impact moved axially and voltage generated across a 10-ohm resistor connecting the electrodes was recorded. The shock pressure and the shock-particle velocity relation for the impacted and impacting materials were obtained from the impact velocity. An expression for the voltage has been obtained in terms of the ratio of the dielectric constants across the shock front and the resistivity behind, assuming that the material behind the shock front has a uniform resistivity, a uniform dielectric constant, no spontaneous polarization, and the induced polarization is linear with the field. Comparison of experiment and theory indicates that, measured at 100 kilobars, the ratio of the dielectric constants is about 2 and that the resistivity is 10^4 ohm-cm or greater.

10,388 A CONTRIBUTION TO THE STATICS OF 90° WEDGE-SHAPED DOMAINS IN $BaTiO_3$ CRYSTALS by J. Fousek and B. Brezina (Czech. Acad. Sci., Prague); Czech. J. Phys., Vol. 11B, pp. 261-267, 1961

A study of 90° domains of wedge and parallel-piped shape in $BaTiO_3$ crystals of different form is reported. The condition responsible for their origin is discussed on the basis of a simple model.

CARRIER PROPERTIES

10,389 HOT ELECTRONS IN SEMICONDUCTORS AND THEIR APPLICATIONS by L. W. Davies (Amalgamated Wireless Valve); Proc. IRE Aust., Vol. 22, pp. 151-156, Mar. 1961

As the electric field strength in semiconductors is increased, departures from Ohm's law associated with carrier heating in the semiconductor are observed. At sufficiently large fields, avalanche increases in carrier density are observed. A brief survey of electron heating phenomena in semiconductors, and of their application in some useful devices is given. These include avalanche injection diodes, avalanche transistors and p-n-p-n diodes.

Injection of Hot Electrons from Au Film into Al-Al_2O_3 Films - See 10,395

Free Carrier Concentration at the Surface of a Semiconductor - See 10,412

Noise Spectrum Method of Measuring Excess Carrier Relaxation Time in InSb - See 10,411

10,390 GENERATION-RECOMBINATION IN P-TYPE GOLD DOPED GERMANIUM by L. J. Neuringer and W. Bernard (Raytheon); Phys. Rev. Lett., Vol. 6, pp. 455-457(L), May 1, 1961

Preliminary estimates of the capture cross sections of free holes by the 0.041 ev donor level and the 0.145ev acceptor level in p-type gold doped germanium derived from measurements of the generation-recombination noise spectrum in the range 10^4-10^7 cps are reported. Good agreement was obtained with a two impurity level model used to predict the observed noise for total cross section values of $\sigma_A = 1.55 \times 10^{-12} cm^2$ and $\sigma_D = 3.75 \times 10^{-18} cm^2$. The experimental noise spectrum clearly shows two characteristic relaxation times corresponding to the gold impurity levels. The significance of a small discrepancy between theory and experiment associated with the donor level is not as yet clear.

10,391 MEANS FOR REDUCING SURFACE RECOMBINATION by K. Lehovec and R. Zuleeg (Sprague); U.S. Pat. 2,980,831, Issued Apr. 18, 1961

A method for the reduction of surface recombination of minority carriers in a semiconductor is described. Surfaces where recombination may occur are covered with a coating which has a high minority carrier injection efficiency and is electrically insulated from the device electrodes. Layers of indium doped p-type material on n-type germanium bodies are cited as specific examples and a photodiode and transistor utilizing such layers are discussed.

10,392 PRODUCTION OF A LOW SURFACE RECOMBINATION VELOCITY ON <111> FACES OF N-TYPE INDIUM ANTIMONIDE AT 77°K by J. L. Davis (U.S. Naval Ord. Lab., and U. Maryland); Bull. Am. Phys. Soc., Ser. II, Vol. 6, p. 18(A), Feb. 1, 1961

It has been difficult to measure the bulk lifetime of added carriers in n-type InSb because of uncontrollable surface effects. This was confirmed by initial experiments which indicated a surface recombination velocity s of the order of 10^4 cm/sec, which varied with time and from point to point in the sample. In the work reported, s was measured on the <111> face which was polished by CP-4-A, using the spectral response of the photoconductivity. Low surface recombination velocities were obtained with a two-step process. The first step is etching in CP-4-A, with rinses of demineralized water and absolute methyl alcohol. This gives an s of about 4×10^3 cm/sec at 77°K. Dried nitrogen is then admitted to the vacuum space of the cryostat in which the sample is mounted, until a bright glow discharge can be excited with a Tesla coil. This discharge is applied to the sample for 30 to 60 sec. The resulting surface recombination velocity is approximately 200 cm/sec or less, which is low enough to make surface effects negligible. The uniformity of the surface is also substantially improved.

Electron Effective Mass in $CdSnAs_2$ - See 10,420

10,393 ELECTRON TRANSPORT IN A SEMICONDUCTOR by H. L. Frisch (Bell Labs.) and J. L. Lebowitz (Yeshiva U.); Bull. Am. Phys. Soc., Ser. II, Vol. 6, p. 29(A), Feb. 1, 1961

The linear transport properties of electrons in a semiconductor-like solid when both phonon and impurity scattering are important were discussed. The problem was treated for the case where Maxwellian statistics apply, and the electrons are described by a classical distribution function in position and velocity, f(r, v) satisfying a linear, space-dependent Boltzmann equation. This equation has been solved formally in the presence of a weak external electric field in a form convenient for perturbation expansions in the relative strength of the different scattering mechanisms, some of which have been carried out explicitly. For the special simplified model where the lattice scattering is represented by a single relaxation time, the change in conductivity due to the addition of impurities may be shown by use of the Wiener-Khinchin theorem to be always negative. In general the magnitude of the first-order change in the conductivity, in powers of the phonon relaxation time, will depend markedly on the sign of the impurity potential. Extension of these results to the case where the electrons are described by a single-particle density matrix was also discussed.

10,394 SCATTERING OF ELECTRONS BY PHONONS AND IMPURITIES IN SEMICONDUCTORS by H. Reiss and A. I. Anderman (NA Aviation); Phys. Rev., Vol. 122, pp. 1135-1140, May 15, 1961

A theory for the mobility of an electron in an n-type semiconductor under the combined scattering of phonons and impurities is developed. An attempt is made to combine the two processes in a rigorous manner by treating the effects of impurities as though due to an applied external field. Although in principle a solution for any value of τ, the phonon scattering relaxation time, should be possible, only a limiting law for the mobility at small values of τ is obtained. In the region of applicability satisfactory agreement with experiment is achieved.

Scattering Processes Deduced from Hot Electron Collection - See 10,395

Carrier-Phonon Interactions in Intrinsic Semiconductors - See 10,378

Ionization of Ge at Liquid He Temperatures - See 10,490

10,395 HOT ELECTRONS IN METAL FILMS: INJECTION AND COLLECTION by J. P. Spratt, R. F. Schwarz, and W. M. Kane (Philco); Phys. Rev. Lett., Vol. 6, pp. 341-342 (L), Apr. 1, 1961

An experiment using a structure in which energetic electrons are injected from a gold film into a 100 A thick Al film by quantum tunneling across a thin Al oxide film is reported. The hot electrons are collected after passing through the Al film across the barrier between the film and the 1 ohm-cm n-type germanium onto which the aluminum was evaporated, while lower energy electrons are rejected by this collector barrier. Information on scattering processes is deduced from collection efficiency data. The electrons appear to undergo many collisions with only a small percentage loss in their excess energy. The structure can be utilized as an amplifier similar to a normal transistor.

CONDUCTIVITY

10,396 THE ELECTRICAL CONDUCTIVITY AND PHOTOCONDUCTIVITY OF LEAD OXIDE LAYERS TREATED WITH SULFUR, SELENIUM, AND TELLURIUM by P. P. Konorov and A. N. Sokolov (Leningrad State U.); Soviet Phys.-Solid State, Vol. 2, pp. 1999-2001, Mar. 1961

The indicated properties of thin layers of lead oxide (PbO) subjected by two methods to vapors of either S, Se, or Te are evaluated. Both methods gave practically identical results. The electrical conductivity of PbO treated with S or Se was in the range of $10^5 - 10^6$ ohm-cm, and infrared photoconductivity was observed in each case, the S-treated layer having a much larger photosensitivity. No appreciable infrared photoconductivity was observed with Te-treated layers, since Te atoms do not enter the PbO lattice in sufficient quantity.

10,397 COMPLEX CONDUCTIVITY OF SOME PLASMAS AND SEMICONDUCTORS by P. H. Fang (NBS); Appl. Sci. Res., Vol. 9B, No. 1, pp. 51-64, 1961

The complex conductivities of plasmas and semiconductors are calculated for several cases where the collision frequency can be expressed as a power function of the energy. From the result some characteristic parameters of the plasma originally investigated by Spitzer are estimated. The problem of determining the relaxation time from a non-symmetrical dispersion is discussed.

Impurity Band Conduction at Low Temperatures in CdS - See 10,406

Effect of Impurities on Semiconductor Conductivity - See 10,393

10,398 A NEW CLASS OF HIGH-CONDUCTIVITY ORGANIC SOLIDS by R. G. Kepler, P. E. Bierstedt, and R. E. Merrifield (du Pont); Bull. Am. Phys. Soc., Ser. II, Vol. 6, p. 11 (A), Feb. 1, 1961

A new class of highly conducting organic solids was discussed. These materials are salts based on the anion-radical of tetracyanoquinodimethan (TCNQ):

$$(NC)_2C = \langle\bigcirc\rangle = C(CN)_2.$$

The highest conductivity materials ($100\,\Omega^{-1}\,cm^{-1}$) exhibit temperature-independent paramagnetism, indicating that the charge carriers are degenerate. In the less conductive compounds the charge carriers appear to be localized with their mobility depending exponentially on temperature. Magnetic susceptibility measurements show that in the less conductive materials the extra electrons on the TCNQ molecules are paired up in quasi-molecular states with a singlet ground state and a triplet state lying a small energy above the ground state. The conductivity of these materials is highly anisotropic. For example, in one material the room temperature conductivities are 4.0, 0.05, and $0.001\,\Omega^{-1}\,cm^{-1}$ in the three principal crystal directions.

Surface Conductivity of Intrinsic Ge Crystals - See 10,415

Conductivity of Rare-Earth Doped Barium Titanate - See 10,383

Conductivity of Moderately Doped Tellurium - See 10,410

Conductivity of Semiconducting Diamonds - See 10,456

10,399 STUDY OF THE ELECTRICAL CONDUCTIVITY OF SILICIDES OF THE TRANSITION METALS by V. S. Neshpor and G. V. Samsonov (Inst. of Metalloceramics and Special Alloys); Soviet Phys.-Solid State, Vol. 2, pp. 1966-1971, Mar. 1961

The electrical resistivity of approximately 35 silicides of transition elements (d-orbital) and the rare-earth elements (f- and d-orbitals) is evaluated. Of those investigated, only the disilicides of barium, chromium, iron, rhenium, and manganese are semiconductors; the others are metallic conductors. The relationship between resistivity and silicon content in a series of silicides of a particular element is determined by the type of conductivity in the highest silicide. The acceptor capacity of the d-orbital in disilicides of elements of groups IV - VI is shown to influence the resistivity in a definite manner.

10,400 SEMICONDUCTING PROPERTIES OF INORGANIC AMORPHOUS MATERIALS by H. L. Uphoff and J. H. Healy (A. O. Smith); J. Appl. Phys., Vol. 32, pp. 950-954, May 1961

The properties of ten compositions in the systems As:Se:Te and As:S:Te are reported. Nine of these compositions are amorphous in structure. The resistivities and Seebeck coefficients of these materials have been measured as functions of temperature. The resistivity varies exponentially with temperature, while the Seebeck coefficient varies linearly. At 298°K, the resistivity values for the amorphous samples range from 4.7×10^4 - 2.5×10^{13} ohm-cm, while the Seebeck coefficient values range from 830 - 1625 μv/°K (p-type). At any temperature, the resistivity decreases with increase in tellurium content. For the amorphous materials, the thermal conductivity values range from 2.4 - 4.4 mw/cm-°K.

10,401 CRITICAL FLUCTUATIONS IN SUPERCONDUCTORS by K. Gottfried (Harvard U.) and L. P. Kadanoff (U. Copenhagen); Bull. Am. Phys. Soc., Ser. II, Vol. 6, p. 65 (A), Feb. 1, 1961

The existence of critical fluctuations follows directly from the Cooper effect. In terms of time-dependent correlation functions, the Cooper pairing manifests itself as an instability of $R(\vec{r},t) = \langle \psi_\uparrow(\vec{r}t)\psi_\downarrow(\vec{r}t)\psi_\downarrow^\dagger(0)\psi_\uparrow^{-\dagger}(0)\rangle_T$ as $T\to T_c$; in fact the form of $R(\vec{r},0)$ is exactly that of the Ornstein-Zernike correlation function. This leads to the question whether any phenomena analogous to critical opalescence occur in the vicinity of T_c. Since $\psi_\uparrow(\vec{r}t)\psi_\downarrow(\vec{r}t)$ cannot be coupled to an external field, R itself is not measurable. R actually describes the effective interaction between electrons; thus its anomalous behavior at T_c results in a resonant electron-electron scattering amplitude near the Fermi surface. The linear response, on the other hand, is described by functions of the type $D(\vec{r},t) = \langle \psi_s^\dagger(\vec{r}t)\psi_s(\vec{r}t)\psi_{s'}^\dagger(0)\psi_{s'}(0)\rangle_T$. Therefore the question reduces to determining the influence of the aforementioned resonance on entities like D. For this purpose Boltzmann-like integral equations which connect D and R were constructed. The results were somewhat inconclusive.

10,402 ABSENCE OF AN ISOTOPE EFFECT IN SUPERCONDUCTING RUTHENIUM by T. H. Geballe, B. T. Matthias, G. W. Hull, Jr., and E. Corenzwit (Bell Labs.); Phys. Rev. Lett., Vol. 6, pp. 275-277 (L), Mar. 15, 1961

Identical superconducting transition temperatures for naturally occurring ruthenium isotopes of mass number 99 and 104 within the accuracy of the measurements (±0.001°K) are reported. Ruthenium is the first transition element checked for the isotope shift. With the exception of ruthenium and osmium, transition element superconductors have transition temperatures which change rapidly enough with small amounts of dissolved oxygen to obscure the expected isotope shift. The transition temperatures of the samples were within 0.001°K, whereas that of Ru^{104} would be expected to be 0.012°K below that of Ru^{99} if they were proportional to the inverse square root of the atomic mass. This indicates that mechanisms other than electron-phonon interaction may lead to superconductivity.

10,403 TRANSVERSE COLLECTIVE OSCILLATIONS IN SUPERCONDUCTORS by R. A. Ferrell (U. Maryland); Bull. Am. Phys Soc., Ser. II, Vol. 6, p. 65 (A), Feb. 1, 1961

Transverse collective waves in superconductors were treated similarly to plasmons in a degenerate electron gas. It was shown that a discrete exciton can separate from the continuum and be pulled down into the energy gap without phonon exchange or Coulomb interaction but as a result of only the magnetic interaction of the quasi-particle and hole. This type of exciton is not an eigenstate of the BCS Hamiltonian and occurs only when the magnetic interaction terms are added to the Hamiltonian. The criterion for the exciton to separate from the continuum is identical to that for free propagation of light at a frequency below the gap frequency. It requires that the positive polarizability due to absorptions above the gap be strong enough to

cancel the negative London polarizability. Although more complicated, such an electromagnetic window in the gap is analogous to the well-known optical window of silver films in the near ultraviolet. A further non-negligible electromagnetic collective effect in superconductors is the excitation of ordinary transverse phonons.

10,404 DIRECT MEASUREMENT OF THE SUPERCONDUCTING ENERGY GAP by J. Nicol, S. Shapiro, and P. H. Smith (A. D. Little); Bull. Am. Phys. Soc., Ser. II, Vol. 6, p. 65(A), Feb. 1, 1961

The phenomenon of electron tunneling through a thin insulating layer between two metals, both of which are maintained in the superconducting state, provides a direct measure of the superconducting energy gap. The tunneling current vs voltage characteristic of an experimental sandwich of Al-Al_2O_3-Pb exhibits negative resistance regions symmetric about the origin. The way in which the negative resistance regions measure the superconducting energy gap directly was analyzed. Measured values for the full limiting gaps for lead and aluminum are, respectively, $(4.35\pm0.10)kT_c$ and $(2.7\pm0.3)kT_c$ with the transition temperatures taken as 7.2°K for lead and 1.2°K for aluminum. Experimental curves were compared with calculations based on the superconducting density-of-states function given by Bardeen, Cooper, and Schrieffer.

10,405 SUPERCONDUCTIVE PROPERTIES OF THIN TIN FILMS by J. N. Cooper and E. C. Crittenden, Jr., (U.S. Naval Postgrad. School and Space Tech. Labs.) and F. W. Schmidlin (Space Tech. Labs.); Bull. Am. Phys. Soc., Ser. II, Vol. 6, pp. 64-65 (A), Feb. 1, 1961

The superconductive properties of a carefully prepared family of eight thin tin films with thicknesses varying from 0.03μ to 1.04μ in the temperature range between 1.5°K and 3.9°K were reported. The films were prepared by vacuum evaporation upon polished glass substrates cooled to −20°C. Film thicknesses were measured by Fabry-Perot interferometry and were also calculated from both mass evaporated and resistance measurements. Critical temperatures, particularly for the thinner films, were substantially above that for bulk tin, presumably because of tensile stresses. The dc critical currents as a function of thickness t can be well approximated by an expression of the form $A(1-e^{-t/\sigma})/(1+e^{-t/\sigma})$, where A is a constant determined by the temperature and σ is about 0.16μ, essentially independent of temperature.

BREAKDOWN

10,406 LOW-FIELD BREAKDOWN, NON-OHMIC CONDUCTIVITY, AND PHOTOCONDUCTIVITY OF CdS AT LOW TEMPERATURES by H. Shenker (U.S. Naval Res. Lab.); J. Phys. Chem. Solids, Vol. 19, pp. 1-7, Apr. 1961

An investigation of low temperature electrical conductivity and photoconductivity effects in highly doped CdS samples having room temperature resistivities in the range 0.08 - 15 ohm-cm is reported. These samples were found to have a low-field breakdown effect at electric fields which varied from 265 v/cm to as high as 5500 v/cm depending on the sample. At fields below the breakdown field, the conductivity was concluded to be of the impurity band conduction type since the Hall mobility at 4.2°K was found to be less than 0.03 cm^2/v-sec. At these fields the conductivity was found to increase markedly as the applied electric field was increased. These crystals were found to exhibit an impurity photoconductivity effect with a maximum response at 28μ and a long-wave cutoff at 32μ.

MAGNETOELECTRIC (GALVANOMAGNETIC) PROPERTIES

10,407 INFLUENCE OF CONDUCTIVITY GRADIENTS ON GALVANOMAGNETIC EFFECTS IN SEMICONDUCTORS by R. T. Bate and A. C. Beer (Battelle Mem. Inst.); J. Appl. Phys., Vol. 32, pp. 800-805, May 1961

An approximate solution of a boundary-value problem arising from the continuity equation in an inhomogeneous semiconductor, leading to rotational current vectors is given. The results are used to predict the effect of carrier-concentration gradients on magnetoresistance. The predicted weak-field effects are especially significant in degenerate semiconductors and n-type III-V intermetallics in which the "intrinsic" magnetoresistance is small. In strong fields, even small gradients in carrier concentration can completely alter the field dependence of the magnetoresistance. Experimental results indicate that transverse currents, which do not occur in the simple case discussed, do appear in general, and further perturb the magnetoresistance. The influence of inhomogeneous magnetic fields is discussed briefly.

10,408 INFLUENCE OF MAGNETOCONDUCTIVITY DISCONTINUITIES ON GALVANOMAGNETIC EFFECTS IN INDIUM ANTIMONIDE by R. T. Bate, J. C. Bell, and A. C. Beer (Battelle Mem. Inst.); J. Appl. Phys., Vol. 32, pp. 806-814, May 1961

Observations in n-type InSb of anomalous galvanomagnetic effects associated with spatial discontinuities in carrier concentration are reported. These discontinuities result from anisotropic segregation of impurities during crystal growth. An increase in the magnitude of the Hall coefficient at 20,000 gauss to nearly twice the weak field value was observed in one case. The magnetoresistance is especially sensitive to inhomogeneities. For an inhomogeneous sample at a particular magnetic field, the measured $\Delta\rho/\rho_0$ may be as much as 100 times larger than that for a homogeneous sample. Negative magnetoresistance has also been observed at room temperature in inhomogeneous samples. All of the above observations are predicted qualitatively by considering a simple model consisting of a long, thin specimen having a discontinuity in resistivity and Hall coefficient in the current direction. The boundary value problem corresponding to this case is solved to predict the electric field and current densities.

10,409 INFLUENCE OF THE HALL EFFECT UPON THE TRANSVERSE MAGNETORESISTANCE IN INDIUM ANTIMONIDE by C. A. Simmons (Burroughs); Bull. Am. Phys. Soc., Ser. II, Vol. 6, p. 18(A), Feb. 1, 1961

A detailed experimental investigation of the influence of the

MAGNETOELECTRIC (GALVANOMAGNETIC) PROPERTIES (Cont'd)

specimen geometry on the transverse magnetoresistance was reported. Differentiation between the bulk properties and the geometrical contributions has been accomplished. It was found that the enhancement of the magnetoresistance effect in rectangular elements is due to the Hall effect rather than to its absence and that the bulk property has an H^2 relationship while the geometry effect is linear with H and inversely proportional to the length-to-width ratio.

New Cyclotron Resonance Effects from Magnetoplasmas - See 10,416

Effect of Stress on Spin Resonance of III Acceptor Impurities in Si - See 10,436

Spin Resonance Spectrum of Stretched Polyethylene - See 10,441

Electron Spin Relaxation in B and P Compensated Si - See 10,433

Impurity Studies by Electron Spin Resonance - See 10,443

Passage Effect in Electron Spin Resonance of Fe-Doped Si - See 10,445

Electron Spin Relaxation in P-Doped Si - See 10,434

Excited States in P-Doped Si - See 10,435

F-Center Spin Resonance in LiH - See 10,438

10,410 MEASUREMENT OF THE GALVANOMAGNETIC EFFECTS IN MODERATELY DOPED TELLURIUM by W. B. Teutsch, H. Roth, and H. T. Harper (Genl. Atomic); Bull. Am. Phys. Soc., Ser. II, Vol. 6, p. 27(A), Feb. 1, 1961

Measurements of a type previously made on pure tellurium that have been carried out on moderately doped tellurium are reported. Oriented samples, with their long axis either parallel to or perpendicular to the c axis, were taken from a Czochralski-grown single crystal. The two resistivities, two Hall coefficients, and eight magnetoresistance coefficients were studied from 70°K to 300°K in magnetic fields up to 13 kgauss. The samples are extrinsic and p-type in this entire range. As was anticipated, the present results differ from the work on pure tellurium and – being free of the anomalies exhibited by the latter – are perhaps more indicative of the properties of the valence band. The two Hall coefficients have the same value and indicate a carrier density of $\sim 10^{17}\,cm^{-3}$. The most striking feature is the vanishing of $\rho_{11,33}$, its value being about 100 times smaller than other corresponding coefficients. This unusual result seems to preclude any straightforward explanation of the conduction processes in the valence band.

OTHER ELECTRICAL PROPERTIES

10,411 GENERATION-RECOMBINATION NOISE IN P-TYPE InSb by F. M. Klaassen, J. Blok, and F. J. de Hoog (Vrije U.); Physica, Vol. 27, pp. 185-196, Feb. 1961

Measurements of the current noise spectra of p-type single crystals of InSb in the range 175°K-275°K are reported. Although the magnitude of these spectra is extremely small, relaxation times of excess carriers are accurately obtained from these spectra. The temperature dependence of these times, being on the order of 10^{-8} sec, suggests a Shockley-Read recombination mechanism. Good agreement is found between the noise spectra and the theory of generation-recombination noise. It is shown that the noise equivalent power has a minimum for that temperature at which the Hall constant has a maximum. A minimum value of 1.8×10^{-10} watt at 220°K was found in the samples which were studied.

10,412 EXTENDED CURVES OF THE SPACE CHARGE, ELECTRIC FIELD, AND FREE CARRIER CONCENTRATION AT THE SURFACE OF A SEMICONDUCTOR, AND CURVES OF THE ELECTROSTATIC POTENTIAL INSIDE A SEMICONDUCTOR by C. E. Young (Bell Labs.); J. Appl. Phys., Vol. 32, pp. 329-332, Mar. 1961

Previously published curves of the space charge, electric field, and change in free carrier concentration for a semiconductor surface are extended to permit their application to materials with wide energy gaps such as silicon and gallium arsenide. Several curves of electrostatic potential inside a semiconductor are also given.

10,413 FIELD EMISSION FROM SILICON AND GERMANIUM FIELD DESORPTION AND SURFACE MIGRATION by F. G. Allen (Bell Labs.); J. Phys. Chem. Solids, Vol. 19, pp. 87-99, Apr. 1961

The successful use of field desorption to produce clean germanium patterns in the electron field emission microscope is reported. The field-cleaned pattern transforms upon annealing to one very similar to that obtained from silicon cleaned by heating in vacuum. Changes in impurity concentration at the surface during cleaning, heretofore a problem, are avoided by the desorption technique. Surface atom mobility becomes appreciable at ~250°C on clean germanium and at ~800°C on clean silicon. Field emission current-voltage characteristics for both clean Ge and Si are presented. The results are discussed in the light of existing theory, and the need for a theory including emission from surface states and the valence band is pointed out.

10,414 EMISSION OF NEGATIVE IONS OF OXYGEN FROM DISPENSER CATHODES. PART I. CATHODES OF BARIUM OXIDE IN SINTERED NICKEL by N. A. Surplice (U. Coll Staffordshire); Brit. J. Appl. Phys., Vol. 12, pp. 214-219, May 1961

The use of sintered nickel and barium oxide cathodes as ion sources in simple mass spectrometers is reported. These cathodes have been found to emit negative ions of atomic oxygen for at least 24 hours during their activation at 1250°K-1350°K. The evidence suggests that the oxygen is produced by the dissociation of barium oxide and is removed from the cathode by positive ion bombardment. At voltages greater than the ionization potential of the residual gases, the variation of the oxygen ion current I with time t could be expressed as the sum of two exponentially decreasing terms: $I = a \exp(-pt) + b \exp(-qt)$ where p and q were of the order of 2 and 0.2 per hour respectively. Similar results have been obtained with a commercial cathode containing triple carbonates. There appear to be two processes operating in parallel, corresponding to the two terms of the equation. It is postulated that the first process is the

diffusion of oxygen through the bulk of the crystals to the nickel part of the cathode's surface, and its removal therefrom by bombardment with positive ions of oxygen and nitrogen. The second process is the diffusion of oxygen through the pores of the cathode, and its removal from the end of the pores by bombardment with positive ions of barium as well as of the residual gases. The first process has the slower rate of replacement of oxygen and in an hour or two this process is insignificant compared with the second one. If the cathode surface is temporarily poisoned with oxygen from an external source, it rids itself of the extra oxygen within a few seconds.

10,415 THE ADSORPTION OF OXYGEN GAS ON GERMANIUM AND SURFACE CONDUCTIVITY by M. J. Sparnaay and J. Van Ruler (N.V. Philips); Physica, Vol. 27, pp. 153-162, Feb. 1961

A new method for studying electrical surface properties of semiconductors is described. The method consists of measuring the electrical conductivity of thin cylindrical germanium single crystals as a function of oxygen gas pressure and thickness of the germanium cylinder. The thickness of the cylinder can be varied by "burning off" the germanium at 700°C in an oxygen gas pressure of 10^{-2}mm Hg. The method permits the roles played by surface conductivity and bulk conductivity to be separated. Results for intrinsic germanium are given. These are in quantitative agreement with the results of Handler.

Surface Space Charge of Semiconductors - See 10,412

10,416 MAGNETOPLASMA EFFECTS IN SOLIDS by B. Lax (Lincoln Lab.); IRE Trans., Vol. MTT-9, pp. 83-89, Jan. 1961

Plasmas in solids show a more complex behavior than in gases since they reflect the symmetry properties of crystals. Because the carrier concentration has a wide range in semiconductors and metals, the plasma phenomena can be studied from microwaves to the ultraviolet. The effect of magnetic fields on the electromagnetic properties of plasmas at microwave and infrared frequencies is discussed and its use to measure dielectric constant and band structure of such solids in the limit of low magnetic fields is reported. The magnetoplasma exhibits effects analogous to the galvanomagnetic phenomena. However, near resonance in the classical limit, they show up as depolarizing effects in semiconductors and also give rise to a new type of cyclotron resonance under anomalous skin conditions in metals.

10,417 COHERENT EXCITATION OF PLASMA OSCILLATIONS IN SOLIDS by D. Pines (Genl. Dynamics, and U. Illinois); IRE Trans., Vol. MTT-9, pp. 89-92, Jan. 1961

Considerations concerning the feasibility of observing the coherent excitation of plasma oscillations in a two-component plasma of electrons and holes in semiconductors or semimetals are given. By coherent excitation is meant the onset of a high-frequency ("two-stream") instability arising from an appreciable drift of electrons versus holes under the action of an applied electric field. Conditions favorable to coherent excitation include a sizeable difference in electron and hole masses, and long relaxation times for both kinds of particles. The extent to which such conditions are present in InSb is discussed.

10,418 OSCILLATIONS IN THE LONGITUDINAL TUNNEL CURRENT OF TUNNEL DIODES by R. R. Haering and P. B. Miller (IBM); Phys. Rev. Lett., Vol. 6, pp. 269-271 (L), Mar. 15, 1961

An explanation of the oscillation of the tunnel current in InSb tunnel diodes with the longitudinal magnetic field at low temperatures is proposed. It is pointed out that the observed oscillations are far too large in amplitude and number to be explained as due to density of state fluctuations in the highest occupied Landau level as is suggested by analogy to the de Haas-Schubnikov type oscillations in galvanomagnetic properties. The alternative explanation is advanced that in a magnetic field the electron Fermi level oscillates about its zero field value, resulting in a small charging or discharging of the junction capacitance and hence a small oscillating change of the junction field F. The tunneling rate is strongly dependent on F and large current oscillations result. The magnitude, field dependence and observed period of the oscillations are accounted for.

10,419 ESAKI TUNNELING IN THE PRESENCE OF MAGNETIC FIELDS by R. R. Haering and E. N. Adams (IBM Res. Ctr.); J. Phys. Chem. Solids, Vol. 19, pp. 8-17, Apr. 1961

The theory for Esaki tunneling in the presence of a magnetic field is given for both transverse and longitudinal magnetic fields; it is shown that there are important qualitative differences between the two cases. Expressions are given for the normalized current I (B)/I(0) in both field orientations in the limit of strong magnetic fields. It is found that oscillations of the de Haas-Van Alphen type are not to be expected.

Calculation of Elastic Tunneling Current in Esaki Diodes - See 10,375

10,420 ELECTRICAL AND OPTICAL PROPERTIES OF $CdSnAs_2$ by W. G. Spitzer, J. H. Wernick, and R. Wolfe (Bell Labs.); Solid-State Electronics, Vol. 2, Nos. 2/3, pp. 96-99, Mar. 1961

An investigation of the electrical and optical properties of n-type $CdSnAs_2$ for samples having carrier concentrations between $10^{18}cm^{-3}$ and $3\times10^{18}cm^{-3}$ is reported. Resistivity and Hall coefficient measurements yield room-temperature electron Hall mobilities between 5500 and 6200 cm^2/v-sec in this carrier concentration range. Measurements between room temperature and liquid-helium temperature show degenerate behavior. Above room temperature the beginning of the intrinsic range was observed with an approximate energy gap of 0.3ev. A thermal-conductivity measurement yielded a phonon thermal conductivity of 0.071 w/cm°C. For the same carrier concentrations, the thermoelectric power ranged from -100 to $-70\mu v/°C$, indicating a thermoelectric figure of merit on the same samples used to obtain the electrical data. An electron effective mass between $0.04m_0$ and $0.06m_0$ and a lattice dielectric constant of 12.1 ± 0.4 were deduced from the reflectivity data. The shift in the absorption edge with increasing carrier concentration and the free-carrier absorption yielded electron effective masses in qualitative agreement with the values obtained from the reflectivity data.

MAGNETIC PROPERTIES

10,421 HYPERFINE STRUCTURE OF Fe^{57} IN PARAMAGNETIC AND ANTIFERROMAGNETIC FeF_2 FROM THE MÖSSBAUER EFFECT by G. K. Wertheim (Bell Labs.); Phys. Rev., Vol. 121, pp. 63-66, Jan. 1, 1961

Use of gamma-ray resonant absorption measurements in oriented slabs of FeF_2 to determine the magnitude and direction of the magnetic field at the iron nucleus in the antiferromagnetic state (3.40×10^5oe at 0°K) and the quadrupole splitting in the paramagnetic state (31.2 Mc/sec) of this material is described. The observed electric and magnetic hfs in the antiferromagnetic state is interpretable in terms of an asymmetric electric field gradient tensor with its major axis perpendicular to the c axis, an asymmetry parameter of 0.33, and a quadrupole splitting of 30.3 Mc/sec at 45°K.

10,422 NUCLEAR MAGNETIC SPECIFIC HEAT IN TWO FERROMAGNETIC IRON ALLOYS by C. T. Wei (Michigan State U.), C. H. Cheng, and P. A. Beck (U. Illinois); Phys. Rev., Vol. 122, pp. 1129-1130, May 15, 1961

Calculated values of the effective magnetic field in two ferromagnetic iron alloys are reported. These values, which are derived from measurements of nuclear specific heat at 1.6°K to 4.2°K, are $H_{eff} = 312$ koe at the Co nuclei in $Co_{0.3}Fe_{0.7}$ and $H_{eff} = 61$ koe or less at the V nuclei in $V_{0.33}Fe_{0.67}$. Both of these alloys are body-centered cubic and ferromagnetic. The large difference in the H_{eff} values may be associated with the fact that in $Co_{0.3}Fe_{0.7}$ the Co^{59} nucleus is located in an atom with appreciably polarized 3d electrons, while in $V_{0.33}Fe_{0.67}$ the V^{51} nucleus is the only abundant nuclide with a nuclear magnetic moment and the atomic moment of V is very small or zero. Since in ferromagnetic alloys the polarization of the core s electrons is expected to be much stronger in those atoms which do have polarized d electrons than in adjacent atoms which do not, the above results suggest that, in the alloys investigated, the dominant contribution to H_{eff} arises through Fermi contact interaction from the polarization of the core s electrons, as found for iron by Hanna et al.

10,423 HYPERFINE FIELD AND ATOMIC MOMENTS IN FERROMAGNETIC ALLOYS by C. E. Johnson, M. S. Ridout, T. E. Cranshaw, and P. E. Madsen (Harwell); Phys. Rev. Lett., Vol. 6, pp. 450-451 (L), May 1, 1961

Measurements of the Mössbauer absorption spectrum at room temperature over the whole range of Fe-Co and Fe-Ni alloys for the 14.4 kev radiation of Fe^{57} are reported. The resulting spectrum showed six lines arising from the Zeeman splitting of the nuclear levels of Fe^{57}, and the hyperfine field was computed from their separations. The variation of the magnetic field at iron nuclei in the alloys is shown graphically against the excess electron number x over that of iron and is generally remarkably similar to the corresponding region of the Slater-Pauling curve for the saturation moments. Both curves show a maximum near $x = 0.3$. The results are contrary to the localized magnetic moment theories.

10,424 THERMAL FLUCTUATION EFFECTS IN THIN MAGNETIC FILMS by E. P. Wohlfarth (Imperial Coll.); J. Electronics Control, Vol. 10, pp. 33-37, Jan. 1961

The observation that the coercive force of thin films is time dependent is interpreted quantitatively on the basis of the theory of thermal fluctuation effects, and values of the anisotropy field and mean effective crystallite size are deduced and discussed.

Magnetic Excitation Inside a Thin Film Ferromagnet - See 10,496

Magnetic Properties of Ferrite Thin Films - See 10,359, 10,360

Kerr Effect in Ferromagnetic Films - See 10,461

10,425 ON THE MAGNETICALLY DILUTE HEISENBERG AND ISING FERROMAGNETICS by G. S. Rushbrooke and D. J. Morgan (U. Durham); Mol. Phys., Vol. 4, pp. 1-15, Jan. 1961

The lowering of the Curie temperature of a ferromagnetic substance by random dilution with nonmagnetic elements is studied on the basis of Heisenberg and Ising models having nearest neighbor interactions between magnetic elements only. It is proved that the limiting concentration, p_c, of magnetic elements, below which there is no Curie temperature, is the same for all such models, whether Heisenberg or Ising, and regardless of the spin value concerned. p_c depends only on the lattice structure. Numerical estimates of p_c for various lattices are given. Successive approximations are developed to the full Curie temperature curve, and it is found that whereas for the Ising model $T_c(p)$ approximates to $pT_c(1)$ near $p = 1$, $T_c(p) < pT_c(1)$ for the Heisenberg model.

10,426 ANOMALIES IN THE TEMPERATURE DEPENDENCE OF THE COERCIVE FORCE IN RARE EARTH ELEMENT GARNET FERRITES IN THE NEIGHBORHOOD OF THE COMPENSATION POINT by K. P. Belov and A. V. Ped'ko (Moscow State U.); Soviet Phys.-JETP, Vol. 12, pp. 666-668, Apr. 1961

Anomalous maxima of the coercive force found in the region of the compensation point in rare earth garnet ferrites are discussed. In polycrystalline ferrites the height and breadth of these maxima depend on the specimen density and, in addition, a doubling of the peaks is observed. There are also anomalous maxima in single crystal specimens, but they are narrower than in polycrystalline specimens. A qualitative explanation of the observed phenomena is given. It is suggested that the strong broadening of the ferromagnetic resonance absorption lines in ferrites on approaching the compensation point previously observed is due to a cause related to that underlying the anomalous increase in coercive force near this point.

10,427 FIRST MAGNETOCRYSTALLINE ANISOTROPY CONSTANTS OF SOME IRON-SILICON ALLOYS by S. Arajs, H. Chessin, and D. S. Miller (U.S. Steel Res. Ctr.); J. Appl. Phys., Vol. 32, pp. 857-859, May 1961

First magnetocrystalline anisotropy constants $K_{1\infty}$ of 3.6, 6.7, 8.8, and 12.4 wt% silicon in iron alloys have been measured at 77°K and 297°K by determining the torque exerted on {100} single-crystal disks in uniform magnetic fields. The following results on disordered alloys are reported:

Composition (wt% Si)	Temperature (°K)	$K_{1\infty} \times 10^3$ (erg cm^{-3})
3.6	77	430 ± 10
	297	360 ± 10
6.7	77	290 ± 10
	297	205 ± 10

(Table cont'd)

Composition (wt% Si)	Temperature (°K)	$K_{1\infty} \times 10^3$ (erg cm^{-3})
8.8	77	245 ± 10
	297	165 ± 10
12.4	77	120 ± 5
	297	78 ± 5

The measurements of this investigation are compared with earlier studies. The agreement, where an overlap occurs, is satisfactory.

10,428 REMARKS ON THE MAGNETIC PROPERTIES OF Au-Mn SYSTEM by H. Sato (Ford Motor); J. Phys. Chem. Solids, Vol. 19, pp. 54-60, Apr. 1961

Au-Mn alloys show magnetic behavior which depends upon the various types of superlattice existing in this system. The comparison of the magnetic properties of Au_2Mn and Au_4Mn, however, clearly shows the difficulty of interpreting the magnetic structure of Au_2Mn, which is supposed to be helical, from competing positive and negative exchange interactions as is often suggested. In both Au_4Mn and Au_2Mn, the Mn atoms form a body-centered tetragonal lattice with c/a ratio of 0.62 and 2.60 respectively. Although the first- and second-neighbor distances between Mn atoms for these two compounds are practically the same, the former is ferromagnetic but the latter is metamagnetic. The first-neighbor distance corresponds to the ferromagnetic interaction range of Mn atoms, but geometrically this alone cannot cause any cooperative alignment of spins. The second-neighbor distance, on the other hand, is too long to expect any appreciable interaction. However, it is proved that the existence of a minor interaction between the second neighbors is sufficient to produce the expected cooperative phenomena. The magnitude of such an interaction is found to be of the same order as the magnetic dipole interaction. Although, at present, it is hard to conclude what kind of interaction is operative, it is suggested that at least the difference of the magnetic behavior of Au_2Mn and Au_4Mn is explained if magnetic dipole interaction is assumed for the weak interaction.

10,429 THEORY OF FERROMAGNETIC RESONANCE. II. (Genl. Relations) by S. V. Tyablikov (Acad. Sci. USSR); Soviet Phys.-Solid State, Vol. 2, pp. 1805-1813, Mar. 1961

An expression for the susceptibility tensor is derived with the aid of two-time temperature Green's functions and some of its general properties that are independent of the specific form of the Hamiltonian are established. The calculations are carried through in an approximation that is linear with respect to the RF-field intensity. Information about the behavior of the susceptibility at ferromagnetic resonance is obtained by considering some analytic properties of the Green's functions. Energy absorption by the spin system is considered.

10,430 NEUTRON DIFFRACTION INVESTIGATION OF ANTIFERROMAGNETISM IN $CrCl_3$ by J. W. Cable, M. K. Wilkinson, and E. O. Wollan (Oak Ridge Natl. Lab.); J. Phys. Chem. Solids, Vol. 19, pp. 29-34, Apr. 1961

Neutron diffraction observations made on powder and single crystal samples of anhydrous $CrCl_3$ at temperatures from 4.2°K to 298°K are reported. This hexagonal layer-type crystal undergoes a transition at 16.8°K to an antiferromagnetic state in which the magnetic moments within each hexagonal layer of metal ions are aligned parallel but adjacent layers of moments are oppositely directed. The axis of spontaneous sublattice magnetization is closely perpendicular to the c-axis. Observations of the (003) antiferromagnetic reflection in an external magnetic field show that the antiferromagnetism can be destroyed with fields of only a few kilo-oersteds, and lead to the conclusion that a net magnetization can be produced with very small magnetic fields.

10,431 PARAMAGNETISM: A KEY TO THE KNOWLEDGE OF CHEMICAL BONDING by J. A. McMillan (Inst. de Fisica de San Carlos de Bariloche); Am. J. Phys., Vol. 29, pp. 207-210, Mar. 1961

The phenomenological classification of substances on the basis of their magnetic behavior is considered. The nature of paramagnetism is explained and cases in which this property changes with coordination are discussed. Simple qualitative experiments are also described.

Crystalline Field Distortions Due to Pressure - See 10,446

10,432 THE ROLE OF PHONONS IN PARAMAGNETIC RELAXATION by B. W. Faughnan and M. W. P. Strandberg (MIT); J. Phys. Chem. Solids, Vol. 19, pp. 155-166, Apr. 1961

The coupled spin-lattice-bath system is investigated under conditions of microwave power saturation and the conditions for the existence of a steady-state nonthermal equilibrium phonon distribution are determined. The spin-lattice-bath equations are solved numerically for a few special cases involving a non-equilibrium distribution of phonons. The results of an experiment designed to detect the presence of nonequilibrium phonons are reported. No indication of the presence of such phonons was found. The experiments were performed using Cr^{3+} impurities in MgO, Al_2O_3 and $K_3Co(CN)_6$ and at T = 4.2°K and 2°K. The sensitivity of the experiment was such that for ruby a phonon temperature rise at $\Delta T = 0.005T$ could have been observed. Finally, the validity of the theory is discussed in view of the experimental results.

10,433 COMPENSATION DEPENDENT ELECTRON SPIN RELAXATION IN N-TYPE SILICON by G. Yang and A. Honig (Syracuse U.); Bull. Am. Phys. Soc., Ser. II, Vol. 6, p. 20(A), Feb. 1, 1961

An investigation of spin-lattice relaxation of phosphorus donor electrons in a compensated silicon sample containing $6 \times 10^{15}/cm^3$ phosphorus impurities and $2 \times 10^{15}/cm^3$ boron impurities at liquid helium temperatures was reported. By subtracting the relaxation probabilities due to mechanisms found in uncompensated samples from the measured relaxation probability, the relaxation probability due to compensation is obtained. The temperature and magnetic field dependences for this compensation dependent mechanism have been determined. In addition, the dependence of this relaxation probability on concentration of charged impurities has been obtained by employing a recently developed technique. This technique permits control of the concentration of ionized impurities in compensated samples by supplying charged impurities with photoexcited electrons and holes from the valence band. The results of these experiments are

consistent with a previously suggested interpretation that relaxation results from spin diffusion from relaxation centers consisting of phosphorus ion-phosphorus neutral pairs, i.e., the analog of the hydrogen molecular ion.

10,434 ELECTRON SPIN RELAXATION IN PHOSPHORUS-DOPED SILICON by T. Castner (GE Res. Lab.); Bull. Am. Phys. Soc., Ser. II, Vol. 6, p. 304(A), Apr. 24, 1961

An investigation of the spin-lattice relaxation of phosphorus donor electrons in a silicon sample containing $9 \times 10^{15}/cm^3$ phosphorus impurities between 4.2°K and 20.4°K at 9.3kMc was reported. The steady-state saturation method was used between 20.4°K and 10°K, and fast passage techniques were used between 10°K and 4.2°K to measure T_s ($\Delta M_s = \pm$, $\Delta M_I = 0$ process). The T^{-7} temperature dependence of T_s found by Feher was shown to continue up to 6.5°K. Between 6.5°K and 8.3°K the temperature dependence can best be fitted by $T_s T^n$ = constant, with $12 < n < 14$. Analysis of the saturation curves taken between 10°K and 20.4°K on the basis of the Portis theory for inhomogeneously broadened lines assuming $T_1 = T_2$ yields an exponential dependence of T_s on temperature. The dependence of T_s on the direction of the static magnetic field with respect to the crystallographic axes was also considered. The results were interpreted in terms of various Raman-type relaxation processes based on relaxation taking place via the intervalley states of the phosphorus donor electrons.

Relaxation Processes in Ruby - See 10,452

10,435 INFRARED PUMPED PARAMAGNETIC EXCITED STATE IN PHOSPHORUS-DOPED SILICON by A. Honig (Syracuse U.); Bull. Am. Phys. Soc., Ser. II, Vol. 6, p. 118(A), Mar. 20, 1961

Production of an appreciable excited state population in a crystal of silicon containing $\sim 10^{15}$ phosphorus impurities/cm^3, by photoionizing the neutral phosphorus impurities, and observation of electron spin resonance in the excited state were reported. The lifetime of an electron in the excited state exceeds several hours at liquid helium temperatures, but the state can be rapidly emptied by infrared radiation of wavelength greater than $\sim 30\mu$. This radiation has insufficient energy to photoionize phosphorus impurities from their ground state, but has sufficient energy to depopulate the excited state. The electron spin resonance associated with this excited state is a single line at $g \cong 1.998$, and the spin-lattice relaxation time is only slightly shorter than the relatively long times associated with the 2 hyperfine lines of the ground-state spin resonance. Identification of this excited state as part of the fivefold nearly degenerate 1S state in the Kohn-Luttinger theory of impurity states in silicon is suggested by the experiments. Other conceivable identifications were discussed, as well as possible explanations of why most silicon samples do not exhibit this photoinduced resonance.

10,436 SPIN RESONANCE OF ACCEPTOR IMPURITIES IN SILICON by G. W. Ludwig and H. H. Woodbury (GE Res. Labs.); Bull. Am. Phys. Soc., Ser. II, Vol. 6, p. 118(A), Mar. 20, 1961

Spin resonance measurements of column III acceptor elements in silicon crystals subjected to uniaxial stress ($\sim 10^4$ kg/cm^3) in the temperature range 1.3° to 10°K were reported. The width of the single line detected at low stresses passes through a minimum at intermediate stresses. Structure, apparently due to hyperfine interaction, has been resolved at larger stresses in some cases. The spin-lattice relaxation time increases by as much as a factor of 10^5 with increasing stress. Resonance due to the deep-level acceptor zinc has also been observed.

10,437 PARAMAGNETIC RESONANCE OF F CENTERS IN LiF by H. Blum (U. Illinois) and W. C. Holton (Texas Instr.); Bull. Am. Phys. Soc., Ser. II, Vol. 6, pp. 112-113(A), Mar. 20, 1961

A study of the electron spin resonance (ESR) of x-rayed LiF crystals was reported. The resonance exhibits partially resolved structure which depends on the crystal orientation in the magnetic field (H_0). For the [100], [110], and [111] directions parallel to H_0, there are ~35 partially resolved lines with spacings of 14.3, 12.1, and 14.7 gauss, respectively. At 72° from the [001] direction in a [110] plane, there are over 70 lines with a spacing of 6.75 gauss. Kim et al. have observed the same ESR structure pattern, and suggest that it is not due to the F center. However, using previously obtained electron-nuclear double resonance data for the F center in LiF, the detailed F-center ESR line shape for the [111] and 72° directions has been calculated on an IBM 704 computer; the computer and experimental results agree to within 3 per cent. Thus the structure is believed to be due to the F center as originally proposed.

10,438 PROPERTIES OF LITHIUM HYDRIDE-III. PARAMAGNETIC RESONANCE OF COLOR CENTERS by W. B. Lewis and F. E. Pretzel (U. California); J. Phys. Chem. Solids, Vol. 19, pp. 139-146, Apr. 1961

Production of F-center concentrations in excess of $10^{17}/cm^3$ in single crystals of LiH by neutron irradiation at 78°K is reported. The electron spin resonance absorption of the F-centers has been observed at $g = 2.004 \pm 0.001$. The saturation parameter of the ESR absorption $(T_1 T_2)^{\frac{1}{2}}$ is close to that for F-centers in KCl. From rms line width measurements on LiH crystals of various isotopic compositions (Li^7H, Li^7D, Li^6H and Li^6D), spin densities of the F-center electron at the Li^+ and H^- sites have been estimated.

10,439 ELECTRON SPIN RESONANCE OF IRRADIATED FERROELECTRIC TRI-GLYCINE SULFATE by R. Blinc, S. Detoni, L. Levstek, M. Pintar, S. Poberaj, and M. Schara (Ljubljana U., Yugoslavia); J. Phys. Chem. Solids, Vol. 20, pp. 187-189, Aug. 1961

Electron spin resonance spectra of γ-irradiated ferroelectric tri-glycine sulfate single crystals are analyzed. Stable free radicals of NH_3CH-, formed in irradiated TGS, are fixed in the crystal lattice; the NH_3 group is found to rotate in the ferroelectric phase. Approximate values of the $H_{(c)}$, the three $H_{(n)}$ and the N Fermi coupling constants are found to be 21.0, 14.5, and 3.2 respectively.

10,440 ELECTRON SPIN RESONANCE IN IRRADIATED KH_2PO_4 AND KD_2PO_4 by F. Jeffers (New Mexico A. and M.) P. E. Wigen, and J. A. Cowen (Lockheed Res. Labs.); Bull. Am. Phys. Soc., Ser. II, Vol. 6, p. 118 (A), Mar. 20, 1961

Observations of electron spin resonance in electron irradiated KH_2PO_4 and KD_2PO_4 in the ferroelectric state were reported. The spectrum in the deuterated crystal consists of two essentially

isotropic lines split by 50 gauss with an average g = 2.02. This splitting is attributed to an isotropic hyperfine interaction with the phosphorus nucleus. The spectrum in the normal crystal consists of eight anisotropic lines which can be associated in four pairs, each pair showing a 50 gauss splitting. For rotation about the ferroelectric axis the lines show fourfold symmetry and an average g = 2.03. The anisotropic splitting is attributed to a hyperfine interaction with protons which is not resolved in the deuterated crystal due to the smaller moment of the deuteron. The data do not fit a simple analysis involving interaction with a single proton but rather appear to be due to an I = 3/2 hyperfine term.

10,441 ELECTRON SPIN RESONANCE SPECTRUM OF STRETCHED POLYETHYLENE by D. Libby and M. G. Ormerod (Roy. Mil. Coll., Canada); J. Phys. Chem. Solids, Vol. 18, pp. 316-319, Mar. 1961

Observations of the electron spin resonance spectrum of stretched polyethylene, irradiated at 77°K, for various orientations of the applied magnetic field with respect to the axis of stretch are reported. The different spectra obtained have been explained in terms of the anisotropy of the α-hydrogen atom which has been resolved due to the orientation of the molecule chains on stretching. Values obtained for the α-hydrogen hyperfine component separation are in good agreement with those found by other workers for irradiated single crystals.

10,442 DOUBLE QUANTUM TRANSITION IN ELECTRON SPIN RESONANCE OF DIPHENYL-PICRYL HYDRAZYL AT LOW MAGNETIC FIELDS by T. Hashi (Kyoto U.); J. Phys. Soc. Japan, Vol. 16, pp. 1243-1248, June 1961

The results of applying two radiation fields (ν_1 of about 150 Mc and ν_2 of 30, 20, and 15 Mc) to dipheny-picryl hydrazyl at static fields of about 50 gauss are reported. The line shape, the peak position, and the intensity of the signal are well interpreted on the basis of the Bloch phenomenological equation choosing $T = 4.8 \times 10^{-8}$ sec, except for slight discrepancies near $H_0 = \omega_1 / |\gamma|$. Some experimental results at $\nu_2 = 4.5$ Mc are also given.

10,443 IMPURITY STUDIES IN COMPOUND SEMICONDUCTORS BY ELECTRON SPIN RESONANCE by H. H. Woodbury and G. W. Ludwig (GE Res. Lab.); Bull. Am. Phys. Soc., Ser. II, Vol. 6, p. 118(A), Mar. 20, 1961

The use of electron spin resonance techniques to obtain information about dilute impurities in single crystals of the II-VI and III-V type semiconductors was discussed. These systems are of interest for crystal field studies in that they present sites of fourfold (tetrahedral) symmetry. A table listing recent results obtained with such semiconductors at a temperature of 10°K was shown. For V and Co in CdS the hyperfine interaction A was given parallel and perpendicular to the c axis.

Paramagnetic Resonance of Cr^{3+} ion in Ruby - See 10,452

Paramagnetic Resonance of Cr^{3+} in Ruby - See 10,453

10,444 AN ELECTRON SPIN RESONANCE STUDY OF MANGANESE IMPURITY IN BRUCITE by W. A. Pieczonka, H. E. Petch, and A. B. McLay; Can. J. Phys., Vol. 39, pp. 145-157, Jan. 1961

The results of investigating a single crystal of brucite, $Mg(OH)_2$, containing manganese impurity to the extent of 100 ppm, by means of the electron spin resonance (ESR) technique are reported. The study was made at room and liquid air temperatures. The observed absorption spectrum has been successfully interpreted in terms of parameters found in the appropriate spin Hamiltonian. The measured values of these parameters at room temperature were found to be:

$g_{\parallel} = 2.0001 \pm 0.0005$ $\quad g_{\perp} = 2.0005 \pm 0.0005$
$D = -7.20 \pm 0.25 \times 10^{-4} cm^{-1}$ $\quad a = +10.82 \pm 0.45 \times 10^{-4} cm^{-1}$
$A = -85.7 \pm 0.4 \times 10^{-4} cm^{-1}$ $\quad B = -84.9 \pm 0.6 \times 10^{-4} cm^{-1}$.

10,445 PASSAGE EFFECT IN THE ELECTRON SPIN RESONANCE OF Fe-DOPED SILICON by T. Igo (Elect. Commun. Lab., Tokyo); J. Phys. Soc. Japan, Vol. 16, p. 1472(L), July 1961

The passage effect in electron spin resonance of p-type, Fe-doped silicon, obtained by studies on the dispersion signal in a manner similar to Weber's [see abst. 6711] is discussed. The in-phase dispersion signal is displayed as a function of magnetic field for several values of H_m. With H_m small, the adiabatic passage line has a typical line shape; increasing H_m broadens the peak and at large H_m a saddle appears. The relaxation time, T_1, estimated from these conditions and from preliminary saturation measurements is of the order of 10^{-4} sec.

Paramagnetic Resonance of Sm^{2+} in CaF_2 - See 10,454

OPTICAL PROPERTIES

Differential Absorption Spectrometer for Impurity Measurement - See 10,329

10,446 EFFECT OF PRESSURE ON THE SPECTRA OF RARE EARTH IONS IN CRYSTALS by K. B. Keating and H. G. Drickamer (U. Illinois); J. Chem. Phys., Vol. 34, pp. 142-151, Jan. 1961

Measurements of the effect of pressure to 180 000 atm on the absorption spectra of crystalline rare earth ions are reported. The effects observed include: (1) an increase of intensity due to increased mixing of 5d and 4f orbitals in the excited state due to an increase of the mixing potential with decreased interionic distance; (2) small shifts accompanied by increases in half-width. Except for the shifts of $^3P_0$, $^3P_1$, and $^3P_2$ levels of Pr^{+3}, these can be accounted for by an increase in the splitting of the individual levels due to intensification of the crystal field; (3) changes in shape of several of the bands, possibly due to changes in occupation of the various states which make up the bands.

10,447 A THEORY OF THE MAGNETO-OPTICAL ABSORPTION by M. Okazaki (U. Tokyo); Prog. Theoret. Phys., Vol. 25, pp. 163-177, Feb. 1961

A theory of magneto-optical absorption is developed by means of the Luttinger-Kohn theory of the effect of magnetic field on the energy bands in the case of a simple band model. In

particular, the absorption line shape is studied. The calculated value of the absorption line width agrees with the experimental value. The line width does not exhibit appreciable dependence on the magnetic field and temperature. The absorption coefficient in the absence of a magnetic field is also discussed.

Coloration of Alkali Halides - See 10,372

10,448 VACUUM-ULTRAVIOLET ABSORPTION STUDIES OF IRRADIATED SILICA AND QUARTZ by C. M. Nelson and R. A. Weeks (Oak Ridge Natl. Lab.); J. Appl. Phys., Vol. 32, pp. 883-886, May 1961

Observations of the optical absorption properties of Co^{60}-irradiated fused silica and crystalline quartz in the vacuum-ultraviolet region are reported. The most prominent absorption band found in both materials has a maximum at 7.6ev (1620A). Optical and thermal bleaching experiments indicate that this band is not necessarily complementary to a band at 5.9ev (2100A), as has been assumed. Though the 7.6-ev band has approximately the same intensity in both materials for the same irradiation, the 5.9-ev band is >20 times more intense in fused silica. The 7.6-ev band is still present after the 5.9-ev band has been thermally bleached. Additional absorption bands occur at 8.0 and 8.2ev. Also, optical and thermal bleaching experiments suggest other absorption bands at 7.2, 7.4, 7.8, and 7.9 ev. Since these bands (particularly the 7.6-, 8.0-, and 8.2-ev bands) occur in high-purity silica and quartz, it is suggested that they are associated with defects in the quartz structure and are not caused by impurities.

Luminescence of Tl-Activated Alkali Halides - See 10,372

10,449 INJECTION ELECTROLUMINESCENCE by A. G. Fischer (RCA Labs.); Solid State Electronics, Vol. 2, pp. 232-246, May 1961

Previous literature on injection electroluminescence is reviewed briefly. It is shown that the theoretical limit for brightness and efficiency of injection EL can be expected to be higher than that of impact ionization EL. A survey of promising host crystal materials is given, and the unusual difficulties encountered in making junctions in wide-band-gap materials are pointed out. It is concluded that p-i-n junctions offer a more favorable approach to efficient injection EL than p-n junctions. The properties of varied band gaps at the contacts are described and the source of loss is discussed.

Thermoluminescence of Irradiated NaCl Crystals - See 10,367

10,450 THE MÖSSBAUER EFFECT by H. Lustig (U. Illinois); Am. J. Phys., Vol. 29, pp. 1-18, Jan. 1961

The recent discovery and several important applications of recoilless gamma-ray fluorescence are reviewed and an introduction to this field of research is given. The importance of the fluorescence technique and its limitations, before Mössbauer's discovery, are discussed. Mössbauer's pioneering experiments are briefly described and Lipkin's simple theoretical explanation of recoilless gamma-ray emission is presented. From among the large number of recent experiments which make use of the Mössbauer effect, two groups are selected for discussion. The first is concerned with the discovery of nuclear and magnetic properties of iron-57; the other with a test of the principle of equivalence in general relativity, by a measurement of the gravitational shift in the frequency of radiation.

Mössbauer Effect in Fe-Co and Fe-Ni Alloys - See 10,423

10,451 EMISSION SPECTRA OF TRIVALENT THULIUM by L. G. Van Uitert and R. R. Soden (Bell Labs.); J. Chem. Phys., Vol. 34, pp. 276-279, Jan. 1961

Trivalent thulium can be caused to fluoresce selectively from different levels by choice of the wavelength of exciting radiation. This has made it possible to correct the assignments of emission transitions occurring in the visible range. As a consequence, the detailed data of Gobrecht have been found to be in much closer agreement to the theoretical predictions than formerly realized.

10,452 RELAXATION TIMES BETWEEN EXCITED STATES OF RUBY by I. Wieder and L. R. Sarles (Varian Assoc.); 1961 Spring Mtg. Opt. Soc. Am.

The use of population inversion between the excited states $\bar{E}(^2E)$ and $2\bar{A}(^2E)$ of Cr^{+++} ions in Al_2O_3 to obtain coherent emission of 1/3-mm radiation was discussed. Such a scheme depends critically on the rate of nonradiative transfer of atoms from upper to lower excited states. To investigate this parameter the relative intensities of R_1 and R_2 fluorescence have been monitored following a pulse of exciting radiation. In order to provide different initial population conditions three excitation methods were used: (1) short pulses of white light in the temperature range 300°K to 1.5°K, (2) coherent pulses of R_1 light at 77°K, and (3) pulses of a mixture of R_1 and R_2 light at 1.5°K. In all cases the observed intensity ratio of fluorescent R_1 and R_2 light did not deviate from the Boltzmann distribution. These observations place an upper limit on the thermal relaxation time between the two levels.

10,453 FLUORESCENCE OF THE Cr^{+++} PAIR SPECTRUM IN SYNTHETIC RUBY by R. T. Daly (TRG); 1961 Spring Mtg. Opt. Soc. Am.,

Measurements of the excitation spectrum of the strong ruby satellite lines at 7008A and 7040A made at 77°K and 2°K are reported. The low-lying and excited levels of these lines appear to arise from two non-equivalent cation pairs in the corundum lattice. Results of experiments to produce stimulated emission in a three-level optical maser using these levels were also given.

10,454 FLUORESCENCE AND OPTICAL MASER EFFECTS IN RARE-EARTH-DOPED CALCIUM FLUORIDE by C. G. B. Garrett and W. Kaiser (Bell Labs.); 1961 Spring Mtg. Opt. Soc. Am.

Measurements of emission spectra, absorption spectra, absolute activation spectra (quantum efficiency vs exciting wavelength), and fluorescent decay lifetime that have been made on samples of rare-earth-doped calcium fluorides with a view to finding suitable materials for optically pumped solid-state optical masers were reported. Information of this sort, taken in conjunction with measurements of the absolute spectral brightness of the pumping lamp, enables one to decide when optical maser action is possible — for example, $CaF_2:Sm^{++}$ is found from these experiments to be a favorable case because of the strong

absorption and high quantum efficiency. Results of fluorescence and optical maser experiments on $CaF_2:Sm^{++}$ were discussed.

Fluorescence of U^{3+} and Sm^{2+} Ions in CaF_2 - See 10,508

10,455 POLARIZED LUMINESCENCE OF CALCIUM FLUOROPHOSPHATE by P. D. Johnson (Gent. Electric Res. Lab.); Bull. Am. Phys. Soc., Ser. II, Vol. 6, p. 30(A), Feb. 1, 1961

The luminescence of synthetic single crystals of apatite, $3[Ca_3(PO_4)_2]\cdot CaF_2$, activated with Sb^{+3} and Mn^{+2}, is spontaneously polarized when excited with unpolarized 2537A or 1850A radiation. The luminescence due to manganese is completely polarized with its electric vector parallel to the crystal c axis. Antimony luminescence is partially polarized perpendicular to the c axis. These results lead to the conclusion that luminescent manganese substitutes for calcium in the "Ca_I" position. This site is on a trigonal symmetry axis which is parallel to the c axis of the apatite structure. Most, if not all, of the luminescent antimony substitutes for calcium which is in the reflection plane perpendicular to the c axis. This "Ca_{II}" site is one of low symmetry adjacent to a fluoride and five oxygen atoms. The effect on the emission spectra of substituting chloride for fluoride and the electron spin resonance of Mn^{+2} in apatite can be correlated with these results. Qualitative conclusions as to the nature of the states involved in antimony luminescence can be deduced from the polarization measurements and other optical data.

10,456 SOME OPTICAL AND ELECTRICAL PROPERTIES OF SEMICONDUCTING DIAMONDS by A. Halperin and J. Nahum (The Hebrew U.); J. Phys. Chem. Solids, Vol. 18, pp. 297-306, Mar. 1961

Measurements of the optical and electrical properties of two semiconducting (Type IIb) diamonds are reported. The energies of the extra absorption bands in the infrared typical of Type IIb specimens were found to fit very well the thermal activation energies obtained both from the dark conductivity and the thermoluminescence. The experiments indicate discrete levels of 0.21, 0.30, 0.37, 0.52 and about 0.7ev above the valence band. Nearly the same spectral distribution was found for the ultraviolet excited luminescence, the electroluminescence, and the thermoluminescence, all having their main maximum at about 0.48 μ. Excitation spectra for the thermoluminescence and the photoconductivity have also been measured. Some other experiments describe the conductivity and voltaic glow curves of the same specimens.

10,457 ONE-SPECIES ANALYSES OF DRIFT AND DIFFUSION CONTRIBUTIONS TO PHOTOCURRENTS AND THEIR INTERRELATION by G. K. Lindeberg (Minn. Mining and Mfg.); Bull. Am. Phys. Soc., Ser. II, Vol. 6, p. 30(A), Feb. 1, 1961

A method for studying photoconductivity in systems in which very little is known at the outset about the natures of the current carrying species and the mechanisms governing their transport and recombination was proposed. Independent species contributions were introduced abstractly as being quantities which obey continuity equations and which determine variations of conductivity and emf. It is reasonable to use a minimal number of these species. Therefore a one-species analysis was developed. This suggests a sequence of two specific experiments, criteria for consistency of the one-species analysis within the experimental context, and possible directions of microscopic interpretation. The conductivity, emf, and recombination can be determined as functions of the species if analysis is consistent. The diffusion coefficient is obtainable, but the effective mobility is not completely specified in the experimental context. If the species are electronic carriers, and if the emf is identifiable with their Fermi level, the distribution of electronic states is available as the solution of an integral equation.

Photoconductivity of Thin Films of S, Se or Te Treated PbO - See 10,396

10,458 STRUCTURES OF PHOTOCONDUCTIVITY SPECTRA NEAR THE FUNDAMENTAL ABSORPTION EDGE OF CADMIUM SULFIDE by H. Mitsuhashi (Japan Broadcasting); J. Phys. Soc. Japan, Vol. 16, pp. 989-995, May 1961

An investigation of the photoconductivity structures of CdS single crystals near the adsorption edge using polarized light at about 81°K is described. Field dependence of wavelengths of peaks and spectral dependence of decay time of the response were measured as well. From these experimental results, the structures are classified into two groups; one, which occurs in the shorter wavelength range ($\lambda < 4870$ A), is attributed to the photoconductivity due to excitons, and the other, which appears on the longer wavelength side, to that due to imperfections in the crystal.

Impurity Photoconductive Effect in CdS Crystals at Low Temperatures - See 10,406

10,459 PHOTOVOLTAGES IN SILICON AND GERMANIUM LAYERS by H. Kallmann, B. Kramer and E. Haidemenakis (New York U.) and W. J. McAleer, H. Barkemeyer and P. I. Pollak (Merck); J. Electrochem. Soc., Vol. 108, p. 247, Mar. 1961

Observations of photovoltages up to a few hundred volts at room temperature and up to a few thousand volts at liquid nitrogen temperatures under strong illumination in silicon and germanium layers with a distance of about 1 cm between electrodes are reported. Only samples with a thickness gradient of evaporated material exhibited these photovoltages. In both the Ge and the Si layers the photovoltage showed an almost linear relationship with illuminating intensity. Both the magnitude and sign of the voltage depended on which side of the film was irradiated, the wavelength of incident light, and the temperature. The dark resistance of these layers varied between 10^{11} and 10^{14} ohms. A theoretical interpretation of the origin of these voltages is given.

10,460 OPTICAL CONSTANTS OF GERMANIUM IN THE REGION 0-27 EV by O. P. Rustgi, J. S. Nodvik, and G. L. Weissler (U. South. California); Phys. Rev., Vol. 122, pp. 1131-1134, May 15, 1961

Measurements of the reflectivity R for a Ge crystal over the energy range 7.6 - 18.0ev and the transmissivity T for an evaporated Ge film over the range 16.6 - 27.4ev are reported. The reflectivity data near normal incidence, combined with existing data at lower energies, have been used in the Kramers-Krönig dispersion relation to evaluate the index of refraction

n and extinction coefficient k of Ge over the range 0-18 ev. Electron characteristic losses are predicted at 10 and 15ev, consistent with those observed at 11 and 16ev. The plasma frequency of bulk Ge as determined by the optical data is $\hbar\omega$ = 10 ev.

10,461 MEASUREMENT OF THE PARAMETERS FOR THE LONGITUDINAL KERR MAGNETO-OPTIC EFFECT IN FERROMAGNETIC FILMS by C. C. Robinson (MIT); 1961 Spring Mtg. Opt. Soc. Am.

The longitudinal Kerr magneto-optic effect can be characterized by four parameters n, k, Q_0, and q. The first two parameters, n and k, are the ordinary optical refractive index and index of absorption, and the last two parameters, Q_0 and q, are the magneto-optic amplitude and phase that were originally introduced by Voigt. Measurements of these parameters for opaque, high-vacuum deposited films of iron, nickel, and Permalloy for wavelengths between 0.360 and 0.620μ were reported. To find n, k, Q_0, and q, the rotation and the ellipticity of the light reflected from the surface of these films were measured with a photoelectric ellipsometer. This ellipsometer employed a Faraday cell which sinusoidally rotated the polarization of the reflected light. The rotational modulation made it possible to cross the analyzer with the original azimuth of the major axis of the elliptic polarization to within 5-15 sec of arc. To find the ellipticity, a calibrated retardation plate was placed in front of the Faraday cell. From these data and from the reflection coefficient expressions derived by Voigt the four parameters were computed. As a check, the Kerr rotation and ellipticity for angles of incidence between 16° and 65° were then calculated from Voigt's theory. These results compared satisfactorily with the experimental measurements made at these same angles of incidence.

Optical Properties of $CdSnAs_2$ - See 10,420

THERMAL PROPERTIES

10,462 EFFECT OF MAGNETIC CLUSTERS ON THE SPECIFIC HEAT OF Ni-Cu AND Fe-V ALLOYS by K. Schröder (U. Illinois); J. Appl. Phys., Vol. 32, pp. 880-882, May 1961

Recent experiments with Ni-Cu and Fe-V alloys indicate that the specific heat at low temperature cannot be described by electronic and lattice terms alone. An additional term in the specific heat of these alloys is explained on the basis of ferromagnetic clusters.

10,463 NORMAL PROCESSES IN THERMAL CONDUCTIVITY by J. Callaway (U. California); Bull. Am. Phys. Soc., Ser. II, Vol. 6, pp. 76-77(A), Feb. 1, 1961

Since normal three phonon scattering processes conserve the total wave vector of the phonon system, addition of reciprocal relaxation times for all phonon scattering mechanisms is not valid when normal processes are dominant. A formula previously proposed for the computation of lattice thermal conductivities was analyzed in the limit of strong normal processes. In this limit the thermal resistivity is the sum of contributions from defect scattering, boundary scattering, and residual Umklapp scattering. If the relaxation time for defect scattering is $\tau_D^{-1} = A\omega^4$, then the resistivity due to point defects is, in this limit, $W_D = 120\pi^2 VAT/h$, where V is the velocity of sound, in agreement with the theory of Ziman. If defect scattering is not weak, addition of thermal resistivities is not valid, and the Ziman formula is an overestimate. The thermal conductivity was exhibited as a function of the ratio of the relaxation times of point defect to normal three phonon scatterings.

10,464 PHOTOTHERMAL (PT) EFFECT IN SEMICONDUCTORS by W. W. Gärtner (CBS Labs.) and H. Mette and C. Loscoe (USASRDL); Bull. Am. Phys. Soc., Ser. II, Vol. 6, p. 28(A), Feb. 1, 1961

When a sample of semiconducting material is illuminated with photons of sufficient energy, electron-hole pairs are generated which diffuse through the crystal from the place of their generation to regions of lower excess-pair concentration. Each pair transports an amount of energy approximately equal to the band separation, thus contributing to the thermal conductivity. This energy is deposited where the pair undergoes nonradiative recombination, increasing the local (measurable) temperature of the crystal. A nonuniform temperature distribution is therefore established in the sample which depends on the nature of the incident radiation, on the characteristics of optical absorption, on the bulk and surface recombination mechanisms, on the boundary conditions for temperature and energy flux and on the ordinary thermal conductivity of the material. This establishment of a temperature distribution in a solid by optically excited diffusing and recombining carriers and the attendant modification in the thermal conductivity is called the Photothermal (PT) Effect. It is the thermal analog to the Dember effect. Its deflection by a magnetic field is called the Photomagnetothermal (PMT) Effect. A simple theory of the PT effect which appears applicable to germanium and silicon was presented and experimental problems were discussed.

10,465 SURFACE DEPENDENCE OF THE THERMOELECTRIC POWER IN GERMANIUM AT ROOM TEMPERATURE: EXPERIMENTAL by J. N. Zemel (U.S. Naval Ord. Lab.); Bull. Am. Phys. Soc., Ser. II, Vol. 6, p. 27(A), Feb. 1, 1961

A series of experiments undertaken to determine the dependence of thermoelectric power on the excess charge in the surface space charge region in the room temperature range was described. The experiments were carried out on a thin sample of very pure intrinsic germanium, and gas ambients were used to vary the surface space charge. Extreme care was taken to reduce or eliminate spurious thermal gradients in the apparatus. The reproducibility of the data indicated that the apparatus was adequate. Measurements were carried out in the temperature range from 15°C to 35°C. A 1.5°C temperature difference was used to produce the thermal emf. Comparison of the experimental results with the theoretical predictions of Greene gave remarkably good agreement. However, the role of the surface scattering mechanism in the experimentally achievable range of surface potential increments was not great enough to provide a clear proof of the scattering's existence, let alone its magnitude. At lower temperatures, the surface thermoelectric power may have some interesting applications to the study of phonon scattering at surfaces.

10,466 SURFACE DEPENDENCE OF THE THERMOELECTRIC POWER IN GERMANIUM AT ROOM TEMPERATURE: THEORETICAL by R. F. Greene (U.S. Naval Ord. Lab.); Bull. Am. Phys. Soc., Ser. II, Vol. 6, p. 27(A), Feb. 1, 1961

A Boltzmann equation treatment of the thermoelectric effects associated with excess carriers in the surface space charge region (SSCR) of a semiconductor was given. In the SSCR, potential variations $>>kT$ within a mean free path are common so that conductance, thermoelectric power, etc., are nonlocal transport quantities. When these are properly defined, however, the Boltzmann equation treatment of them satisfies the Kelvin-Onsager relation. Constant relaxation times and spherical energy surfaces are assumed to reduce the labor of evaluating the transport integrals. These integrals remain complex because no approximations have been made in the solution of the Poisson equation for the shape of the SSCR. The resulting integrals, which are similar to those arising in the theory of surface mobilities, have been evaluated by electronic computer for various surface scattering conditions and for a range of bulk conditions corresponding to near-intrinsic germanium near room temperatures. Under these conditions the resulting thermoelectric power vs surface conductance curves are rather insensitive to the degree of specularity of the surface.

Seebeck Coefficients of Amorphous Inorganic Materials - See 10,400

Thermal Properties of $CdSnAs_2$ - See 10,420

MECHANICAL PROPERTIES

10,467 EFFECT OF INTERSTITIAL Li ON THE DENSITY OF Si by J. S. Prener, E. M. Pell, and F. E. Williams (GE Res. Lab.); Bull. Am. Phys. Soc., Ser. II, Vol. 6, p. 76(A), Feb. 1, 1961

Densities of Merck vacuum grown floating zone Si and of Si containing 10^{19} Li/cm^3 in solution determined using a density gradient column, were reported. The density was also measured during the room-temperature aggregation of Li which was monitored by resistivity measurements. At 27.4°C, the measured density of pure Si was 2.32906 g/cm^3, in rather close agreement with Smakula. When Li dissolves in Si, there is a volume increase of 4.7×10^{-24} cm^3/Li. This is interpreted as due to electrostatic repulsion between Li^+ and the partly shielded Si^{+4} cores. A simple model involving Si^{+4} cores and spherically symmetric bonding electrons centered between the cores yields a potential at the Li^+ consistent with an effective charge on the Si of approximately +0.1 calculated from the expansion. During the initial conversion of Li^+ to aggregated Li^0, the volume increases by 6.0×10^{-24} cm^3/Li. This is interpreted as due to overlap repulsion between interstitial Li^0 and Si. The coincidence of deionization and aggregation appears plausible from the properties of Li_2 and Li metal. A subsequent nonlinear expansion may involve formation of a separate phase.

10,468 DETERMINATION OF ELASTIC CONSTANTS OF CRYSTALS USING DIFFUSELY REFLECTED X-RAYS by W. A. Wooster; Czech. J. Phys., Vol. 11B, p. 291(A), 1961

The theory of the scattering of X-rays from a crystal by thermally generated travelling elastic waves is developed in two parts. The first part concerns the direction of travel of the X-ray beam due to a given wave which perturbs the regular lattice. The second part concerns the relation between the amplitude of the vibration and the intensity of the corresponding diffuse beam. An optical analogy, involving a simple diffraction arrangement, is used to illustrate the first part of the theory. The second part of the theory is developed from the usual diffraction theory of a sinusoidally perturbed lattice. The thermodynamic requirement that each mode of vibration shall carry the same energy per unit cell of the crystal is used to relate the amplitude of vibration to the frequency. Lastly, the classical theory of the transmission of elastic waves through crystals is used to connect the intensity of diffuse scattering with the elastic constants. Details of the experimental methods, both photographic and ionization, are given. An example of the application of this method to vanadium metal is discussed. In summarizing the advantages of the method it is pointed out that it can be applied to smaller crystals than any other method. It can be used with soft or fragile crystals and at any temperature, since only the temperature of the crystal is relevant. The disadvantage of the method is its poor accuracy, which is not better than 5 per cent and is usually less.

Residual Thermoelastic Stresses in Bonded Si Wafers - See 10,484

10,469 CREEP BEHAVIOR OF PORE-FREE POLYCRYSTALLINE ALUMINUM OXIDE by R. C. Folweiler (GE Res. Lab.); J. Appl. Phys., Vol. 32, pp. 773-778, May 1961

A study of creep in pore-free polycrystalline aluminum oxide as a function of temperature, grain size, and strain rate is reported. The behavior may be described by $\sigma \propto d^2 \epsilon$, where d is the mean grain diameter. Deformation is not controlled by basal slip but by a diffusional creep process as described by Nabarro and Herring, [F. R. N. Nabarro, Conference on Strength of Solids, (The Physical Society, London, 1948), p. 75; C. Herring, J. Appl. Phys., Vol. 21, p. 437(1950)].

10,470 SMOOTH SPALLS AND THE POLYMORPHISM OF IRON by J. O. Erkman (Stanford Res. Inst.); J. Appl. Phys., Vol. 32, pp. 939-944, May 1961

Observation of smooth spalls in Armco iron loaded with a transient wave in which the pressure exceeds 0.131 megabar is reported. The two distinct compression shocks which are transmitted by the iron are followed by a steep rarefaction which may be called a rarefaction shock. At a free surface, the first compression shock is reflected as a backward-facing rarefaction wave. This wave may also steepen into a rarefaction shock which eventually meets the forward-facing rarefaction shock. The interaction of these waves results in a localized tension of destructive magnitude, which produces a smooth fracture. Location of the plane of this interaction has been calculated by applying hydrodynamic theory. These calculations are inexact because the speed of sound for relief waves was taken from Hugoniot data since no other data are available. Fair agreement was obtained between experimental and calculated results. The work indicates that, in the case of a double spall, the fracture furthest away from the original free surface may sometimes be formed first.

Ultrasonic Absorption in Intrinsic Semiconductors - See 10,378

10,471 INTERNAL FRICTION IN LIGHTLY DEFORMED PURE IRON WIRES by J. D. Fast and M. B. Verrijp (Philips); Philips Res. Rep., Vol. 16, pp. 51-65, Feb. 1961

Measurements of the internal friction of pure (99.99 per cent) iron wires before and after they have been subjected to a very small plastic deformation are reported. The damping after deformation is found to be strongly dependent on amplitude, temperature of deformation and temperature of measurement. Wires subjected to deformation at temperatures below $-30^{\circ}C$ show a spontaneous increase of internal friction; wires deformed at temperatures above $-30^{\circ}C$ a spontaneous decrease as time passes. In the latter case, plotting log Q^{-1} against t^p results in straight lines provided that p is allotted values ranging from 0.2 to 1.0 and differing for each experiment. By increasing the vacancy concentration and the carbon content it is shown that the process responsible for the spontaneous falloff in damping is the diffusion of point defects toward dislocations. The phenomenon whereby damping increases with time is tentatively attributed to a dispersion of pile-ups of dislocations.

SOLID STATE DEVICES

DIODES

10,472 A NEW METHOD OF CONSTRUCTION FOR TRANSMISSION EQUIPMENT III. ELECTRICAL COMPONENTS by P. O. Harris and N. Hellkvist (Ericsson); Ericsson Rev., Vol. 38, pp. 2-15, 1961

A survey on the electrical characteristics and construction of components employed in transmission equipment is presented Passive and active components, such as transistors, diodes, magnetic devices, resistors, capacitors, inductors, transformers, relays and the like are all briefly discussed. Aging characteristics on these components are also shown. The construction of the components and their most important characteristics are described, especially those which have been a deciding factor in the choice of component type.

10,473 THE APPLICATION AND PROTECTION OF SILICON RECTIFIERS by P. B. Free (Standard Tel. & Cables Pty. Ltd.); Proc. IRE Austral., Vol. 22, p. 191 (A), Mar. 1961

A brief review of the history and development of semiconducting rectifiers was presented. The range of devices currently available was outlined and the method of rating these devices as regards peak inverse voltage and forward current given. The problems of protecting the units against transient voltage surges and heavy current surges was described and some solutions indicated The use of assemblies of the units in series or parallel and a description of some typical applications in both the electronic and power fields were cited.

10,474 EFFECTS OF ELECTRONS AND HOLES ON THE TRANSITION LAYER CHARACTERISTICS OF LINEARLY GRADED P-N JUNCTIONS by C. T. Sah (Fairchild); Proc. IRE, Vol. 49, pp. 603-618, Mar. 1961

The dc theory of p-n junctions, extended for the consideration of the mobile carriers or electrons and holes in the transition region, is discussed. The linearized Poisson-Boltzmann equation is solved by using a linearization parameter a, which is a measure of the relative importance of the fixed, ionized impurity space charge compared with the mobile carrier or electron and hole charges in the transition region of the p-n junction. It is found that both the transition layer width and the transition carrier capacitance associated with the electrons and holes in the transition region increase exponentially with applied voltage under forward bias condition. A calculation of the recombination-generation current at a forward bias beyond the built-in or diffusion voltage is now possible with the present theory The dc theory of junction capacitance compares favorably with experimental measurements of a wide variety of nearly linear-graded diffused silicon junctions.

10,475 PARAMETRIC DIODES FOR HIGH FREQUENCY APPLICATIONS by R. E. Aitchison (U. Sydney); Proc. IRE Austral., Vol. 22, p. 180 (A), Mar. 1961

The effect of impurity distribution on the capacitance voltage relationship of parametric diodes is analyzed and modifications introduced by intervening layers of other material were discussed. The factors governing diode cut-off frequency and the way in which the realization of good high frequency performance is affected by packaging were considered. Methods of fabricating diodes for high frequency use were considered with particular reference to experimental results for gallium arsenide and silicon diodes, and the problem of obtaining both low spreading resistance and small junction were discussed. The possibility of using high speed silicon computer diodes as parametric diodes was considered and the effect of the gold recombination centres on the operation as parametric diodes analyzed.

Electron Heating Phenomena in Avalanche Injection Diodes - See 10,389

Oscillations in the Longitudinal Tunnel Current of Tunnel Diodes - See 10,418

Stability of Tunnel Current in the Presence of a Magnetic Field - See 10,419

10,476 FIELD-EFFECT PINCH-OFF OF SURFACE LEAKAGE IN HIGH-VOLTAGE DIODES by T. Kan (Shindengen Res. Div., Japan); Solid State Electronics, Vol. 2, pp. 68-69 (L), Jan. 1961

The use of the insulating properties of the depletion layer of a reverse-biased junction to reduce the leakage current and increase the breakdown voltage of an alloyed germanium diode is discussed. The n-side of the junction consists of two concentric cylinders, the smaller of which has the same diameter as the base metal contact. As the voltage across the junction is increased, the depletion layer extends completely across the n-type material exterior to the smaller cylinder and effectively insulates the junction from the adverse effects of the leakage current. Measurements made with various thicknesses of exterior material are discussed.

10,477 BREAKDOWN IN P-N JUNCTIONS by E. M. Cherry (U. Melbourne); Proc. IRE Austral., Vol. 22, p. 190(A), Mar. 1961

A survey of the histories of the theories for junction breakdown at a high reverse bias was presented. Breakdown in the body of the crystal and the classical Zener theory and its failure were treated. The development of the McKay-Miller theory of avalanche breakdown was covered, and the empirical $\{1-(V/V_B)^n\}^{-1}$ breakdown law derived from first principles. Breakdown on the surface of the crystal was described and evidence for the existence of surface inversion layers presented. Complications arising from the junction effects in such layers were considered.

TRANSISTORS

10,478 A CONTROLLED-TEMPERATURE DEVICE FOR TRANSISTOR TESTS by E. F. King and F. L. Walker (UCLA); IRE Trans., Vol. E-4, pp. 21-22, Mar. 1961

A laboratory device for operating transistors at selected, known temperatures in the 15 - 95°C range is described. After a simple, one-time calibration no further temperature measurements are necessary The unit is simple, rugged and easily constructed.

10,479 SOME EXTENSIONS OF THE CHARGE CONTROL CONCEPT TO H.F. TRANSISTOR DESIGN AND APPLICATIONS by D. E. Hooper (U. Melbourne), and A. R. T. Turnbull (Aeronautical Res. Labs.); Proc. IRE Austral., Vol. 22, p. 188(A), Mar. 1961

The application of the charge control concept to the design of high frequency transistors was discussed. An analysis of device behavior, utilizing the stored charge concept, was cited and HF transistor performance, derived without recourse to advanced mathematical techniques, was cited. The particular physical parameters concerning transmission and switching applications were derived using this approach. The device designer can therefore optimize input parameters for specified applications and the circuit engineer is able to assess the potential and range of a particular device. Fundamental parameters which should be specified by the manufacturers were discussed in detail.

Characteristics of Junction Transistors - See 10,561

Survey of P-N Junction Breakdown Theory - See 10,477

Field Effect Pinch Off of Leakage Current in High Voltage Junctions - See 10,476

10,480 THE FREQUENCY DEPENDENCE OF THE Y_e PARAMETERS OF THE π401 TYPE TRANSISTOR [in Czech.] by M. Pajgrt; Slaboproudý Obzor, Vol. 22, pp. 145-148, Mar. 1961

Measurement of the Y_e parameters of the π401 type transistor in the frequency range 1 kc to 5 Mc is discussed. A matrix method for transforming these Y_e parameters to other matrix forms is pointed out.

10,481 TRANSISTOR UPPER NOISE CORNER FREQUENCY by H. F. Cooke (Texas Instr.); Proc. IRE, Vol. 49, p. 648(L), Mar. 1961

An expression for transistor upper noise corner frequency, f_A, is discussed. The expression is derived by equating the frequency dependent term in Nielsen's formula for noise figure to the sum of the four non-frequency dependent terms and solving for f_A. The expression is more exact than the form derived by considering only the collector noise term in Nielsen's formula. Very good agreement is found between measured upper noise corner frequencies and those calculated by means of the new expression when the cutoff frequency, f_x, is used. When f_x is replaced by f_T, the transition frequency, poor agreement is found.

Electron Heating Phenomena in Avalanche Transistors - See 10,389

10,482 SELF-POWERED SEMICONDUCTIVE DEVICE by P. Rappaport (RCA); U.S. Pat. 2,976, 426, Issued Mar. 21, 1961

A self-powered device comprising a transistor structure and a radioactive power source common to a semiconductor body is described. Radioactive materials, such as Strontium^{90}, are employed to irradiate a junction region to generate power across a resistive load. With fifty millicuries of Sr^{90} employed, the open-circuit voltages obtained are between thirty and several hundred millivolts, depending on the kind of semiconductor material; power expended in a load is of the order of several microwatts. Voltage so generated is applied as bias to the adjacent transistor structure.

10,483 MICROMASKING FOR CHEMICAL ETCHING OF SEMICONDUCTORS by S. Denda (Electrotech. Lab., Tokyo); Solid State Electronics, Vol. 2, p. 69(L), Jan. 1961

A method for producing mesas down to 30μ or less in diameter in diffused transistors and diodes without utilizing the photomasking technique is described. A thin thread of picein, black wax used for sealing vacuum systems, is positioned by means of a mechanical holder so that it touches the semiconductor surface. The tip of the thread is melted by passing a current pulse through a platinum heater supporting the semiconductor. The masked pellet is then etched, with the height of the mesa being limited to one third the diameter to prevent removing the mask during the etching. The mask is dissolved by benzol after the etching.

Reduction of Surface Recombination in Junction Transistors - See 10,391

10,484 RESIDUAL THERMOELASTIC STRESSES IN BONDED SILICON WAFERS by T. D. Riney (Bell Labs.); Bull. Am. Phys. Soc., Ser. II, Vol. 6, p. 77(A), Feb. 1, 1961

The residual thermoelastic stresses produced in a silicon strip when eutectic-bonded to a gold-plated molybdenum block have been investigated photoelastically using near infrared light and an image converter tube. This is the two-dimensional analog of a problem arising when silicon wafers are bonded to headers in semiconductor devices. It was shown that with the proper orientation of the crystal the specimen may be studied by the methods normally employed with isotropic birefringent materials. This simplifies the quantitative evaluation of the

stresses. It is found that, though the mean longitudinal stress near the center of the strip is compressive, a transverse tensile stress of greater magnitude occurs near the ends of the strip. This "tearing stress" is determined to be approximately 1.1×10^9 dynes/cm^2 at room temperature.

10,485 GRAPHICAL ANALYSIS OF THE OPERATION OF THE TECNETRON I. [in French] by A. V. J. Martin and J. Le Mée (Carnegie Inst. Tech.); J. Phys. Radium, Suppl. to No. 2, pp. 1A-12A, Feb. 1961

The operation of the Tecnetron is analyzed in the subcritical field region where the carrier mobility can be considered as constant. The analysis is mainly graphical and is a second approximation of an analytic theory previously published by Martin. A set of universal curves giving the main characteristics of the device is derived and the preceding theories and the present study are compared.

10,486 EXAMINATION OF A NEW TETRODE FIELD EFFECT DEVICE: THE ALCATRON [in French] by J. Grosvalet (Cie. Gen. Telegraphie); Onde Elect., Vol. 41, pp. 114-122, Feb. 1961

A field effect device of annular construction in which the two grids have been separated is discussed. The small grid is used as a control grid and the larger grid aids power dissipation and modifies the equivalent circuit at high frequency. Experiments performed on a germanium device have exceeded the limits of previous field effect theories. These theories are examined and it is shown why they do not apply directly to the new device. The possibilities of further development of such a device are briefly outlined with particular attention to new semiconductor materials.

Injection and Collection of Hot Electrons in Metal Films - See 10,395

MAGNETOELECTRIC DEVICES

10,487 APPLICATIONS OF HALL EFFECT IN THIN SEMICONDUCTOR FILMS by A. R. Billings (U. Western Australia); Proc. IRE Austral., Vol. 22, p. 180(A), Mar. 1961

Alternative techniques of producing thin films of semiconductor compounds were discussed. Evaporation techniques allow the use of unusual geometries which in turn can lead to novel devices. Some such devices which make use of the Hall Effect were described and a simple generator of a function of one or more variable was developed. The way in which the performance of a practical device de iates from that of the idealized device was discussed in some detail and it was shown that a Hall plate can usefully be employed as a low-pass balanced to unbalanced converter.

10,488 SOME APPLICATIONS OF HALL-GENERATORS by E. Laisk (U. New South Wales); Proc. IRE Austral., Vol. 22, p. 188(A), Mar. 1961

The use of Hall generators for magnetic field measurements, hysteresis measurements and oscillators was discussed. A single, simple and robust Hall device able to replace delicate instruments and complex circuitry such as fluxmeters, multipliers and the like, was shown. The characteristics and circuitry of a Hall-effect gaussmeter, an oscillator and a clip-on-ammeter were discussed.

Hall Effect Isolator in Tunnel Diode Amplifier - See 10,533

10,489 CHARGING SURFACE ACTIVITY IN THE OSCILLISTOR by K. T. Rogers (Varian Assoc.); Bull. Am. Phys. Soc., Ser. II, Vol. 6, p. 116(A), Mar. 20, 1961

Studies on the "charging" at the surfaces of the "oscillistor" were presented. Larrabee and Steele have found that both parallel and transverse magnetic field components must be present to obtain oscillations; the transverse field points out the importance of pair accumulation at a "Hall surface". "Charging surfaces" to which carriers tend in drifting parallel to the magnetic field and the "Hall surface" were considered. Modification of the "charging" by applying high polarizing electric fields was found to alter oscillistor periods. Symmetries were found upon the reversal of magnetic field and/or angle of field; they were verified by considering the behavior of both sets of surfaces.

CRYOGENIC DEVICES

10,490 THE CRYOSISTOR – A NEW LOW-TEMPERATURE THREE-TERMINAL SWITCH by I. Melngailis (Carnegie Inst. Tech.); Proc. IRE, Vol. 49, pp. 352-354(L), Jan. 1961

The characteristics and some possible applications of the Cryosistor are described. The device, which consists of a thin wafer of germanium with two ohmic contacts and an indium-alloyed p-n junction, exhibits a negative resistance characteristic between the high and low resistance states at liquid helium temperatures. Bistable switching is feasible with the device using pulses of no more than 2×10^{-8} seconds duration. The Cryosistor is also suited as an experimental structure for the investigation of the ionization of germanium at liquid helium temperatures.

PHOTODEVICES

10,491 SPECTRAL RESPONSE OF PHOTOVOLTAIC CELLS by J. J. Loferski and J. J. Wysocki (RCA Labs.); RCA Rev., Vol. 22, pp. 38-56, Mar. 1961

A theoretical and experimental study of the spectral response of p-n junction photovoltaic cells is discussed. The current flowing across the junction is calculated as a function of the absorption constant of the radiation for various values of the semiconductor parameters. The results of machine calculations on some cases are shown in the figures. The use of normalized spectral-response curves to determine the values of minority-carrier diffusion lengths is demonstrated. Using certain approximations it is possible to determine minority-carrier diffusion lengths on both sides of the junction with relative ease. These principles have been applied to experimental GaAs and silicon photovoltaic cells to determine the values of diffusion lengths in the finished junctions.

10,492 THE EFFECT OF SERIES RESISTANCE ON PHOTOVOLTAIC SOLAR ENERGY CONVERSION by J. J. Wysocki (RCA Labs.); RCA Rev., Vol. 22, pp. 57-70, Mar. 1961

The component contact and sheet resistances of the series resistance of photovoltaic cells are examined and a qualitative agreement between theory and experiment is discussed. The contact resistance was shown to reduce the conversion efficiency more than sheet resistance.

Reduction of Surface Recombination in Photodiodes - See 10,391

OTHER PHOTODEVICES

10,493 ELECTROLUMINESCENCE – ITS CHARACTERISTICS AND APPLICATIONS by D. H. Smith (Naval Res. Lab., N. Zeal.); Electronic Engrg., Vol. 33, pp. 68-72, Feb. 1961; pp. 164-170, Mar. 1961

The characteristics of the light emitted from electroluminescent cells energized by sine waves, square waves, and pulses of voltage are described, the mechanism of electroluminescence is discussed, and some of the many applications are reviewed. Examples cited include electroluminescent cells used as light sources and for the visual display of information, and light amplifiers made from a combination of electroluminescent and photoconductive elements. The possibility that an array of very small electroluminescent cells could be used as a thin-screen television display is cited.

10,494 PHOTOCONDUCTIVE MODULATION OF MICROWAVE ELECTRIC FIELDS by W. E. Bulman (Ohio Semiconductors); B. C. Potts, and R. B. Green (The Ohio State U.); IRE Trans., Vol. AP-9, pp. 193-199, Mar. 1961

Thin films and coatings of photoconductive cadmium sulfide material used to modulate electric fields are discussed. An analysis of these films in terms of the physics involved and the effect upon microwave fields is presented. Experimental procedures show the validity of the analyses and indicate possible applications of the principle. Practical significance of the technique is illustrated by experimentally determining the areas of a particular flat plate that produce the first sidelobe of the scattering pattern.

FERRITE DEVICES

10,495 THE APPLICATION OF FERRITE TYPE MATERIALS AT LOW MICROWAVE FREQUENCIES by D. F. Hewitt (Postmaster-General's Dept.); Proc. IRE Austral., Vol. 22, p. 183(A), Mar. 1961

Limitations of ferrite materials in linear devices at low microwave frequencies were reviewed. Reference was made to measurements carried out on various ferrite materials in rectangular and circular waveguides. Application in various microwave devices, such as filters, doublers, limiters, amplifiers and the like, is described.

10,496 THE MAGNETIC EXCITATION INSIDE A CYLINDRICAL THIN-FILM FERROMAGNET by T. H. O'Dell (UKAEA Atomic Energy Res. Est.); Proc. IEE, Vol. 108C, pp. 79-82, Mar. 1961

An expression for the magnetic excitation inside a cylindrical thin film ferromagnet is derived and a table of computed values is given. The results are relevant to work on thin ferromagnetic films for digital storage applications.

10,497 FLUX DISTRIBUTION IN FERRITE CORES UNDER VARIOUS MODES OF PARTIAL SWITCHING by R. H. James, W. M. Overn, and C. W. Lundberg (Sperry Rand Corp.); J. Appl. Phys., Suppl. to Vol. 32, pp. 38S-39S, Mar. 1961

The flux distribution in a ferrite core after partial switching to the same flux density is described by three different methods. These methods are: (1) applying a fixed pattern of alternate-polarity pulses with diminishing amplitude, (2) amplitude limiting, and (3) time limiting. Discontinuities in the residual magnetization curve in the first case show the existence of regions of oppositely-directed magnetization. A comparison of the curves shows that the time-limited state can be represented by a model consisting of a large number of regions magnetized in alternate directions.

10,498 THE TESTING OF METAL TAPE MAGNETIC CORES FOR USE IN A CODE TRANSLATOR by J. D. Andrews (P. O. Engrg.); Electronic Engrg., Vol. 33, pp. 21-26, Jan. 1961

An acceptance test for magnetic cores, reproducing the conditions which will occur in the equipment for which the cores are intended, is described. The tests made on two types of metal tape magnetic cores are discussed. With one type of core it is important that the voltage x time area and '1' to '0' signal ratio exceeds a certain value. The second type of core is tested for a form of coincident current working and for switching speed. The acceptance test of these cores has been made simple by reducing it to a plug-in operation which produces an oscilloscope display behind a test mask.

10,499 FERRITE TOROID CORE CIRCUIT ANALYSIS by R. Betts and G. Bishop (IBM); IRE Trans., Vol. EC-10, pp. 51-56, Mar. 1961

An analysis of the terminal characteristics of thin ferrite toroid cores under arbitrary drive and load conditions is presented. The analysis is founded only on the following two experimentally confirmed conditions: 1) the time required for a complete reversal of flux under unloaded conditions is inversely proportional to the magnitude of a step-driving field which is in excess of the critical field required to initiate flux change; 2) the open circuit voltage-time output waveforms caused by step-driving currents are identical when normalized with respect to amplitude and time. The normalized output voltage waveform $f'(x)$ is used to develop a terminal characteristic equation. It is shown that $f'(x)$ may be obtained by using a nonideal step-input current. Utilizing a modified Gaussian equation to represent $f'(x)$, equations are developed to allow the prediction of core response to arbitrary input waveforms, using 4 parameters easily obtained from voltage response vs NI step-drive plots, and $f(x)$, which is the integral of the normalized expression for the open circuit voltage $f'(x)$, and is proportional to the flux switched in the core. The equations are expanded to include a load circuit and to test the validity of the

expressions developed. Theoretical and experimental results are compared for a core loaded with series RL and RLC circuits with both ramp and step-drive currents. Agreement is shown to be good, even though the core used was not particularly thin.

10,500 MAGNETIZATION AND PULL CHARACTERISTICS OF MATING MAGNETIC REEDS by R. L. Peek, Jr., (Bell Labs.); Bell Sys. Tech. J., Vol. 40, pp. 523-546, Mar. 1961

Expressions for the magnetization and pull relations of the mating flat magnetic reeds used as contacting members in reed relays are presented. The results of an experimental study expressed in dimensionless form give the force or pull between the reeds in terms of their dimensions, the gap between them, and the flux density. Since the attainable flux density is limited by saturation, the pull expression leads to conditions which must be satisfied by the reed and gap dimensions to provide desired levels of contact and retractile force. The ampere-turn sensitivity of a relay using mating magnetic reeds depends on the flux required and on the reluctance of the magnetic path through the reeds. Expressions are given for the reluctance in the case of an air return path and in that where the air return is partially replaced by a shielding member. Expressions are also given for the operate time of such reed relays. This depends on the concurrent flux development and motion of the reeds. The time of flux development varies inversely with the power input to the coil, but the motion time cannot be less than that required when the flux density is raised abruptly to its maximum value at the start of motion.

10,501 AN APPROXIMATE SOLUTION TO SOME FERRITE FILLED WAVEGUIDE PROBLEMS WITH LONGITUDINAL MAGNETIZATION by S. S. Sandler (Electronic Commun.); IRE Trans., Vol. MTT-9, pp. 162-168, Mar. 1961

An approximate solution for the field structure and propagating modes in parallel plane, circular, and coaxial ferrite filled waveguide is presented. Bundles of plane waves are assumed to propagate in these structures which bounce back and forth along the guide. The solutions are classified into two types depending on the negative or positive equality of the incident and reflected waves. In the case of the circular guide the waves form a cone, and in the coaxial guide they form a frustrum of a cone about the axis. The elemental plane waves are also assumed to satisfy Polder's relation and the boundary conditions at the guide walls. Simple relations are obtained with this equivalence for the propagation constant and the field. Comparison to rigorous theory is made in the case of the parallel plane and circular guide. Some experimental verification for the completely filled coaxial waveguide is presented.

MASERS AND LASERS

Theory of Relaxation Times in Ruby Masers - See 10,452

10,502 ADIABATIC RAPID PASSAGE IN RUBY AT 8MM WAVELENGTHS by J. S. Thorp, J. H. Pace, and D. F. Sampson (RRE); J. Electronics Control, Vol. 10, pp. 13-24, Jan. 1961

An investigation of adiabatic rapid passage made in ruby at 8mm wavelengths is discussed. Performance data for a two-level ruby maser operated both as a pulsed amplifier and as an oscillator at these wavelengths are given. When amplifying, values of gain and bandwidth of up to 14 db and 10 Mc at 1.4° were obtained, giving root gain-bandwidth products of up to about 50 Mc. In preliminary measurements, using the maser as an oscillator, output powers of about 70 μw at 33.1 Gc and 1.4°K were obtained. The inversion technique used, which incorporates magnetic field modulation with the use of the crystal as a cavity, could be readily scaled to considerably higher frequencies.

10,503 CHARACTERISTICS OF THE RUBY LASER by C. Zarowin and R. L. Martin (TRG); 1961 Spring Mtg. Opt. Soc. Am. p. 10(A), Mar. 1961

A number of definite cavity modes were observed in the beam of the ruby laser. Off-axis modes appeared to contribute to the observed beam width of 15 min of arc. The analysis of these modes as well as the conditions under which they are observed were discussed. Other operating characteristics of the ruby laser also were given.

10,504 TIME DEVELOPMENT OF THE BEAM FROM THE RUBY LASER by R. L. Martin (TRG); 1961 Spring Mtg. Opt. Soc. Am. p. 11(A), Mar. 1961

High-speed streak moving pictures of the beam from the ruby laser were presented. The pictures were taken with a film speed of about 300 ft per sec and a variety of focusing conditions. The relaxation oscillations during the excitation pulse are clearly visible as well as variations in the laser characteristics as a function of time. An analysis of these characteristics was given.

10,505 CONFOCAL MULTIMODE RESONATOR FOR MILLIMETER THROUGH OPTICAL WAVELENGTH MASERS by G. D. Boyd and J. P. Gordon (Bell Labs.); Bell Sys. Tech. J. Vol. 40, pp. 489-508, Mar. 1961

A multimode resonator of high quality factor which may be applied in maser devices is discussed. The resonator consists of two identical concave spherical reflectors which are separated by any distance up to twice their common radius of curvature. Mode patterns and diffraction losses for the low-loss modes of such a resonator are obtained analytically, using an approximate method. The results show that the diffraction losses are generally considerably lower for the curved surfaces than for the plane surfaces. Diffraction losses and mode volume are a minimum when the reflector spacing equals the common radius of curvature of the reflectors. For this case the resonator may be termed confocal. A further property of the concave spherical resonator is that the optical alignment is not extremely critical.

10,506 RESONANT MODES IN A MASER INTERFEROMETER by A. G. Fox and T. Li (Bell Labs.); Bell Sys. Tech. J., Vol. 40, pp. 453-488, Mar. 1961

A theoretical investigation of diffraction of electromagnetic waves in Fabry-Perot interferometers when they are used as resonators in optical masers is presented. An electronic digital computer was programmed to compute the electromagnetic field across the mirrors of the interferometer where an initially

launched wave is reflected back and forth between the mirrors. It was found that after many reflections a state is reached in which the relative field distribution does not vary from transit to transit and the amplitude of the field decays at an exponential rate. This steady-state field distribution is regarded as a normal mode of the interferometer. Many such normal modes are possible depending upon the initial wave distribution. The lowest-order mode, which has the lowest diffraction loss, has a high intensity at the middle of the mirror and rather low intensities at the edges. Therefore, the diffraction loss is much lower than would be predicted for a uniform plane wave. Curves for field distribution and diffraction loss are given for different mirror geometries and different modes. Since each mode has a characteristic loss and phase shift per transit, a uniform plane wave which can be resolved into many modes cannot, properly speaking, be resonated in an interferometer. In the usual optical interferometers, the resolution is too poor to resolve the individual mode resonances and the uniform plane wave distribution may be maintained approximately. However, in an oscillating maser, the lowest-order mode should cominate if the mirror spacing is correct for resonance. A confocal spherical system has also been investigated and the losses are shown to be orders of magnitude less than for plane mirrors.

Maser Radiometer for Centimeter Wavelengths - See 10,544

10,507 RESONATORS FOR MILLIMETER AND SUBMILLIMETER WAVELENGTHS by W. Culshaw (NBS); IRE Trans., Vol. MTT-9, pp. 135-144, Mar. 1961

Further considerations on the mm-wave Fabry-Perot interferometer are presented. Computed Q values for parallel metal plate resonators indicate that at spacings around 2.5 cm, values ranging from 60,000 at 3 mm, to 300,000 at 0.1 mm wavelengths are possible. The plates, however, must be quite flat. These results are important for many investigations, and in particular for mm and sub-mm wave maser research. For the aperture per wavelength ratios possible here, diffraction effects should be small. Consideration is given to using curved reflectors or focused radiation in applications where the fields must be concentrated. For this purpose, re-entrant conical spherical resonators are treated in detail, as regards operation in the TEM mode at high orders of interference. Expressions for the Q and shunt impedance are given and high values are possible at mm and sub-mm wavelengths. Quasi-optical methods of coupling into and out of such a resonator are proposed, and the higher modes possible in such a resonator are considered. Results indicate that it could have application to the mm-wave generation problem, and that it represents a good resonant cavity for solid state research at mm and sub-mm wavelengths and for maser applications in particular.

Optical Ruby Maser - See 10,453

10,508 SOLID STATE OPTICAL MASERS USING U^{+++} AND Sm^{++} by P. P. Sorokin and M. J. Stevenson (IBM Res. Ctr.); 1961 Spring Mtg. Opt. Soc. Am., p. 10(A), Mar. 1961

Oscillations of two solid-state optical masers were observed using as the active maser medium U^{+++} and Sm^{++} ions substituted for Ca^{++} ions in calcium fluoride. One of the principal characteristics of both of these systems is that the maser oscillations take place in transitions terminating on states lying sufficiently far above the ground state to be depopulated at low temperatures. As a result, the amount of pumping power required to reach threshold for oscillation is less by a factor of more than 500 than in the case of the ruby optical maser. In the U^{+++} system the stimulated emission occurs at 2.5μ from the lower of two metastable states approximately 4525 cm^{-1} above the ground state. The terminal state lies approximately 515 cm^{-1} above the ground state. The strongest absorption bands used to excite the U^{+++} ions into the metastable level are in the green and blue portions of the visible spectrum. Characteristic relaxation oscillations were observed in detail. In the Sm^{++} system the maser oscillation takes place at 7082 A in a transition from a metastable state 14,500 cm^{-1} above the $^7F_0$ ground state to $^7F_1$ level 369 cm^{-1} above the ground state. The principal absorption band is centered at 6320 A, and there are a few additional bands at shorter wavelengths. In contrast to both U^{+++} and the ruby optical masers, no relaxation oscillations were observed in the pulsed output of the Sm^{++} optical maser.

Maser Effects in Sm^{2+} Doped CaF_2 - See 10,454

10,509 RECTANGULAR TE AND TM MODES IN ANISOTROPIC DIELECTRICS by G. J. Troup (Weapons Res. Est.); Proc. IRE Austral., Vol. 22, p. 183(A), Mar. 1961

The conditions for the propagation of pure TE and TM modes, obtained from simple heuristic considerations based on the optics of anisotropic dielectrics, were described. These conditions were verified by the solution of Maxwell's equations, and propagation constants for TE and TM modes in uniaxial and biaxial crystals were derived. The application to maser cavity design was indicated, and a discussion as to what will occur when the conditions for pure TE and TM mode propagation are not completely fulfilled was given.

OTHER SOLID STATE DEVICES

10,510 THEORY FOR THE OPERATION OF A MAGNETIC REFRIGERATOR AT TEMPERATURES BELOW 1°K by J. E. Gordon (Amherst Coll.), H. B. Silsbee (U. California); Rev. Sci. Instr., Vol. 32, pp. 572-578, May 1961

A theory for determining the optimum cycle of a magnetic refrigerator is developed. The refrigerator consists of a helium bath, a paramagnetic working substance, and an isothermal reservoir. The working substance is connected to the bath and to the reservoir via thermal values. In the theory the values are presumed to be superconducting wires, but no assumptions are made concerning the characteristics of the working substance. The expected behavior of a refrigerator utilizing both He^4 and He^3 baths is investigated. It is predicted that a magnetic refrigerator operating from a bath temperature of 0.3° or 0.4°K will be able to maintain an isothermal reservoir temperature of 0.05°K or lower with heat inputs of 10-20 ergs/sec, providing the effects of thermal contact resistance can be kept small. The effect of thermal resistance on refrigerator performance is investigated. The same theoretical techniques have been used to predict the behavior of a magnetic refrigerator

utilizing a mechanical switch. The theoretical and experimental results are compared and moderately good agreement is obtained.

10,511 DIELECTRIC BOLOMETER: A NEW TYPE OF THERMAL RADIATION DETECTOR by R. A. Hanel (NASA); J. Opt. Soc. Am., Vol. 51, pp. 220-224, Feb. 1961

A thermal infrared detector, which is not limited in sensitivity by Johnson noise, constructed by utilizing materials which exhibit a high dielectric constant temperature dependence, is discussed. The basic theory of the dielectric bolometer is discussed and it is shown that noise figures below 3 db can be obtained even at chopper frequencies well above the $1/\tau$ value of the detector. Ferroelectrics such as barium-strontium titanate and others seem to be well suited for radiation-cooled dielectric bolometers.

10,512 PRODUCTION OF MAGNETIC FIELDS EXCEEDING 15 KILOGAUSS BY A SUPERCONDUCTING SOLENOID by J. E. Kunzler, E. Buehler, F. S. L. Hsu, B. T. Matthias, and C. Wahl (Bell Labs.); J. Appl. Phys., Vol. 32, pp. 325-326 (L), Feb. 1961

A superconducting solenoid and its operation at fields as high as 15.5 kgauss at a temperature of 1.5°K is discussed. The device was constructed by winding 0.007cm diameter gold-coated Mo_3Re wire on a coil form that was 3cm long and had a core of 0.3 cm. About 30,000 turns were used and the outside diameter of the solenoid was nearly 2 cm. The solenoid was wound so that several sections could be operated with the current in parallel. The preparation of the Mo_3Re wire is described.

Piezoelectric Ceramic Resonators - See 10,550

10,513 DEMAGNETIZATION OF TWISTOR BITS by W. A. Barrett (Bell Labs.); J. Appl. Phys., Suppl. to Vol. 32, pp. 35S-36S, Mar. 1961

A search-coil technique for measuring the effect of demagnetizing fields on twistor wire is described. A coincident-current bit select followed by a single-current read select is used to form and to "erase" the magnetized regions. It is found that the shape of the magnetized regions thus formed are a complex function of the two currents used and that the bits are not fully erased by the single current. The results suggest that demagnetization must be reduced by reducing thickness and/or bit density unless a more complex solenoid structure can be found to control the magnetization of the bit regions.

BASIC SOLID STATE DEVICE CIRCUITS

THEORY AND DESIGN OF CIRCUITS

10,514 NEGATIVE RESISTANCE FOR LOW FREQUENCY APPLICATIONS by B. J. Lancaster (U. New South Wales); Proc. IRE Austral., Vol. 22, p. 185(A), Mar. 1961

A negative resistance that has been developed from the Negative Impedance Converter was described. The Converter is ideally a transformer with a −1:1 ratio between two ports forming a quadripole. A transistorized version of such a device has been developed and with some modification this type of converter has proved quite successful in the desired frequency range. The device has a negative resistance characteristic which is stable with respect to frequency from dc to at least fifty cycles per second. The negative resistance is of the series or current operated type but it is quite simple to rearrange the circuit so that the device is voltage operated. The current range is between 0.5 and 0.2 ma maximum depending on the value of the resistance to be converted and the type of active element being used. Examples of the use of the negative resistance at very low frequency were also discussed.

10,515 A METHOD OF TREE EXPANSION IN NETWORK TOPOLOGY by H. Watanabe (Nippon Electric); IRE Trans., Vol. CT-8, pp. 4-10, Mar. 1961

A systematic method of obtaining the total sum of all possible tree admittance products of a complicated network is presented. First, the network is partitioned into several simple subnetworks by a set of independent cut sets. Then, the relationship between trees or tree admittance products of the network and multitrees or multitree admittance products of each subnetwork is found and presented as the tree expansion theorem. Finally, an effective method for decomposition of the large network into simple subnetworks is discussed. The methods described in this paper are very applicable to solution by automatic computation.

10,516 ON THE REALIZABILITY OF A SET OF TREES by S. L. Hakimi (U. Illinois); IRE Trans., Vol. CT-8, pp. 11-17, Mar. 1961

A matrix with entries 0's and 1's whose rows correspond to the trees of a graph G and whose columns correspond to the elements of G is introduced. Many interesting properties of such a matrix are derived. The concept of the rank (modulus 2) of the tree matrix is found to be very useful in determining the number of separable parts of the corresponding graph. A simple algebraic way is presented by which one can find, from a given set of trees (or tree matrix), the fundamental circuit (or cut-set) matrix with respect to a prespecified tree. It is also shown that one can easily find, from the tree matrix, the set of all paths between the vertices of an element of a graph. Some interesting conjectures are stated concerning graphs with a given rank and nullity which have a minimum number of trees.

10,517 ON THE SYNTHESIS OF R-NETWORKS by D. P. Brown and Y. Tokad (Michigan State U.); IRE Trans., Vol. CT-8, pp. 31-39, Mar. 1961

A study of a class of real symmetric matrices is made, and a new set of necessary and sufficient conditions are defined on the entries of these matrices such that they can be synthesized, without using ideal transformers, as an R-network with a minimum number of terminals. The conditions are stated in terms of the terminal graph used in representing the terminal characteristics of multiterminal components. The new class of matrices then represents "terminal equations" corresponding to a path-tree terminal graph. It is also shown that one of the well-known class of matrices, referred to as dominant matrices, represent

the terminal equations for a Lagrangian-tree terminal graph. It is further indicated that any such class of real symmetric matrices is distinguishable by a particular terminal graph. For the cases when a real symmetric matrix of order n cannot be synthesized by an R network with (n + 1) terminal vertices, an "enlarged" matrix is formed, and the necessary and sufficient conditions for realizability of these matrices are given.

10,518 ANALYSIS AND SYNTHESIS TECHNIQUES OF ORIENTED COMMUNICATION NETS by D. T. Tang and R. T. Chien (IBM Res. Ctr.); IRE Trans., Vol. CT-8, pp. 39-43, Mar. 1961

An oriented communication net, a communication network in which channel capacities between pairs of terminals are not symmetrical, is discussed. Such a system can be represented by an oriented graph. The concept of a minimum-valued cut is used to determine the terminal-capacity matrix which gives the maximum possible communication between any ordered pair of terminals. Necessary conditions for a terminal capacity matrix to be realizable as an oriented communication network are obtained. These conditions are shown to be sufficient when the order of the terminal capacity matrix is three or less. They are not sufficient for higher-order cases in general. Synthesis techniques based on matrix partition and matrix addition are used to realize any three-by-three terminal capacity matrix with extensions to some higher-order cases.

10,519 FLOWGRAPHS FOR THE REPRESENTATION OF NON-LINEAR SYSTEMS by T. A. Bickart (The Johns Hopkins U.); IRE Trans., Vol. CT-8, pp. 49-58, Mar. 1961

The development of a nonlinear flowgraph notation for the representation of a large class of nonlinear systems is described. By the definition of power operator branches, exponential operator branches, switching operator branches, and limiting operator branches, it becomes possible to represent in a very simple manner a number of different types of hyteretic systems. A study of the rules for manipulation of nonlinear flowgraphs is made, so as to bring out the procedures that might be used in reducing the complexity of such a system as that represented by the flowgraphs. Generalized flowgraph inversion procedures are developed as a consequence of the defined nonlinear branch transmittances. A variety of nonlinear systems are illustrated to indicate the broad applicability of the notation in representing such systems.

10,520 THE SEG: A NEW CLASS OF SUBGRAPHS by M. B. Reed (Michigan State U.); IRE Trans., Vol. CT-8, pp. 17-22, Mar. 1961

A presentation of a new class of subgraphs (segs) which includes stars and cust sets as special cases is discussed. The matrix associated with the seg can be shown to be the general coefficient matrix of the Kirchhoff current equations. In addition to adding to the structure of linear graph theory, knowledge of currents in electric networks is increased, opening new phases of network theory.

10,521 APPLICATION OF GRAPH THEORY TO THE ANALYSIS OF ACTIVE AND MUTUALLY COUPLED NETWORKS by W. H. Kim (Columbia U.); J. Franklin Inst., Vol. 271, pp. 200-221, Mar. 1961

A unified graphical approach to the analysis of an electrical network which contains linear multi-terminal devices such as vacuum tubes, transistors, transformers, gyrators, circulators, etc. is presented. The concept of the mathematical equivalent circuit of an active device or a passive but mutually coupled device is related to the indefinite admittance matrix of a multipole defined by Zadeh and Shekel. Various graphical formulas for the evaluation of network functions of a multipole, including the node-condensation techniques, are given. A number of examples are presented.

10,522 OPTIMAL SYNTHESIS OF A COMMUNICATION NET by O. Wing and R. T. Chien (IBM Res. Ctr.); IRE Trans., Vol. CT-8, pp. 44-49, Mar. 1961

Solutions to the problem of realizing a communication network at minimum cost are described. The network is composed of a set of nodes connected by a set of branches. Every branch has associated with it a capacity. The required amount of flow between every pair of nodes is specified. The unit costs of the branch capacities are given. The problem is to find the network and the branch capacities such that the total cost is minimum. The set of branch capacities and the set of terminal demands are shown to satisfy a set of linear inequalities. Linear programming is used to obtain the optimal solution. In the case of identical unit costs, several realizations are given which require fewer branches than previously reported.

10,523 DARLINGTON'S SYNTHESIS AND RMS ERROR EVALUATION by A. Papoulis (Tech. Hochschule, Darmstadt); IRE Trans., Vol. CT-8, pp. 58-60, Mar. 1961

A theorem relating the integrated square of the impulse and step response of a two terminal-pair network to its input impedance is developed. This theorem is in a sense the time domain equivalent to the gain-bandwidth relationship in steady state. As an application, a simple method is presented for evaluating the integrated square,

$$\int_0^\infty \left[r(t) - r_{ss} \right]^2 dt,$$

of the difference between a signal $r(t)$ and its steady state value r_{ss}; the method is based on Darlington's procedure for determining a reactive network from its transfer function.

10,524 POLYTYPE-PORT DEVICES AND NETWORKS by E. E. Loebner (RCA Labs.); Proc. Symp. Active Networks and Feedback Systems Polytechnic Press, 1961, pp. 449-456

Various classes of solid state multiport devices are described and algebraic rules for combining such devices into networks are discussed. Such networks combine several types of power-flow branches within the same volume. These do not necessarily interact with each other, permitting an isolation between a number of intertwined sub-networks. Coupling of the sub-networks is accomplished by polytype-port transducer nodes. A specific polytype-port network representing a shift register is described and the analogy and correspondence between various types of solid state devices is developed.

10,525 ON THE SYNTHESIS OF RESISTIVE N-PORT NETWORKS by G. Biorci and P. P. Civalleri (Inst. Elettrotecnico

Nazionale Galileo Ferraris); IRE Trans., Vol. CT-8, pp. 22-28, Mar. 1961

A new approach to the problem of the synthesis of resistive n-port networks with (n + 1) nodes is given. First it is shown that, given a conductance matrix G of order n, the signs of its elements define the complete tree of the n port uniquely (if it exists). The case of two (or more) ports in "series" is exceptional: the order of such ports in the complete tree can be found by comparing the absolute values of a couple (or more couples) of elements of G. Once the complete tree has been determined, the synthesis becomes very simple, since the G matrix can be transformed into another matrix G_0 referred to a set of node-to-datum independent voltages, whose conditions of realizability are well known.

10,526 PARAMOUNT MATRICES AND SYNTHESIS OF RESISTIVE N PORTS by I. Coderbaum (Columbia U.); IRE Trans., Vol. CT-8, pp. 28-31, Mar. 1961

A method of reducing the main diagonal elements of a paramount matrix and its inverse without destroying their paramount character is described. It is shown that in not more than 2 n steps the irreducible remainder of a given matrix can be found. Also, the conditions are formulated for a paramount matrix with nonpositive off-diagonal elements to be the impedance matrix of an n-port network with the minimum number of independent circuits.

10,527 FORMAL REALIZABILITY OF LINEAR NETWORKS by Y. Oono (Kyushu U.); Proc. Symp. Active Networks and Feedback Systems Polytechnic Press, 1961, pp. 475-486

The synthesis of linear passive or active networks is described. An n-port is defined by the "system matrix" which represents n homogeneous linear relations between the terminal voltages and currents, and is synthesized by the linear transformation of the system matrix. The paradoxical network for which the scattering matrix cannot be defined and which forces the input to be simultaneously open and shorted is presented and discussed. As an application of the general synthesis procedure, two-ports with real system matrices are synthesized in the canonical form containing one ideal gyrator and two positive or negative resistors. It is shown that system matrices of which the elements are real rational functions of the frequency variable can always be synthesized.

Design of Multi-Level Switching Circuits - See 10,543

Properties and Applications of Si Rectifiers - See 10,473

AMPLIFIERS

Analysis of Parametric Traveling-Wave Amplifier - See 10,536

Temperature Stability of High Impedance Amplifiers - See 10,541

Shot Noise in Tunnel Diode Amplifiers - See 10,538

10,528 TRANSISTOR CASCODE CIRCUIT IMPROVES AUTOMATIC GAIN CONTROL IN AMPLIFIERS by J. F. Perkins, Jr. (Raytheon); Electronics, Vol. 34, pp. 49-51, June 2, 1961

An improved method of applying automatic gain control to transistor IF tuned amplifiers is presented. In an ordinary one stage grounded-emitter tuned amplifier with AGC, frequency response is usually degraded by the change of the Q and the center frequency f_0 of the tuned circuit when the emitter current I_E changes. To prevent these parameters (Q and f_0) from changing, a grounded-base stage serving as a buffer is provided between the grounded-emitter stage and the tuned circuit. Major characteristics of transistor types 2N1143, 2N384, 2N588, and the schematic and test results of a 10 Mc IF amplifier with AGC using these transistors are included.

10,529 SYNTHESIS USING TUNNEL DIODES AND MASERS by L. Weinberg (Hughes Res. Labs.); IRE Trans., Vol. CT-8, pp. 66-75, Mar. 1961

Methods for the realization of multistage amplifier networks containing negative resistances are described. These methods concern exact synthesis procedures which are based on reverse predistortion, both uniform and nonuniform. They thus realize a specified function of frequency – its magnitude, its phase, and its constant multiplier. The methods apply to the realization of tunnel-diode amplifiers if the equivalent circuit of a tunnel diode is considered to be a parallel connection of the junction transition capacitance and a negative resistance. They can be used to realize cascaded maser amplifiers if the equivalent circuit of a maser amplifier is taken to be a parallel connection of an inductance, a capacitance, and a negative resistance, or a series connection of these three elements. The methods used automatically provide for the stability of the multistage active networks. The straightforward technique of predistorting the complete system function may for some applications require too many active elements. Simple modifications of this technique are given which allow a control over the position in the network, the time constants, and the required number of the active elements.

10,530 SIGNAL TRANSMISSION IN NONRECIPROCAL SYSTEMS by J. H. Mulligan, Jr. (New York U.); Proc. Symp. Active Networks and Feedback Systems Polytechnic Press, 1961, pp. 125-153

Some methods for the computation of signal transmission in transistor and vacuum tube amplifiers are described. Bode's definitions of return difference and return ratio are applied to a general system matrix. The relation between returned quantity and the models used to represent a particular nonreciprocal device employed in a system is discussed. It is shown and illustrated by examples that a given nonreciprocal device may have associated with it a family of return differences, one corresponding to each different model chosen to characterize the device. In general these return differences are not equal to one another, although under some conditions the members of the family can have the same value. The usefulness of the different return differences in various circuit calculations is also illustrated. Signal transmission is then considered in terms of both driving point and transfer admittances and impedances. Blackman's impedance relation is generalized to show the dependence of a driving point function on the return differences associated with an arbitrary number of nonreciprocal elements connected in an arbitrary fashion. The counterpart of this generalized result which applies to transfer

admittances and impedances is also given. The use of these relations is illustrated by calculations on transistor and vacuum tube amplifiers. The examples include the derivation of a general equivalent representation for the driving point impedance of a feedback system.

10,531 AMPLIFIER CIRCUIT by R. Silberbach (Motorola); U. S. Pat. 2,972,114, Issued Feb. 14, 1961

A temperature compensated transistor amplifier circuit, suitable for use in audio frequency amplifiers, which permits distortionless operation over a wide temperature range, is described. Temperature compensation at the transistor is provided by a series coupled positive temperature coefficient resistor and negative temperature coefficient thermistor bias divider network. The resistor tends to linearize the response of the thermistor at higher temperatures and to add cumulatively to the response of the thermistor at low temperatures, offsetting changes in transistor conduction characteristics.

Ruby Maser Millimeter Amplifier - See 10,502

10,532 TRANSISTOR IF AMPLIFIER USING DOUBLE-TUNED COUPLING TRANSFORMERS by D. L. Jones (Mullard Semicon. Measurement and Appl. Lab.); Mullard Tech. Commun., Vol. 5, No. 47, pp. 259-275, Mar. 1961

The design of a two-stage, 470 kc, IF amplifier using OC45 transistors and double-tuned transformers is described. The circuit uses two double-tuned and one single-tuned transformers as coupling elements between stages. An over-all nominal gain of 53 db (63 db, exluding the loss in the first IF transformer) can be obtained with a satisfactory margin of stability during and after alignment even with the worst possible spread in transistor characteristics. The effect of AGC on over-all bandwidth is found to be small, and the bandpass characteristics are about -3 db at ± 3 kc and -35 db at ± 9 kc.

10,533 A UNIDIRECTIONAL AMPLIFIER WITH ESAKI DIODES by W. J. Grubbs (Bell Labs.); IRE Trans., Vol. ED-8, pp. 163-169, Mar. 1961

An Esaki diode amplifier, which can furnish unidirectional amplification when used in conjunction with a Hall-effect isolator, is described. The input and output impedances of this amplifier are greater than the absolute value of the negative resistance of the diodes by a factor which is proportional to the voltage gain. The voltage gain-bandwidth product of such an amplifier is $g_T/4\pi RC$, where g_T is determined by the isolator and RC is the usual RC time constant of the Esaki diodes. Typically, g_T is between 0.1 and 1. If one of the diodes is removed, the remaining network still amplifies unilaterally, but the impedance at the diode-less end drops to that of the isolator alone. It is noted that a Hall-effect gyrator or circulator can be made essentially lossless by the addition of Esaki diodes.

10,534 A NEW DESIGN APPROACH FOR FEEDBACK AMPLIFIERS by M. S. Ghausi and D. O. Pederson (U. California); Proc. Symp. Active Networks and Feedback Systems Polytechnic Press, 1961, pp. 155-177

A new design procedure for feedback amplifiers through which closed loop bandwidth, gain amount of feedback and response shape specifications can be realized is described. The amount of feedback obtainable is at least as large as through conventional procedures. It is also possible in principle to achieve designs in which not only the low-frequency or long-time response is desensitized, but also the high-frequency or short-time effects such as rise time and minimum overshoot. Transistor amplifiers are used as a focal point in developing the design procedure. Initially a dominant pole model for the transistors is assumed. For such models root locus techniques are used together with "Phantom Zeros", the transmission zeros of the feedback path. Of the natural frequencies of the idealized closed-loop amplifier, two can be made dominant. The loci of these dominant natural frequencies tend to terminate at the phantom zeros. This assures large densitivity of both the short-time and long-time response characteristics. In both analytical and experimental evaluations of the design procedures, the effects of imperfections of the transistor model are troublesome and can lead to instability. These effects can be remedied by more complicated passive structures in the amplifier or alternate bounds can be established on the validity of the first-order design procedure.

Parametric Diodes for High Frequency Applications - See 10,475

10,535 DESIGN AND PERFORMANCE OF A 450 Mc PARAMETRIC AMPLIFIER by D. J. Mudgway (Weapons Res. Est.); Proc. IRE Austral., Vol. 22, pp. 167-173, Mar. 1961

The design and performance of a 450 Mc parametric amplifier using the up-convertor configuration is described. The bandwidth is 12 Mc and the noise figure and gain of 1.5 db and 9 db respectively are in agreement with theoretical prediction. Some of the problems involved in carrying out measurements on the amplifier and its practical application are discussed.

10,536 TRAVELING-WAVE PARAMETRIC AMPLIFIER ANALYSIS USING DIFFERENCE EQUATIONS by H. Zucker (Armour Res. Found.); Proc. IRE, Vol. 49, pp. 591-598, Mar. 1961

A second-order difference equation is derived for both periodically and uniformly distributed parametric amplifiers. Using a two-frequency approximation the gain and the voltage output of the amplifier are computed. The results are specifically applied to an LC-distributed parametric amplifier and the gain computed for a capacity modulation index of 0.5, and for different normalized pump frequencies.

10,537 ON STABLE PARAMETRIC AMPLIFIERS by F. A. Olson (AF Cambridge Res. Labs.); Proc. IRE, Vol. 49, pp. 629-630 (L), Mar. 1961

The stabilization of traveling wave parametric amplifiers by utilizing distributed ferrite isolators is discussed. The isolation should be equal to or greater than the net forward gain and the insertion loss should be small; the bandwidth should extend over the range of signal, idler, and pump frequencies. The distributed isolator does not affect the noise performance of the amplifier and provides some isolation between diodes, which reduces the effect of internal reflections. The structure recently developed by Anderson and Hines is suggested for use in traveling wave parametric amplifier circuits.

10,538 SHOT NOISE IN TUNNEL DIODE AMPLIFIERS by

J. J. Tieman (GE Res. Lab.); Proc. IRE, Vol. 49, pp. 622-623(L), Mar. 1961

Chang's method of relating the IR product of an I-V characteristic to the noise performance of a tunnel diode amplifier [see abst. 6261] is questioned. The second derivative of the I-V characteristic does not affect the minimum IR product, nor is a low value of I_m required to assure a low $(IR)_{min}$. Several assumptions about tunnel diode characteristics from which Chang draws his conclusions about an ideal characteristic for a low possible IR product are called arbitrary. The second and third derivatives of the I-V characteristic are correct only for Chang's free hand sketches. They are not, however, typical of Ge, GaAs, GaSb or Si tunnel diodes and hence his dI^2/dV^2 disagrees with experiment, and dI^3/dV^3 may even be of opposite sign in the region of interest. The simultaneous occurrence of a small first derivative together with a large second derivative is insufficient to guarantee a small $(IR)_{min}$ since this situation has to apply at V_m and one is not free to choose V_m.

10,539 THEORY OF NONRECIPROCAL CIRCUITS WITH EQUAL INPUT AND OUTPUT FREQUENCY USING NONLINEAR SEMICONDUCTOR DEVICES [in German] by R. Maurer and K-H. Löcherer (Telefunken); Arch. Elekt. Uebertragung, Vol. 15, pp. 71-83, Feb. 1961

The four pole and the transducer gain equations for nonreciprocal amplifiers consisting of cascaded tunnel diode up- and down-converters are derived. If the tunnel or parametric diodes are fed with pump voltages of different phases, decoupling between output and input can be achieved by means of an additional linear, passive and reciprocal coupling admittance. For mixed devices containing one tunnel diode and one parametric diode such decoupling between output and input is possible even for pump voltages of equal or opposite phases. In the non-inverting case power matching at the input and output is always possible. If two tunnel diodes or one tunnel diode and one parametric diode are used, the numerical transducer gain in the forward direction can exceed unity if the pump power is properly chosen. With two parametric diodes the device operates as an isolator. In the inverting case the value of the numerical transducer gain can always be made to exceed unity, but simultaneous power matching at input and output is then possible only with the use of two tunnel diodes.

10,540 TRANSISTOR AMPLIFIER CIRCUIT by R. J. Molnar (Bendix); U.S. Pat. 2,977,546, Issued Mar. 28, 1961

A technique for increasing the voltage gain and input resistance and decreasing the output resistance of a common emitter amplifier is described. These results are obtained by connecting the biasing resistors so that they do not shunt the circuit input or output. It was found in a particular circuit that the technique increased the voltage gain 23 per cent and the input resistance 71 per cent.

Magnetic Core Amplifier - See 10,572

10,541 NOTE ON HIGH INPUT IMPEDANCE SINGLE TRANSISTOR STAGES by J. H. Giddy (U. Melbourne); Proc. IRE Austral., Vol. 22, pp. 174-177, Mar. 1961

Three circuits are presented and analyzed in regard to input impedance, low noise characteristics and frequency response. The unbypassed emitter resistor configuration is used with the base biasing resistor split and a capacitor connected from the junction to the emitter. The divider resistance is in shunt with the emitter resistor, allowing practical values of resistance for temperature stability without seriously degrading the input resistance. The second circuit is the standard bypassed emitter resistor. In the third circuit, the input is applied between collector and base. The circuit has a high input impedance and low noise figure, but neither side is grounded. A mathematical analysis of each circuit is presented and theoretical values and experimental results given.

OSCILLATORS

Ruby Maser Millimeter Oscillator - See 10,502

10,542 THE SATURATING CORE OSCILLATOR by H. S. Wragge (Postmaster-General's Dept.); Proc. IRE Austral., Vol. 22, p. 185(A), Mar. 1961

The theory and operation of the saturating core oscillator using square loop core material was considered briefly. The behavior in the case where conventional transformer materials such as mumetal or stalloy is used was discussed. The effects of load and transistor characteristics on frequency stability was examined, and methods of controlling this were indicated. Various commonly used starting circuits were examined in detail and certain design procedures were suggested. The complete design and performance of a small 400 cycle oscillator was described in detail.

SWITCHING CIRCUITS

10,543 DETECTION OF DISJUNCTS OF SWITCHING FUNCTIONS AND MULTI-LEVEL CIRCUIT DESIGN by A. Mukhopadhyay (U. Calcutta); J. Electronics Control, Vol. 10, pp. 45-55, Jan. 1961

A method for the detection of component functions of fewer number of variables, disjunct of which forms a given switching function, is described. The multi-level electronic circuit synthesized from the component functions yields better economy in several cases with regard to the number of logical circuit elements compared with the case when the same function is synthesized from the "minimal" two-stage forms.

10,544 A LOW-LOSS SEMICONDUCTOR MICROWAVE SWITCH by D. L. Rebsch (Westinghouse Elect.); Proc. IRE, Vol. 49, pp. 644-645(L), Mar. 1961

A microwave switch in which a semiconductor diode is mounted in the arm of symmetry of an H-plane tee is described. A IN419 diode exhibits 14 db peak isolation, with less than 0.1 db insertion loss and 1.08 VSWR. A switch in which the same diode was mounted in the center of the transmission line had a 28 db peak isolation, with a minimum insertion loss of 0.7 db and 1.3 VSWR. The isolation in the tee switch as a function of frequency for fixed position of the diode and the sliding short which blocks the symmetry arm is discussed. For a fixed position of the diode, the short may be tuned to give a maximum

isolation for any frequency in the range. Mounts may be cascaded to produce higher isolations or wider bandwidths than a single mount.

10,545 ONE-TUNNEL-DIODE FLIP-FLOP by R. A. Kaenel (Bell Labs.); Proc. IRE, Vol. 49, p. 622(L), Mar. 1961

A flip-flop circuit comprising a single GaAs tunnel diode is described. A series resistor that intersects the static tunnel diode characteristic in two stable points is used. A timing inductor is placed in series with the resistor and diode. The trigger pulse consists of a large negative trigger with a slight positive pip. The negative portion switches the diode from a high to a low voltage state. The inductor time constant is larger than the trigger pulse duration to prevent reswitching by the positive trigger excursion. The positive portion of a subsequent trigger pulse switches the diode to its high voltage state. The circuit is ready for retriggering after the inductor current decreases to its quiescent level.

10,546 A TUNNEL DIODE UNIVIBRATOR AND PULSE HEIGHT DISCRIMINATOR by Y. Hazoni (C.E.N.); Nuc. Instr. Methods, Vol. 10, pp. 231-233, Mar. 1961

A univibrator and a pulse height discriminator using tunnel diodes and backward diodes and their application in pulse shaping and fast coincidence circuits are described. The main advantages of the circuits are simplicity of design and speed of operation.

10,547 D-C VOLTAGE COMPARATOR CIRCUIT USES TUBE AND TRANSISTOR by R. D. Valentine (Avco); Electronics, Vol. 34, p. 66, June 16, 1961

A hybrid dc comparator circuit, which compares a long-duration sawtooth input with a dc reference and generates a pulse when the two inputs coincide, is described. A dc reference voltage is applied to a cathode-follower. A Zener diode in the cathode sets the voltage across a transistor comparator. The transistor reference voltage follows the input reference voltage, while the voltage across the transistor remains constant; the transistor is normally saturated. A sawtooth input is applied to a second cathode-follower and when the sawtooth voltage exceeds the reference voltage, a diode conducts, reducing the transistor base drive to cutoff to produce an output pulse. The sawtooth duration range is from a few microseconds to several minutes.

10,548 OUTPUT-COUPLING NETWORKS FOR USE WITH LOGICAL CIRCUITS OF THE EMITTER-CURRENT SWITCHING TYPE by R. J. Miles (Mullard); Mullard Tech. Commun., Vol. 5, No. 47, pp. 295-300, Mar. 1961

Coupling networks, emphasizing zener-diode coupling with catching diodes to define the output-signal amplitude, are discussed. This system is one of the easiest to design, and is very satisfactory in practice. Practical circuits embodying this type of network are cited. Disadvantages of passive output-coupling networks are that the coupling efficiency is low when allowance is made for limit circuit parameters and the coupling networks increase cost without performing any additional logical function. Against these disadvantages is set the greater versatility of the standard logical elements which results from the use of the coupling networks.

Diode Logic Switching Circuits - See 10,570, 10,571

Cryosistor Switch - See 10,490

SIGNAL CONVERTERS

10,549 DIODE DETECTOR WITH FILTER by S. Vojtásek; Czech. J. Phys., Vol. B11, p. 305(A), 1961

A circuit of a detector with a semiconducting diode and a filter is derived. The derivation is carried out from the point of view of the theory of non-linear differential equations by the method of a small parameter. The problem of the approximation of the characteristics of the semiconducting diode used is analyzed, relations are given determining the steady state of the output current of the detector and conditions are found for the asymptotic stability of this steady state. Higher approximations for the periodic solution of the differential equation determine the residual alternating component of the output current of the detector. On the basis of this, the question of the filtration ability of a filter behind the detector is discussed. The results of the calculations are adapted for practical use.

Tunnel Diode Pulse Height Discriminator - See 10,546

FILTERS

10,550 DESIGN DATA FOR BAND-PASS LADDER FILTERS EMPLOYING CERAMIC RESONATORS by R. C. V. Macario (IBM Brit. Labs.); Electronic Engrg., Vol. 33, pp. 171-177, Mar. 1961

Piezoelectric ceramics which have high electromechanical coupling coefficients and medium Q factors, when in the shape of small circular disks resonating in a radial mode and in conjunction with or without capacitors, utilized in band-pass ladder filters are described. Design feasibility data for a variety of networks are examined and given in the form of graphs with tables of exact design data. These are based on image parameter theory, the justification of which is established by comparing actual filter responses. The ranges of centre frequency, bandwidth and image impedance achievable are discussed.

10,551 THE EFFECT OF TOLERANCES IN THE ELEMENTS OF IMAGE PARAMETER FILTERS by J. W. Scholten (Philips); Philips Telecommun. Rev., Vol. 22, pp. 63-77, Jan. 1961

The effect of deviation in the elements of image parameter ladder filters on attenuation, phase shift and input impedance is calculated. A number of simple approximative formulae are derived. The pass-range attenuation of a filter is affected by reactive deviations of the elements practically only in those frequency ranges where a mismatch exists between the filter and its terminating impedances. When matching is satisfactory, the phase shift and the input impedance in the pass range are considerably more sensitive to reactive deviations of the elements than the attenuation. An example of calculation for a simple bandpass filter is given, and the results of tuning the filter circuits are discussed. Finally the conjecture is put forward that the attenuation in the pass range of filters that are

not terminated at one end is more easily affected by reactive deviations in the elements than it is in filters terminated at both ends. The appendix gives formulae for calculating the tolerances in different filter sections.

10,552 A FILTER SYSTEM WITH FAVORABLE IMPULSE PROPERTIES [in German] by K. Uhl (Tech. Hochsch. Stuttgart); Arch. Elekt. Uebertragung, Vol. 15, pp. 109-114, Mar. 1961

To supplement the relationships known from system theory between the transmission performance and the pulse performance of a filter, an analysis of a filter arrangement as devised by W. Wolman is given. Simple relations are derived for determining the poles of the transfer function on the basis of given pulse criteria. The regularity of the locations of these poles permits a simple method for realizing the pulse filter by a branch circuit with exact consideration of the losses in the circuit components. This special circuit yields a very simple equation for determining the pulse amplitude.

10,553 MODULATION IN NONLINEAR FILTERS WITH PARAMETRIC FEEDBACK by D. A. Robinson (Airpax Electronics); IRE Trans., Vol. CT-8, pp. 60-66, Mar. 1961

A class of nonlinear second-order filters which may be described and analyzed by the theory of quasi-linear differential equations is considered. It is shown that the effect of nonlinearity in these equations is equivalent to that obtained by parametric feedback where the system parameters are functions of the output amplitude. This leads to an extension of the filter class by admitting phase parametric feedback. Filters of this class exhibit startling characteristics in comparison with the behavior of LLFPB circuits. The methods of Mandelstam and Papalexi, and Andronow and Witt in complex notation underlie the derivations. After examining the solution under sinusoidal inputs, the more interesting problem of modulation response is considered. Under small signal conditions a second-order linear differential equation with complex coefficients is derived to describe the modulation response. One example is offered of a filter with phase feedback that discriminates between amplitude and phase modulation by passing the former and rejecting the latter.

APPLICATIONS OF SOLID STATE DEVICES

SCIENTIFIC, MEDICAL, AND COMMERCIAL

10,554 A RUBY MASER RADIOMETER, AND THE MEASUREMENT OF CENTIMETER WAVE RADIATION FROM VENUS, MARS, AND JUPITER by J. A. Giordmaine (Columbia U.); Diss. Abstr., Vol. 21, pp. 2760-2761 (A), Mar. 1961

The measurement of radiation at 3 cm wavelength associated with the planets Venus, Mars, and Jupiter by means of a maser type radiometer in conjunction with the U.S. Naval Research Laboratory 50 ft reflector was discussed. The radiometer utilized a ruby maser preamplifier of the three-level type proposed by Bosov and Prokhorov and by Bloembergen. The over-all input noise temperature of the radiometer was 85°K, including contributions from antenna spillover and from atmospheric radiation. This noise level represents an enhancement in sensitivity of about 12 over a comparable superheterodyne radiometer. The theory of maser amplification and noise is applied to the maser preamplifier. The observed gain in sensitivity was found to be in good agreement with theory.

10,555 MEDICAL ELECTRONICS PART IV: PROSTHETICS — HEARING AIDS AND BLIND GUIDANCE DEVICES by W. E. Bushor (Associate Ed., Electronics); Electronics, Vol. 34, pp. 43-49, June 23, 1961

A broad survey of electronic hearing aids for the deaf and of guidance devices for the blind is presented. The two major types of hearing defect, perceptive impairment and conductive deafness, are described, together with the principal features of various kinds of hearing aids and the corresponding products of major manufacturers. A list of different approaches to the design of guidance devices for the blind is given. Several experimental systems are included.

10,556 THE SIGNAL SENTRY: A SOLID STATE MONITORING AND ALARM SYSTEM by M. L. Klein and J. P. Hart (Commun. Control); Electronic Engrg., Vol. 33, pp. 344-348, June 1961

A monitoring system for use in process control, medical work, and quality checking is described. The "Signal Sentry" provides 0.1 per cent monitoring accuracy on multiple input dc levels. In addition, internal monitoring of the unit itself on twelve critical voltages is provided. The unit consists of a solid state multiplexor, all transistor digital voltmeter, and utilizes punched card programming and logic. All data that agrees with the program is discarded. Thirty channels can be scanned in less than 300 msec permitting use for critical process control.

AERONAUTICAL AND SPACE

10,557 AN AUTOMATIC CHECK-OUT AND RECORDING NETWORK by R. Mansey (De Havilland Aircraft Ltd.); Elect. Engrg., Vol. 33, pp. 284-291, May 1961

An existing British automatic check-out equipment, designed for a missile system, which has proved suitable for any aircraft or similar system where the parameters are predominantly electrical is described. The methods of accepting the input signals are discussed, together with selection and comparison with a standard. The design of a unique self-balancing potentiometer is described, showing how the standardized input is used to operate a bidirectional staircase generator until parity is reached between the staircase output and the input. A brief summary of the application of the equipment to the check-out of aircraft is given.

10,558 BEACON TRANSMITTERS AND POWER SUPPLY FOR ECHO 1 by J. G. McCubbin and H. B. Goldberg (RCA); RCA Rev., Vol. 22, pp. 147-161, Mar. 1961

Transmitters and power supplies for "Echo 1", a 100-foot-diameter passive communication satellite designed to reflect radio waves, are discussed. The special beacon transmitter and power

supply were designed for attachment to the external surface of the satellite. The beacon permits tracking of the satellite and assists in establishing ephermeris data. A design was required which would be compatible with the folding and packing procedures for the satellite and which would operate reliably in space environment after withstanding the rigors of launching. The transmitter, which produces an output of 5 to 10 mw at 107.94 Mc, is mounted along with silicon solar cells, batteries, and antenna on a 10-inch diameter printed circuit board. The package is 0.35 inch thick and weighs 11 ounces.

10,559 ULTRA-LOW-NOISE ANTENNA AND RECEIVER COMBINATION FOR SATELLITE OR SPACE COMMUNICATION by R. W. DeGrasse, D. C. Hogg, E. A. Ohm, and H. E. D. Scovil (Bell Labs.); Proc. Natl. Electronics Conf., Vol. 15, pp. 370-379, 1959

An ultra low-noise receiving system formed from a combined traveling-wave solid state maser and low side-lobe reflector antenna is reported. In satellite or space communications, where the antenna is 10° or more above the horizon, this receiving system gives a hundred-fold improvement over present equipment. A zenith sky temperature of 2.7°K at 6 kMc was calculated. The actual value was measured, using the low-noise receiving system, by rotating the antenna and noting the sky-noise variation. From this measurement a zenith sky temperature of 2.5 ± 0.75°K was determined. Improvements under way in the laboratory indicate the feasibility of systems having an over-all noise temperature of 7.5°K at 6 kMc and of 5°K at 2 kMc, respectively.

10,560 TRANSISTOR EQUATORIAL SATELLITE STUDIED FOR EUROPEAN-AFRICAN COMMUNICATION by A. Erikson (McGraw-Hill World News); Electronics, Vol. 34, pp. 26-27, June 23, 1961

The possibilities of adapting a communications satellite to European-African needs is studied. A 33-lb transistor satellite will be put in a synchronized equatorial orbit. The satellite would provide coverage for all of Europe, Africa and the Middle East plus part of South America. This communication system would have a high number of low-capacity telephone channels. Ground to satellite transmission would be in the 460 Mc channel. Satellite to ground transmission would be at 2,000 Mc with 23 Mc bandwidth.

Satellite-Borne Cosmic Radiation Counter - See 10,600

Solar-Cell Power Supply for Satellite - See 10,588

TELEVISION

10,561 THE INFLUENCE OF ALLOY DIFFUSED TRANSISTORS ON DOMESTIC TELEVISION RECEIVER DESIGN by J. R. Goldthorp (Mullard-Austral. Pty. Ltd.); Proc. IRE Austral., Vol. 22, p. 187(A) Mar. 1961

Performance capabilities of alloy diffused transistors in the HF and fast rise time sections of television receivers were discussed. Some interim techniques which have been devised to ease the requirements imposed by normal circuit configurations on transistors impressed for television applications were evaluated. Other application problems appeared more readily solved by modification of existing ancillary components. These trends were discussed with a view towards establishing a clearer over-all picture for the Television Receiver Design Engineer.

TELEMETRY

10,562 A FORTY-EIGHT CHANNEL PULSE SELECTOR FOR THE AUSTRALIAN DME SYSTEM by P. W. Headford (Amalgamated Wireless, Australasia); Proc. IRE Austral., Vol. 22, p. 185(A), Mar. 1961

A new transistorized pulse selector that decodes 48 pulse-duration/pulse-separation codes, and generates a response to the selected code was discussed. The techniques which provide precise timing were reviewed.

10,563 DEVELOPMENT OF A COMMERCIAL TRANSISTORISED DME SET FOR AIRBORNE USE by F. R. Hall, B. R. Johnson (Amalgamated Wireless, Australasia); Proc. IRE Austral., Vol. 22, p. 185(A), Mar. 1961

The development of a production prototype transistorized DME set was described. The design not only provides an equipment of light weight and low power consumption, but a considerable improvement in precision, reliability, and maintenance requirements, has been achieved, when compared with the existing set. Some of the techniques used were described in detail.

10,564 A TRANSISTORIZED AIRBORNE RECEIVER FOR THE AUSTRALIAN DME by J. Ward (Amalgamated Wireless, Australasia); Proc. IRE Austral., Vol. 22, p. 185(A), Mar. 1961

A brief outline of a 224 Mc airborne receiver was given. A more detailed description was presented on the novel 30 Mc IF amplifier; this IF stage comprised a multi-section band-pass filter, followed by a six-stage broad-band transistor amplifier. The advantages of this approach were discussed.

MICROWAVES AND ULTRAMICROWAVES

450 Mc Parametric Amplifier - See 10,535

Ruby Maser Millimeter Amplifier - See 10,502

Ferrite Microwave Devices - See 10,495

DIGITAL COMPUTERS

10,565 THE PHILIPS COMPUTER PASCAL by H. J. Heijn and J. C. Selman (N.V. Philips); IRE Trans., Vol. EC-10, pp. 175-183, June 1961

PASCAL, a binary parallel computer with a word length of 42 bits, a clock-pulse repetition time of 1 1/2 μsec, that performs on the average, 60,000 operations/sec is described. Wired-in floating-point facilities are provided. Core storage is backed by a drum and by magnetic tape. Modification versions for indexing as well as for stepping-up purposes are given. Special instructions include count and repeat instructions, jumps on the results of an earlier comparison, and two kinds of link

instructions for facilitating the use of subroutines and interpretative programs. Transfer instructions enable a simultaneous bidirectional data flow between drum and cores or between tape and cores while computations are going on.

10,566 A SEMICONDUCTOR BINARY COORDINATE CONVERTER by M. F. Williams, A. F. Thornhill, and W. A. Richards (Naval Res. Lab.); U.S. Gov. Res. Rep., Vol. 35, p. 324(A), Mar. 10, 1961 PB 149 297

The characteristics of a semiconductor binary digital coordinate converter are discussed. This equipment converts 18-bit polar-coordinate data to 20-bit rectangular-coordinate data in three milliseconds. The equations used are: $X = \rho \sin\Theta$ and $Y = \rho \cos\Theta$. Sine Θ and cosine Θ are obtained by the use of a rectangular diode matrix and diode trigonometric function tables; X and Y are obtained by summing partial products in a parallel accumulator type multiplier. The converter occupies a volume of less than two cubic feet and requires one ampere at 20 volts and 200 milliamperes at 90 volts. Methods of increasing the operating rate of the converter are considered.

10,567 LINEAR-INPUT LOGIC by R. C. Minnick (Stanford Res. Inst.); IRE Trans., Vol. EC-10, pp. 6-16, Mar. 1961

Techniques for the logical design of magnetic core circuits to produce arbitrary single-output combinational switching functions are developed. The approach is based on the relationship of a single magnetic core circuit to a linearly separable switching function. A synthesis procedure which uses a pair of logical primitives, AND with NOT and OR with NOT, which are similar to the STROKE primitive and its inverse, is developed. Procedures for the synthesis of symmetric functions which require no more than the integral part of $(n + 3)/2$ cores, approximately half the number used in previously published procedures, are given. The synthesis of arbitrary switching circuits is treated as a linear programming problem, and a table of all four-variable circuits in which no circuit requires more than three cores is presented.

10,568 LOGIC CIRCUITS USING SQUARE-LOOP MAGNETIC DEVICES: A SURVEY by J. L. Haynes (Precision Instr.); IRE Trans., Vol. EC-10, pp. 191-203, June 1961

This survey is a capsule view of twenty-four square-loop magnetic logic circuits which have been proposed or developed so far, with a brief description of the way each circuit or circuit family meets the requirements of logic circuitry. All circuits are treated with a consistent terminology, and the generic relationships among circuits are stressed. Included in this survey are parallel and series transfer core-diode schemes, core-transistor schemes, and all-magnetic schemes of various topologies.

10,569 POSSIBILITIES OF ALL-MAGNETIC LOGIC by U. F. Gianola (Bell Labs.); J. Appl. Phys., Suppl. to Vol. 32, pp. 27S-34S, Mar. 1961

A sequential logic circuit must have a capacity for memory undirectionality, and gain. The problem of obtaining these features in magnetic components is considered, and several approaches are described. The organization of a circuit using multiapertured cores is discussed, and a method for introducing added combinational logic in a compatible manner is described. The status of these techniques is summarized.

10,570 HIGH-SPEED LOGIC CIRCUITS USING DIODE LOGICAL NETWORKS AND CURRENT-SWITCHING AMPLIFIERS by R. J. Miles (Mullard); Mullard Tech. Commun., Vol. 5, No. 47, pp. 286-294, Mar. 1961

Practical examples of diode hybrid circuits and circuit performance and design considerations are discussed. It is shown that although satisfactory results may be achieved, worst-limit design yields circuits unattractive as regards power dissipation and close-tolerance components. Circuit capacitances become a major factor when switching times of less than 50 nsec are required, and it is felt that the limiting switching-time of hybrid circuits will be about 10 nsec, even if greatly improved transistors and diodes or circuit techniques are employed. Logic circuits employing only transistors are expected to have a slightly lower limiting switching time.

10,571 ESAKI DIODE NOT-OR LOGIC CIRCUITS by H. S. Yourke, S. A. Butler, and W. G. Strohm (IBM); IRE Trans., Vol. EC-10, pp. 183-190, June 1961

A basic technique enabling the development of Esaki diode NOT-OR logic circuits is presented. Two embodiments of the basic scheme are discussed, which, when combined with an OR-DELAY circuit, provide a logically complete system. Emphasis is placed on the more economical of the two embodiments. A tolerance analysis which demonstrates that the technique enables the practical design of logic circuits is included. The requirements placed on Esaki diode characteristics and the speed limitations of the circuits are discussed. Examples of working circuits, including photographs of voltage wave shapes are shown.

10,572 THE CORE AMPLIFIER, A BASIC CIRCUIT FOR ELECTRONIC SWITCHING EQUIPMENT by H. Kok (Philips); Philips Telecommun. Rev., Vol. 22, pp. 81-93, Jan. 1961

A core amplifier, consisting of a transistor and a ferrite core assembly, is described. The principle and design of this storage and switching element are discussed, and various applications in logical circuits such as counting circuits, code converters and circuits for matrix control are described. Finally, a description is given of a method for the supervision of logical circuits made up of core amplifiers.

10,573 MATRIX SWITCH AND DRIVE SYSTEM FOR A LOW-COST MAGNETIC-CORE MEMORY by W. A. Christopherson (IBM); IRE Trans., Vol. EC-10, pp. 238-246, June 1961

A unique system of ferrite-core matrix switches and drivers for a low-cost magnetic-core memory is reported. The memory uses coincident-current techniques and has a capacity of 10,000 characters with seven bits per character. A 20-μsec read-compute-write cycle features serial-by-character processing. Computing time is approximately 7μsec, and read-write time is 13μsec. The matrix switch requires only two sets of five drivers to select one out of 100 individual outputs. The drivers operate in an unusual three-out-of-five coding arrangement. A Set and a Reset driver, each using four transistors in parallel, are also required for the matrix switch. Two matrix

switches provide the 200 X-Y half-select drives for a 100 x 100 seven-plane core array. At read time, two half-select current pulses of 250 ma to 300 ma are emitted with an effective 10 per cent to 90 per cent rise time of 0.3μsec. At write time, half-select current pulses with 1.2μsec rise time are emitted on the same selected lines, but in the opposite direction. A new method of timing the drive current allows the read pulse to rise in 0.3 μsec, even with a low-voltage power supply and an inductive load that would otherwise limit the rise time to 0.8μsec. All current-driving circuits use alloy junction transistors. The drive current is furnished from a 10 to 12 v power supply, and temperature compensation of the drive currents is accomplished through control of power-supply voltage. Operating temperatures range from 10°C to 40°C.

10,574 CIRCUIT WITH SEVERAL STABLE STATES UTILIZING TUNNEL DIODES [in French] by Y. Hazone (C.E.N.); Nuc. Instr. Methods, Vol. 10, pp. 229-230, Mar. 1961

A tunnel diode circuit which has four stable states is discussed. The time needed for a change of state is of the order of 10^{-8} sec. The circuit could be utilized as a fast prememory for a multichannel analyzer. Since it can count recurrent pulses with repetition rates up to 40 Mc it can also serve as the basic unit for the address scaler associated with such analyzers.

10,575 MULTIAPERTURE-CORE COUNTERS GIVE NONDESTRUCTIVE STORAGE READOUT by W. R. Johnston (Ampex); Electronics, Vol. 34, pp. 62-64, June 16, 1961

A multiaperture-core counter with nondestructive readout, combined with a time-logic matrix which stores command times, is described. A stage consists of two multiply-wound cores with a transistor connected as a blocking oscillator. The first count pulse switches both cores; a reset pulse then resets core one. The second count pulse switches core one, gating the blocking oscillator which drives the next stage and resets core two; a second reset pulse then resets core one. The maximum repetition rate depends on the length of the counter, the propagation delay and the pulse width. A 22 stage counter has been operated at 40 kc. Nondestructive readout is obtained by inserting read and sense windings in holes in the cores. A count pulse sets up the flux conditions around the small hole. An interrogate pulse reverses the flux around the small hole, inducing a pulse in the sense winding. A reset pulse then returns the flux to its initial state. When the counter reaches a time set into a matrix word, a comparison circuit produces a command pulse. The counter can be read serially or in parallel.

10,576 A MAGNETIC ASSOCIATIVE MEMORY by J. R. Kiseda, H. E. Petersen, W. C. Seelbach, and M. Teig (IBM); IBM J. Res. and Dev., Vol. 5, pp. 106-121, Apr. 1961

A computer storage system in which data flows in and out of the memory on the basis of content rather than location (address) is described. A small experimental model of this system, using ferrite cores as novel associative memory storage elements, is discussed.

Magnetic Excitation of Thin Film Ferromagnetic Storage Devices - See 10,496

10,577 RECORDING AND REPRODUCTION OF NRZI SIGNALS by R. S. Schools (IBM); J. Appl. Phys., Suppl. to Vol. 32, pp. 42S-43S, Mar. 1961

A theoretical study of a saturation type of recording and reproduction in digital magnetic tape systems is described. The dependence of tape magnetization and of output signal pulse width and amplitude on the major system parameters has been investigated and determined. These parameters are the magnetic field distribution of the recording head, write current waveform, tape thickness and hysteresis characteristics, head-to-tape spacing, reading gap length, and bit density. A portion of this study concerns the extension of the sinusoidal theory to include the reproduction of signals resulting from saturation recording. This is done by a Fourier analysis of the tape magnetization and a term-by-term summation of harmonic responses to obtain the resultant signal. The results show why high writing field gradients, high tape B-H "squareness," and thin tapes are needed for high-density recording. They indicate possible reasons for EMF pulse peak position asymmetries during readback. Two examples of output calculations are included. One shows the signal amplitude and pulse width vs bit density, compared with experimental measurements. The other presents the field distribution above the magnetized tape, indicating the influence of the presence of the read head.

10,578 MAGNETIC FILM DEVICES USING PASSIVE LOADING by J. M. Daughton, T. A. Smay, A. V. Pohm, and A. A. Read (Iowa State U.); J. Appl. Phys., Suppl. to Vol. 32, pp. 36S-37S, Mar. 1961

Computer solutions of a pair of differential equations based on the Landau-Lifshitz model, which indicate that with passive loading, magnetic film devices may be used as storage and logical elements in digital computers, are reported. Experimental models of a flip-flop consisting of an RLC loaded film device show that successive 20 oe, 0.1μsec drive field pulses can switch the magnetization in the film alternately from one rest orientation to the other with repetition rates of the drive on the order of 10^6 pps. A nondestructive readout memory element consisting of an RL loaded thin film device is shown which allows films with H_k on the order of 3 oe to be driven in the hard direction by 15 oe, 0.05μsec field pulses without destroying the stored information, resulting in output voltages of approximately 25 mv per winding turn. Fabrication of a memory employing such elements by evaporation techniques is discussed.

Demagnetization of Twistors - See 10,513

10,579 A 2.18 MICROSECOND MEGABIT CORE STORAGE UNIT by C. A. Allen, G. D. Bruce and E. D. Councill (IBM); IRE Trans., Vol. EC-10, pp. 233-237, June 1961

A magnetic core memory which has a read-write cycle time of 2.18 μsec, an access time of 1 μsec, and a storage capacity of 1,179,648 bits is described. The array configuration and the design of the driving system are shown. The core and transistor requirements are discussed, and a description is given of the sensing and the driving circuitry. Design factors which governed the choice of the 3-dimensional system organization are presented.

10,580 IMPULSE SELECTION FOR CORE LOGIC by R. H.

Tancrell (Lincoln Lab.); J. Appl. Phys., Suppl. to Vol. 32, pp. 40S-41S, Mar. 1961

Impulse selection, a scheme for operating ferrite cores which have low values of coercive force, is discussed. Two different threshold properties of a core are utilized. One threshold is the dc coercive force, which can be changed electrically. The other threshold results from the inertial magnetic effects within the core which are predominant when pulses of very narrow widths are applied. The switching behavior of ferrite cores when two threshold currents, a low amplitude current and an impulse of current, are combined and the application of this property to core logic are considered.

10,581 FERRITE CORE STORAGE DEVICES IN ELECTRONIC EXCHANGES [in German] by G. Merz (Standard Elect. AG); Nachrichtentech. Z., Vol. 14, pp. 294-299, June 1961

A summary of the most important properties of ferrite cores, as well as of core store matrices, is given. The low frequency hysteresis loop of ferrite cores is investigated and a discussion of magnetization reversal time and read signal amplitude of the cores is provided. The parallel use of several store matrices and the resulting inhibition problem are also considered. The various possibilities for using such cores in fast access stores, in semi-permanent stores and as a means for sampling line conditions in exchanges are described.

Ferrite Core Circuit Analysis - See 10,499

Testing Magnetic Core Switching Times - See 10,498

Flux Distribution in Ferrite Cores - See 10,497

10,582 A MULTIPLE OUTPUT PRECISION TIME CODE GENERATOR by J. L. Harwood and F. A. Hinc (Weapons Res. Est.); Proc. IRE Austral., Vol. 22, p. 183(A), Mar. 1961

A time code generator having special application in data recording systems where a number of simultaneous records require accurate correlation and analysis at a later stage was described. Four separate width-modulated pulse trains are emitted continuously, each describing time but with different pulse repetition frequencies. The unit consists of a number of etched foil circuit cards and a power supply contained in a sheet steel cabinet suitable for rack or bench mounting. Continuous indication of time and date is given through slot windows in the door of the cabinet. Reference was also made to the transistor and cold cathode switching circuit techniques used in the generator.

ANALOG COMPUTERS

10,583 A STRAIGHTFORWARD WAY OF GENERATING ALL BOOLEAN FUNCTIONS OF N VARIABLES USING A SINGLE MAGNETIC CIRCUIT by K. V. Mina and E. E. Newhall (Bell Labs.); IRE Trans., Vol. EC-10, pp. 151-156, June 1961

A correspondence between the topology of relay contact networks and the topology of magnetic circuits, which may be applied to a relay tree to produce a magnetic structure capable of generating, in a simple manner, all Boolean functions of N variables is described. Once the basic magnetic topology is established, it may be distorted to achieve winding simplicity at the expense of magnetic circuit complexity. In the resulting arrangement, the drive, hold (variable) and reset windings are always in the same position, regardless of the function to be generated. Any one of the 2^{2^N} functions of N variables is generated by linking a selected group of the output legs. The structure is such that all switching paths are of equal length, causing all outputs to be equal in amplitude. This balanced arrangement also permits the holding MMF to be significantly smaller than the drive MMF. The holding scheme is a symmetrical one, specifically arranged to overcome shuttle flux problems and reduce noise. An 8-leg manganese-magnesium-zinc ferrite structure is operated easily at a 4-μsec cycle time with an output of 500 mv into 5 ohms. The peak-signal-to-peak noise ratio was at worst 8:1. The structure described is in a sense the complement of the laddic, in that the drive and hold windings are always applied in fixed positions and different functions are generated by linking different sets of output legs.

10,584 DIFFERENTIATION AND INTEGRATION WITH THE AID OF TRANSISTORS [in Czech.] by V. Spany; Elektrotech. Cas., Vol. 12, No. 2, pp. 99-111, 1961

New transistorized integrating and differentiating circuits are presented and a simplified analysis of their function is discussed. It is pointed out that the use of feedback is not advantageous and, in the case of integration, feedback is undesirable

10,585 A HIGH SPEED ANALOGUE TO DIGITAL CONVERTOR by N. Winterbottom and J. S. B. Walters (Armstrong Whitworth Aircraft Ltd.); Electronic Engrg., Vol. 33, pp. 144-149, Mar. 1961

A high speed analog to digital converter capable of performing 55,000 conversions per second from an analog voltage to an 8-bit binary code is described. The equipment uses transistors as the active elements.

10,586 HIGH-SPEED ANALOG-TO-DIGITAL CONVERTERS UTILIZING TUNNEL DIODES by R. A. Kaenel (Bell Labs.); IRE Trans., Vol. EC-10, pp. 273-284, June 1961

Two analog-to-digital sequential converters which combine in one tunnel-diode pair per bit the functions of an amplitude discriminator and memory are described. In addition, one of the two schemes utilizes each tunnel-diode pair as a delay network. The conversion duration of one of these six-bit converters, which employs germanium 2N559 transistors and gallium arsenide 1N651 tunnel diodes, has been set to 1μsec. Shorter conversion times are possible, but are not required in the present application of the converter as an integral part of an electronic high-speed signal processing system. The use of tunnel diodes presents a significant improvement in the art of converter design by virtue of circuit simplicity and performance. The principle and operation of the converters are described and pertinent design considerations are discussed. Particular emphasis is given to the discriminator property of series-aiding tunnel-diode pairs. A comprehensive bibliography relating to tunnel-diode switching circuits is attached.

10,587 SELECTIVE ERASURE AND NONSTORAGE WRITING IN DIRECT-VIEW HALFTONE STORAGE TUBES by N. H.

ANALOG COMPUTERS (Cont'd)

Lehrer (Hughes Res. Labs.); Proc. IRE, Vol. 49, pp. 567-573, Mar. 1961

A new type of direct-view halftone storage tube that can selectively erase as well as simultaneously display stored and nonstored information is described. A dual-effects target is used; one effect (secondary emission) charges the storage surface positively, while the other (bombardment-induced conductivity) charges it toward the backing-electrode potential, which in this case is negative. Selection of the effect and, consequently, the charging direction, is determined by the incident beam energy. At low energies secondary emission predominates and the target is written on, i.e., charged positively. At high energies, the bombardment-induced conductivity prevails and the target is erased, i.e., the positively charged areas are discharged. The two effects cancel at an appropriate intermediate beam energy, thus permitting presentation of nonstored information without otherwise disturbing the display, by means of that portion of the beam current which passes through the backing electrode and strikes the viewing screen. A 5-inch, direct-view halftone storage tube that utilizes such a dual-effects target is described and its characteristics are discussed.

Data Monitoring System - See 10,556

POWER

10,588 POWER SUPPLY FOR THE TIROS I METEOROLOGICAL SATELLITE by S. H. Winkler, I. Stein, and P. Wiener (RCA); RCA Rev., Vol. 22, pp. 131-146, Mar. 1961

The power supply system employed in the TIROS I satellite is discussed. The influence of the system performance requirements on power-supply design and thermal control methods is shown. Detailed discussion covers the problems of thermal control, solar-collector orientation with respect to the sun vector, the method of mounting solar cells to the vehicle surface, the electrical arrangement of the solar-cell circuitry, the solar-cell testing program, and the design factors employed in determining the size and shape of the solar collector. The storage battery is discussed with references to the battery testing program, electrical characteristics of the battery, and the basic factors which governed the battery design. Protective and regulatory circuit functions and specifications are given. Data is given on the performance in orbit of the solar cells, batteries, and thermal control. The factors affecting spatial orientation of the TIROS I satellite in orbit are also discussed. Graphical evidence is provided showing how telemetered solar-cell data compared with computed data on the satellite-to-sun orientation.

Power Generation by Irradiated Junctions - See 10,482

10,589 TRANSISTOR POWER INVERTER by H. E. Schultz (GE); U.S. Pat. 2,971,166, Issued Feb. 7, 1961

Four transistor power inverters in which the frequency of operation is determined by an LC resonant circuit are described. The use of the LC circuit results in an operating frequency which is independent of variations in the dc supply voltage or of changes in the load.

10,590 DC INVERTER FOR FLUORESCENT LAMPS by J. R. Nowicki (Mullard); Mullard Tech. Commun., Vol. 5, No. 47, pp. 276-285, Mar. 1961

A square-wave dc inverter is described which is suitable for driving one or two 40 w fluorescent lamps from a 28 v supply. The operating frequency is about 5 kc and the relative efficiency (compared with mains operation) about 82 per cent for the single-lamp circuit and nearly 100 per cent for the two-lamp circuit. The timing of the inverter is controlled by the decrease of base current, using a RC timing circuit. The peak collector current is very nearly equal to the load current, except for a small increase due to the magnetizing current of the linear (non-saturating) transformer. The inverter combines the advantages of square-wave inverters with low cost of the output transformer and safe operation under no-load conditions.

CONTROL

10,591 A NEW SOLID-STATE CONTROL SYSTEM by R. G. Davis (Siemens Edison Swan); Proc. IRE Austral., Vol. 22, p. 190(A), Mar. 1961

A system, developed to replace relays in nuclear reactor guard and interlock circuits, and applicable to other circuits in which relays have hitherto been used, was described. Trains of pulses are passed through a series of gated amplifiers which are held open by the demodulated sum of at least two out of three sources of pulses which are fed in via conventional trip contracts or from function amplifiers which themselves generate pulsetrains. The gated amplifiers are preferably arranged in a triple line; the pulses from all three lines can then be fed into a similar gated amplifier which in turn feeds a power amplifier which can act as a motor switch or a magnetic clutch release. In this way it is possible to arrange for, say, a flux trip to result in the release of a clutch without the intervention of any mechanical contacts. Systems of this type so far designed have been found to cost less than two-thirds of comparable relay systems. In addition they can be made fully fail-safe and immune to spurious trip; no routine maintenance is required, and great flexibility is available.

Data Monitoring System - See 10,556

10,592 CONTROL OF INDUSTRIAL PROCESSES BY ELECTRONIC COUNTING by D. J. Hancock (Philips Elect. Ind. Pty. Ltd., Sydney); Proc. IRE Austral., Vol. 22, p. 180(A), Mar. 1961

Pick-up systems which convert quantities, such as mass, length, time, etc., into electrical impulses were described. Counting systems, ranging from a simple single stage device to a complex predetermined counter with visual readout provided by numerical indicator tubes, were discussed. A comprehensive bibliography is included and a typical electronic counting system using plug-in units with cold cathode tubes and transistors was demonstrated.

INSTRUMENTATION

10,593 MINIATURE HALL PROBE MAPS MAGNETIC FIELDS

by D. D. Roshon, Jr. (IBM); Electronics, Vol. 34, pp. 68, 70, 71, June 16, 1961

A miniature Hall probe for magnetic mapping of small, sharply discontinuous structures is described. The sensitivity is sufficient to measure magnetic fields having an intensity less than 0.01 gauss. Two thin lines of bismuth are vacuum deposited on a glass slide. One line carries current perpendicular to the magnetic field. A Hall voltage proportional to field strength is developed in the other line. The output is linear within one per cent from 1-1000 gauss. Using 400μa probe current, the minimum detectable magnetic field is 0.25 gauss. Equivalent drift is less than two gauss in 24 hours. Fields down to 0.005 gauss can be measured with 20μa probe current, but thermal drift increases.

Application of Hall Generators in Measurement Devices - See 10,488

10,594 INSTRUMENTATION OF A SMALL NUCLEAR MAGNETIC SPECTROMETER by L. O. Bowen, E. Laisk, and K. H. Marsden (U. New South Wales); Proc. IRE Austral., Vol. 22, p. 189(A), Mar. 1961

A portable nuclear magnetic resonance spectrometer was described. The basic design requirements and characteristics of the associated electronic equipment was outlined. The NMR spectrometer is designed around a small permanent magnet, which has been modified to achieve homogeneity of the magnetic field. The circuitry of the following equipment was discussed: transistorized frequency standards, frequency modulation by means of voltage sensitive capacitors, transistor Q-multiplier and scanning methods. A demonstration was given of the performance and the uses of the NMR spectrometer.

10,595 SEMICONDUCTOR JUNCTIONS AS POSITIONAL INDICATORS OF RADIATION by L. W. Davies (Amalgamated Wireless, Australasia); Proc. IRE Austral., Vol. 22, p. 180(A), Mar. 1961

The lateral photovoltage in the plane of a non-uniformly illuminated semiconductor junction, and of the use of this effect in photocells to indicate the position of a small area of illumination by visible or infrared radiation, such as a light spot or line image was analyzed. An important consequence of the presence of a heavily doped p-region contiguous with an n-region was the enhancement by orders of magnitude of the effective lateral diffusion length for holes in the n-region. Reference was also made to a twin-junction structure, made by alloying to one side of a thin slice of semiconductor, which may also be used to indicate the position of a light spot between the junctions. A comparison of its sensitivity to small movements of the light spot was made with that of the lateral photovoltage diode. Experimental observations were in good agreement with theory.

Thermal Radiation Dielectric Bolometer - See 10,511

10,596 SOLID STATE COUNTERS FOR dE/dx AND TOTAL ENERGY MEASUREMENT AT CYCLOTRON ENERGIES by J. T. Heinrich and T. H. Braid (Argonne Natl. Lab.); Bull. Am. Phys. Soc., Ser. II, Vol. 6, p. 46(A), Feb. 1, 1961

Surface-barrier detectors, produced by evaporating gold onto n-type silicon, were described. Detectors of 1 cm^2 sensitive area have back currents of a few tenths of a microampere at a back bias of several hundred volts. With a charge-sensitive transistor preamplifier due to Higginbotham et al. such detectors have given a resolution width of 60 kev when used to detect α particles from natural sources. Counters of 200 ohm-cm silicon have been reduced to uniform thicknesses of 0.002 to 0.003 in for dE/dx measurements. They can be made sensitive essentially throughout their entire thickness. A resolution width of 10 per cent has been obtained for dE/dx from 43 Mev α particles. After allowance for noise pickup, this agrees well with a value of 7 per cent predicted by the simple theory of the fluctuation in the energy loss. Detectors made from 3000 ohm-cm silicon can be biased to 600 v; the thickness of the sensitive region then approaches 1 mm. The response of a dE/dx, E pair in use by the cyclotron group is linear up to the maximum available α-particle energy, 43 Mev. The resolution width observed, 1.1 per cent, is believed to be limited by the energy spread of the beam and is much better than can be obtained from scintillation detectors.

10,597 SIGNAL-TO-NOISE RATIO OF A P-N-JUNCTION RADIATION COUNTER by J. A. W. van der DOES de BYE (N.V. Philips); Philips Res. Rep., Vol. 16, pp. 85-95, Feb. 1961

The signal-to-noise ratio of the p-n counter is treated in detail. It is found that the spectral-line width caused by noise can be reduced to 3 kev and the discriminator can be set at 6 kev to reject most of the noise. These values are calculated for the case of a thermionic amplifier with RC pulse shaping and are determined mainly by the diode current noise, the tube shot noise and the total input capacitance, which together constitute a figure of merit for the p-n counter. The values found experimentally were about 1.5 times higher.

10,598 P-N JUNCTION SEMICONDUCTOR RADIATION DETECTOR FOR USE WITH BETA- AND GAMMA-RAY EMITTING ISOTOPES by N. A. Baily and J. W. Mayer (Hughes Aircraft); Bull. Am. Phys. Soc., Ser. II, Vol. 6, p. 107(A), Mar. 20, 1961

Detectors for high-energy charged particles and x- and gamma rays were discussed. Increase in energy deposited within the charge sensitive region was accomplished by an increase in the depth of the region. Silicon was diffused with a lithium impurity, and by ion-drift techniques a sensitive volume was established with a width of about 1 mm in comparison with the usual 10- to 100-μ width established when silicon is diffused with phosphorus. Approximate sensitivities to gamma and beta rays was given. On using Bi^{207}, both K and L levels were distinguished. By subtraction of the electron response the Compton edges may be observed.

10,599 MEASUREMENT OF DAMAGE IN A SILICON DIFFUSED JUNCTION FAST-NEUTRON DOSIMETER by W. A. Lindgren, O. J. Mengali (Battelle Mem. Inst.), and W. L. Weiss (GE); Bull. Am. Phys. Soc., Ser. II, Vol. 6, p. 107 (A), Mar. 20, 1961

The equivalence of fast-neutron induced damage in silicon p-n junction dosimeters to that in tissue was discussed. Both monoenergetic neutrons and fission spectrum neutrons hardened by

passage through water were used. The charge carrier lifetime of the device is sensitive to damage resulting from fast neutron irradiation. Annealing studies and calibration of the device with a standard flux have shown the characteristics to be reproducible within 5 per cent. In its present state, the use of an individual device for dosimetry work depends upon calibration of its sensitivity to damage.

10,600 SATELLITE-BORNE INSTRUMENTATION FOR OBSERVING FLUX OF HEAVY PRIMARY COSMIC RADIATION by P. Schwed, H. Hanson, and H. Benjamin (RIAS) and M. A. Pomerantz (Franklin Inst.); J. Franklin Inst., Vol. 271, pp. 275-291, Apr. 1961

A lightweight (1150 gm.) instrument for measuring the flux of relativistic heavy primary cosmic ray nuclei of $Z \geq 6$ and separating these into three categories according to charge is described. The detector is an ionization chamber 11 cm in diameter and 11 cm long filled with 9 atmospheres of argon. The associated electronics which consists of a 400 v supply for the ionization chamber, a high input impedance amplifier, and a three channel pulse height analyzer is completely transistorized and consumes 54 mw.

10,601 TEMPERATURE DEPENDENCE OF SCINTILLATION DETECTORS by J. Skrivánek and M. Veselá; Czech. J. Phys., Vol. 11B, pp. 291-292(A), 1961

The temperature dependence of the efficiency was measured on detectors with organic and inorganic scintillators. In the range from $+5^{\circ}C$ to $+40^{\circ}C$ the coefficients of the organic scintillators are negative and the dependence of NaI(Tl) on the temperature is reciprocal. The form of the amplitude spectrum of the scintillator {ZnS(Ag) + paraffin} does not vary with temperature. The temperature coefficients of RCA 6655- and 6342-type photomultipliers are negative in the range measured.

10,602 THE TIMING OF SCINTILLATION PULSES BY MILLIMICROSECOND COINCIDENCE TECHNIQUES by J. W. Lee and J. H. Green (U. New South Wales); Proc. IRE Austral., Vol. 22, p. 188(A), Mar. 1961

A conventional fast-slow millimicrosecond coincidence system for measurement of positron lifetimes was described. Although matching comparable units overseas in performance, the unit's cost has been considerably decreased. The detectors are high-gain photomultipliers, capable of very high time resolution and the fast coincidence is achieved by feeding limited pulses to a biased Ge diode. The side-channels operate through Moody discriminators, which again provide fast outputs so that modification to a fast-not-so-fast principle is possible.

10,603 A TRANSISTORIZED QUARTZ CLOCK [in Czech] by J. Skotnicky; Slaboproudy Obzor, Vol. 22, pp. 167-169, Mar. 1961

A completely transistorized quartz clock is discussed. The clock achieves a short-time accuracy of 10^{-9}, i.e. 0.1 msec per day, with a five stage decade scaler, on the output of which a time scale is available with seconds pulses localized in time accurately to 10^{-5} sec.

NEW PRODUCTS

10,604 ULTRA-PURE ELEMENTS (Light and Co. Ltd., Colnbrook, Bucks., England)

Availability of over 250 ultra-pure elements and compounds for solid-state and metallurgical research is announced. Notable among these are 99.999% Phosphorus and Boron, and single crystal, Czochralski grown, Indium Arsenide with a mobility in excess of 20,000 cm/sec.

10,605 YTTRIUM IRON GARNET AND LITHIUM FERRITE SINGLE-CRYSTALS (Airtron, 200 E. Hanover Ave., Morris Plains, N. J.)

Yttrium iron garnet (YIG), with resonance linewidth of 0.4 to 0.45 oe, in sizes from 1 to 5 gms and lithium ferrite, with a linewidth of less than 10 oe, in polished spheres from 15 to 30 mils, is now available. Frequency range is 2 to 4 kMc for YIG and 5 to 10 kMc for the lithium ferrite.

10,606 POLISHING AND GRINDING MACHINE (Geoscience Instr. Corp., 142 Maiden Lane, New York 38)

The UNI-POL model UP-1, a laboratory lapping and polishing machine, is announced. Wheel speed ranges from 80 to 1,200 rpm, with constant torque at all loads. Vibration and runout have been minimized and components of the machine can be interchanged in seconds.

10,607 BONDING EQUIPMENT (Kulicke and Soffa, Philadelphia, Pa.)

K and S model 601M Multi-Dice Bonder is announced. The machine positions and bonds dice, foil, and other micromodules to header-mounted microcircuits and is well suited for circuit design research due to its high precision and flexibility. Positioning to a precision of 10 to 15 millionths of an inch is easily attained with an exclusive chessman joy-stick assembly.

10,608 HIGH SPEED COMPUTER DIODES (Microwave Assoc., Inc., Burlington, Mass.)

Two high speed, diffused silicon, computer diodes (MA-4413 and MA-4414) are announced. The diodes have a junction capacitance of 1.8 μμf (max) at −6 v bias, and combine extremely low leakage with very fast switching speeds — typically 1 nsec. The diodes are rated at 10 ma at 1.0 v forward and at 0.1 μa at 40 v (MA-4413) and 30 v (MA-4414) reverse. Recovery time to 1 ma, when switched from 10 ma to −5 v through 100 Ω loop impedance, is 0.004 μsec (max) at 25°C.

10,609 MINIATURIZED DRIFT FIELD TRANSISTORS (Sylvania, Woburn, Mass.)

A miniaturized 2N1699 "Pancake" version of the 2N1225 drift field transistor is announced. The 2N1699 has a V_{CB} of −40 v, V_{EB} of −0.5 v, and a power dissipation of 100 mw in free air.

10,610 PHOTOCELLS (Philco Corp., Lansdale, Pa.)

A gallium arsenide photovoltaic detector, the GAU-401, for application in the visible and near-infrared spectrums, is announced. The device is designed for the 0.4 to 0.9 micron

region and has peak sensitivity at 0.85 microns. The GAU-401 may be employed in celestial body sensing, missile tracking, space vehicle control, computer readout and numerous industrial control systems.

10,611 PHOTOCELLS (Solid State Prod., Inc.,1 Pingree St., Salem, Mass.)

An improved Photran, a bistable silicon p-n-p-n light-actuated switch, is announced. The light sensitivity has been improved by more than a factor of 3 over previous types and the device can now handle dc loads of 300 ma. The Photran s employed in counting, sorting, power control, limit switching, programming and optical logic control applications.

10,612 MAGNETIC COMPONENTS (Torotron Corp., 256 East Third Street, Mount Vernon, N.Y.)

A line of magnetic components, including toroidal inductors, toroidal transformers, wave filters, magnetic amplifiers, static inverters and decade inductors, is available. The components are either open or hermetic cased and epoxy molded and are designed to customer specifications.

10,613 TRANSISTORIZED AMPLIFIERS (Burr-Brown Research Corp., Box 6444, Tucson, Ariz.)

The 1800 Series instruments employing standard sub-modules including differential and chopper stabilized operational amplifiers to provide a variety of gain ranges, gain steps, frequency responses and outputs is announced. A typical instrument provides variable gain of 0 to 1000 over 0 to 20,000 cps with an input impedance greater than 1 Megohm and an output impedance suitable for driving a 100 ma galvanometer.

10,614 S-BAND PARAMETRIC AMPLIFIER (Motorola Inc., Solid State Electronics Dept., 3102 N. 56th St., Scottsdale, Ariz.)

A high gain, low noise parametric amplifier (Model SPA 01) designed for operation at 2480-2520 Mc is announced. The amplifier utilizes a single, silicon p-n diode as the variable capacitance element; signal separation is obtained by employing a ferrite circulator and extremely wideband operation is obtained by the use of filters in the input and idler circuits. The amplifier is flexible and can be used as a broad or narrow band amplifier and as a parametric X-band up-converter.

10,615 FIXED FREQUENCY OSCILLATORS (Burr-Brown Research Corp., Box 6444, Tucson, Ariz.)

A series of transistorized high stability oscillators (designated as the 1391 series) providing a high purity sine wave of fixed frequency through the use of a high gain dc amplifier in a Wein Bridge configuration, and designed for applications requiring a known frequency or bank of fixed frequencies is announced. Measures of frequency stability on a typical unit, model 1391-1 (1000 cps), show ±0.01% per °C from 0°C to 50°C after thermal stabilization. Other models are available in frequencies of from 1 to 100,000 cps.

10,616 HEARING AID (Otarian Listener Corp., P.O. Box 711, Ossining, N. Y.)

The "Normalizer", a dime-sized, transistorized, hearing aid is announced. The device employs a series of subminiature transistors in a p-n-p n-p-n p-n-p sequence and incorporates a subminiature acoustic labyrinth, akin to a baffle chamber, to broaden the frequency range and enhance tone response.

SUBJECT INDEX

A

Absorption:
in Crystalline $SrTiO_3$, Measurements of Microwave 10,384
Edge of CdS, Structures of Photoconductivity Spectra 10,458
of Irradiated Silica and Quartz, Vacuum Ultraviolet 10,448
Line Shape, Magneto-Optical 10,447
Acceptor Impurities in Si, Spin Resonance of 10,436
Activation Energies in AgI and ZnO Crystals 10,331
Admittance Products, Method of Finding 10,515
AGC Circuit for IF Amplifier 10,528
Aircraft Check-Out and Recording System 10,557
Alarm System, 30 Channel DC 10,556
Alcatron, Field Effect Tetrode 10,486
Alkali Halide Crystals,
Cohesive Energy, Coloration and Luminescence of 10,372
Distortion Correction to the Surface Energy of 10,373

Alkali Halides, Diffusion Theory Approach to Electrical Breakdown in 10,381
Alumina, Sintering in 10,342
Aluminum-Oxide:
Annealing of Radiation Induced Color Centers and Defects of 10,321
Creep in Polycrystalline 10,469
Growth of Whiskers: 10,347
and Platelet Crystals of α 10,362

Amorphous Semiconductors, Resistivities and Seebeck Coefficients of Inorganic 10,400
Amplifiers, 10,613
AGC Circuit for IF 10,528
Feedback 10,534
IF 10,564, 10,532
Magnetic Core Switching 10,572
Nonreciprocal 10,539
Parametric: 10,539
Analysis of Traveling-Wave 10,536
S-Band 10,614
Stability of Traveling-Wave 10,537
Up-Converter 10,535
Switching 10,572
Temperature Compensated Audio Frequency 10,531
Transistor:
Common Emitter Input/Output Resistance and Gain of 10,540
High Input 10,541
Low Noise 10,541
Signal Transmission in 10,530
Tunnel Diode:
Shot Noise in 10,538
Unidirectional 10,533
Analog-to-Digital Converters 10,585, 10,586
Anisotropic Photovoltages in Si and Ge 10,459
Anisotropy Constants of Some Fe-Si Alloys, Magnetocrystalline 10,427
Anisotropy Field Values in Thin Magnetic Films 10,424
Antiferromagnetism, Neutron Diffraction Investigation of 10,430
Arsenic in Ge, Diffusion of 10,333, 10,334
Atomic Moments in Ferromagnetic Alloys 10,423
Audio Amplifiers, Temperature Compensation of 10,531
Autoemission from Thin Dielectric Layers, Theory of 10,379
Avalanche Breakdown in Junctions 10,477

B

Band Pass Filters, 10,550
Impedance Mismatch in 10,551
Band Splittings in Zincblende and Wurtzite Structures, Theory of Valence 10,376
Band Structure of Heavily Doped Ge 10,375
Barium Ferrite, Growth of Single Crystals 10,358
Barium Titanate,
Dielectric Constant Across a Shock Front in 10,387
Dielectric Properties of Finely Dispersed 10,386
90° Wedge-Shaped Domains in Crystals of 10,388
Phase Transitions in 10,383
Resistivity of Rare-Earth Doped 10,383
Binary Computer, The PASCAL 10,565
Blind Guidance Devices 10,555
Bolometers Utilizing Temperature Dependence of Dielectric Constant 10,511
Bonded Silicon Wafers, Residual Thermoelastic Stresses in 10,484
Bonding:
Equipment, Dice 10,607
Theory, Paramagnetism in Chemical 10,431
Boolean Function Generators 10,583
Boron, Ultra Pure 10,604
Boron from SiI_4, Zone Melting Removal of 10,330
Breakdown
in Alkali Halides, Diffusion Theory Approach to Electrical 10,381
of CdS, Low Temperature Low Field 10,406
in Junctions, Survey of Theories of 10,477
of n-Hexane, Electric 10,382
Brucite, Electron Spin Resonance Study of Mn Impurity in 10,444
Bulk and Surface Conductivity in Ge, Separation of Roles of 10,415

C

Cadmium, Fermi Surface Area of 10,377
Cadmium Sulfide,
Non-Ohmic Conductivity and Photoconductivity of 10,406
Photoconductivity Spectra of 10,458
Thin Films for Modulation of Microwaves 10,494
Zone Melting of 10,346
Cadmium Tin Arsenide, Electrical and Optical Properties of 10,420
Calcium Cadmium Silicate Phosphors, (Pb + Mn)-Activated 10,353
Calcium Fluoride Maser,
Fluorescence in 10,454
Oscillations in 10,508
Calcium Fluorophosphate, Polarized Luminescence of 10,455
Carrier Concentration of Semiconductors, Curve of Surface Free 10,412
Cathodes, Emission of Negative Oxygen Ions from Dispenser 10,414
Characteristics of Solid State Devices, Survey of 10,472
Chemical Etching of Semiconductors, Study of 10,366
Chromium Chloride, Neutron Diffraction Observations on Single Crystal 10,430
Cleaning Ge and Si Surfaces by Field Desorption 10,413
Cobalt-Iron Alloys, Nuclear Magnetic Specific Heat in 10,422
Coercive Force in Garnet Ferrites, Anomalies in Temperature Dependence of 10,426
Cohesive Energy of Alkali Halide Crystals 10,372
Coincidence System, Measurement of Positron Lifetime by 10,602
Color Centers,
in Al_2O_3, Annealing of Radiation Induced 10,321
in LiF, X-Ray Induced 10,319
in LiH, Electron Spin Resonance of 10,438
in NaCl, Transient Production of 10,320
Coloration of Alkali Halides 10,372
Common Emitter Amplifier, Input/Output Resistance and Gain of 10,540
Communication Nets,
Analysis of 10,518
Synthesis of 10,522
Comparator, Sawtooth-DC 10,547
Computer:
Circuits, Refer to Specific Circuit
Memories, Refer to "Memories", "Magnetic Logic Circuits"
Computers, The PASCAL Binary System 10,565
Conductive Organic Solids 10,398
Conductivity:
of CdS, Low Temperature Low Field Non-Ohmic 10,406
Effect of Impurities on 10,393
of Ge, Surface 10,415
Influence of Gradient on Galvanomagnetic Effects in Semiconductors 10,407
Phonon Scattering Mechanism of Thermal 10,463
of Plasmas and Semiconductors 10,397
of S, Se and Te Treated PbO Layers 10,396
of Silicides of Transition Elements 10,399
Construction Survey on Devices 10,472
Control Systems, Industrial 10,592
Converter,
Analog to Digital 10,585, 10,586
Binary Digital Coordinate 10,566
Copper, Acid Cutting and Acid Polishing Crystals of 10,365
Copper-Nickel,
Effect of Magnetic Clusters on Specific Heat of 10,462
Intermetallic Diffusion in the System 10,332
Copper Oxides, Effect of Environment on Growth of 10,363
Core:
Circuits,
Analysis of 10,499
Design of 10,567
Driver 10,573
Logic, Impulse Selection for 10,580
Matrix Storage System 10,581
Switch 10,573
Cores,
Flux Distribution in 10,497
Testing of Switching Speed of 10,498
Counter, Multiaperture-Core 10,575
Counter-Timer 10,618
Coupling Networks Employing Zener Diodes 10,548
Creep in Polycrystalline Al_2O_3 10,469
Critical Fluctuations in Superconductors 10,401
Cryosistor Switch 10,490
Crystalline Solids,
Description of Sintering in 10,341
Experiments in Sintering in 10,342
Crystallite Size in Thin Magnetic Films, Effective 10,424
Crystallization of YIG and YGG 10,356
Crystals,
Effect of Pressure on the Spectra of Rare Earth Ions in 10,446
Electroluminescent, Survey of 10,449
Growth of Graphite 10,347
Growth Mechanism of 10,340
Hartree-Fock Theory of 10,371
Cupric Oxide, Formation of 10,363
Cuprous Oxide, Formation of 10,363
Curie Temperature of Ferromagnetics Lowering of 10,425
Cutting of Copper Crystals, Acid 10,365
Cyclotron Resonance in Metals, Magnetoplasma Induced 10,416

D

Data Monitoring System 10,556
DC Inverter for Fluorescent Lamps 10,590
Decoder, DME 48 Channel 10,562
Defects in:
Al_2O_3, Annealing of Radiation Induced 10,321
Plastically Deformed LiF, X-Ray Induced 10,319
Demagnetization of Twistors 10,513
Dendritic Growth of:
Al_2O_3 10,347
Ge 10,351, 10,352
Depolarizing Effects in Semiconductors, Magneto-plasma 10,416
Desorption in Si and Ge 10,413
Detector,
Cosmic Radiation 10,600
Radiation 10,599
Radiation, Beta and Gamma-Ray 10,598
Detectors,
Diode with Filter 10,549
Temperature Dependence of Scintillation 10,601
Devices, Construction Survey on 10,472
Diamond, Optical and Electrical Properties of Semiconducting 10,456
Dielectric:
Bolometers 10,511
Cavity for Masers 10,509
Constant Across a Shock Front in $BaTiO_3$ 10,387
Layers, Mechanism of Autoemission from Thin 10,379
Properties of Finely Dispersed $BaTiO_3$ 10,386
Properties of TiO_2, Effects of Oxygen Vacancies on the 10,380
Dielectrics, Electric Breakdown of Liquid 10,382
Differentiating Circuits 10,584
Diffraction Investigation of Antiferromagnetism, Neutron 10,430
Diffusion:
of As in Ge 10,333
of As and P into Ge 10,334
and Drift Contributions to Photocurrent, Analyses of 10,457
in Large Temperature Gradients, Intermetallic 10,332
Paths in AgI and ZnO Crystals 10,331
Sintering Models, Derivation of 10,341
Theory Approach to Electrical Breakdown in Alkali Halides 10,381
of Tin in GaAs 10,335
Diffusional Creep Process in Al_2O_3 10,469
Diode:
Detectors 10,549
Logic Switching Circuits 10,570, 10,571
Diodes,
Application of 10,473
Application as Low-Loss Microwave Switches 10,544
Avalanche Injection in 10,389
High Frequency Application of 10,475
High Speed Si Computer 10,608
Junction:
Breakdown Voltage of 10,476
Electron Heating Phenomena 10,389
Field Effect Pinch Off of Leakage Current in 10,476
High Speed Computer 10,608
Parametric:
Characteristics and Parameters of 10,475
High Frequency Application of 10,475
Protection of 10,473
Tunnel:
Application of 10,574
Oscillations of Longitudinal Tunnel Current 10,418
Diphenyl-Picryl Hydrazyl, Double Quantum Transition in the Electron Spin Resonance of 10,442
Disjuncts of Switching Functions 10,543
Dispenser Cathodes, Emission of Negative Oxygen Ions from 10,414
Display of Stored and Nonstored Information 10,587
Distortion Correction to the Surface Energy of Alkali Halide Crystals 10,373
DME Systems 10,562, 10,563, 10,564
Domains in $BaTiO_3$ Crystals, 90° Wedge-Shaped 10,388
Donor Formation in O_2-Doped Ge 10,322
Dosimeter, Fast-Neutron 10,599
Drift and Diffusion Contributions to Photocurrent, Analyses of 10,457
Driver, Matrix Magnetic Core 10,573

E

Elastic Constants of Crystals, Measurement of 10,468
Electric Field of Semiconductors, 10,412
Electroluminescence,
Characteristics and Application of 10,493
Survey of Host Crystals for 10,449
Theory of Injection and Impact Ionization 10,449
Electroluminescent ZnS Crystals, Growth of 10,354
Electron:
Gun Excitation for Spectrographic Analysis of GaAs 10,326
Heating Phenomena in Avalanche Devices 10,389
Interaction with Acoustic Waves in Intrinsic Semiconductors 10,378
Scattering,
by Metal Films, Energy and Angular Distribution of 10,370
by Phonons and Impurities 10,394
by Thin Foils 10,369
Spin Relaxation,
in n-Type Silicon, Compensation Dependent 10,433
in p-Doped Si 10,434
Spin Resonance,
Application in Impurity Studies of Compound Semiconductors 10,443
of Color Centers in LiH 10,438
of Diphenyl-Picryl Hydrazyl, Double Quantum Transition in 10,442
of Fe-Doped Si, Passage Effect in the 10,445
of Irradiated Ferroelectric Tri-Glycine Sulfate 10,439
of Mn Impurity in Brucite 10,444
Transport in Semiconductors, Theory of Linear 10,393
Electrons in:
Metal Films, Injection and Collection of Hot 10,395
Semiconductors, Hot 10,389
Electroplating, Ge Dendrite Growth Study Using Pulse 10,352
Electrostatic Potential in Semiconductors, Curves of 10,412
Emission:
of Negative Oxygen Ions from Dispenser Cathodes 10,414
from Si and Ge, Field 10,413
Spectra of Trivalent Thulium 10,451
Energy Gap, Direct Measurement of Superconducting 10,404
Epitaxial Layers Thickness of 10,350
Esaki:
Diode NOT-OR Logic Circuits 10,571
Tunneling in Presence of Magnetic Fields 10,419
Excitation:
of Plasma Oscillations in Solids 10,417
Spectrum of Semiconducting Diamond 10,456

F

F Centers in LiF, Paramagnetic Resonance of 10,437
Feedback Amplifiers, Design of 10,534
Fermi Surface Areas of Mg, Zn and Cd 10,377
Ferrite
Core Circuit Analysis 10,499
Core Storage Devices 10,481
Cores, Flux Distribution in 10,497
Microwave Devices 10,495
Waveguides, Analysis of 10,501
Ferrites,
Coercive Force in Garnet 10,426
Frequency Limitations of 10,495
Single Crystals,
Device for Growing 10,357
Growth of Ba 10,358
Thin Films, Preparation of 10,359, 10,360
Ferroelectric Tri-Glycine Sulfate, Electron Spin Resonance of Irradiated 10,439
Ferromagnetic:
Alloys, Hyperfine Field and Atomic Moments in 10,423
Films, Measurement of Parameters for Kerr Effect in 10,461
Resonance, General Theory of 10,429
Ferromagnetics, Lowering of Curie Temperature of 10,425
Ferromagnets, Magnetic Excitation in Thin Film 10,496
Ferrous Fluoride, Mössbauer Effect Hyperfine Structure in 10,421
Ferrous Oxide, Deviations from Stoichiometry in 10,337
Field Effect:
Pinch Off of Leakage Current in High Voltage Junctions 10,476
Tetrode, The Alcatron 10,486
Field Emission from Clean Ge and Si Surfaces 10,413
Films,
Epitaxial, Measurement of Thickness of 10,350
Ferrite, Preparation of 10,359, 10,360
Ferromagnetic, Measurement of Parameters for Kerr Effect in 10,461
Helium Flush in Vacuum Deposition of 10,355
Magnetic, Coercive Force of 10,424
Metal, Energy and Angular Distribution of Electrons Scattered by 10,370
Metal, Injection and Collection of Hot Electrons in 10,395
Superconducting, Properties of Thin Tin 10,405
Filter:
Band Pass 10,550
Band Pass, Mismatch of Impedances in 10,551
Diode Detector 10,549
Filters,
Analysis of Phase Modulated 10,553
Analysis of Pulse 10,552
Fission Spectrum Neutron Irradiation of Ge 10,368
Flip-Flops, Tunnel Diode 10,545
Floating Zone:
Growth of GaP Crystals 10,345
Preparation of Silicon Crystals 10,344
Floating Zones, Stability Limit for 10,343
Flowgraphs: 10,520
for Nonlinear Systems 10,519
Fluorescence,
of Cr^{+++} in Masers 10,453
of Rare-Earth Radicals in Masers 10,454
Techniques, Recoilless Gamma-Ray 10,450
Fluoride Ions, Method for Analyzing 10,366

Flux Distribution in Ferrite Cores 10,497
Foils, Electron Scattering by Thin 10,369
Friction in Lightly Deformed Pure Fe Wires 10,471
Function Generators, Boolean 10,583
Furnace for the Growth of Lead Selenide 10,348

G

Gallium Arsenide,
Diffusion of Tin in 10,335
Spectrographic Determination of Trace Elements and Halogens in 10,326
Gallium Arsenide:
Photocells 10,491
Tunnel Diode Flip-Flop Circuit 10,545
Gallium Phosphide,
Floating Zone Technique for Growing Single Crystals of 10,345
Vapor Phase Preparation of 10,349
Galvanomagnetic Effect, in Semiconductors, Influence of Conductivity Gradients on 10,407
Galvanomagnetic Effects,
in InSb, Influence of Magnetoconductivity Discontinuities on 10,408
in Moderately Doped Te, Measurement of 10,410
Gamma-Ray Fluorescence Techniques 10,450
Generation-Recombination in Au-Doped Ge 10,390
Germanium,
Band Structure of Heavily Doped 10,375
Dendritic Growth Processes 10,351, 10,352
Diffusion of As in 10,333
Diffusion of As and P in 10,334
Donor Formation in O_2-Doped 10,322
Effect of Fission Spectrum Neutrons on n-Type 10,368
Emission, Desorption and Surface Migration in 10,413
Hall Effect Analysis of 10,327
Optical Constants of 10,460
Photovoltages in 10,459
Recombination-Generation in Au-Doped 10,390
Saturation in Chemical Etching Solutions of n-Type 10,366
Surface Conductivity of 10,415
Germanium at Room Temperature,
Measurement of Surface Dependence of Thermoelectric Power in 10,465
Theory of Surface Dependence of Thermoelectric Power in 10,466
Germanium Telluride-Tin Telluride, Lattice Constants and Structural Changes in 10,318
Gold-Doped Ge, Recombination-Generation in 10,390
Gold-Manganese System, Magnetic Properties of 10,428
Gold-Ni, Intermetallic Diffusion in the System 10,332
Graph Theory, Network Analysis by Means of 10,521
Graphite Single Crystals, Growth of 10,347
Growth of:
Barium Ferrite Single Crystals 10,358
Ferrite Crystals 10,357
GaP Crystals 10,349
Ge Dendrites 10,351, 10,352
InSb Crystals 10,316
Lead Selenide 10,348
Sapphire Microcrystals 10,362
YIG Crystals 10,338
Guidance Devices for the Blind 10,555

H

Hall:
Coefficient of $CdSnAs_2$ 10,420
Effect:
Analysis of Ultrapure Si and Ge by 10,327
Generators 10,488
Influence on Transverse Magnetoresistance in InSb 10,409
Isolator in Tunnel Diode Amplifier 10,533
in Moderately Doped Te 10,410
Surface Charging in Oscillistor 10,489
in Thin Films 10,487
Generators, Application of in Field Measurements 10,488
Probes, Magnetic Field Measurement by 10,593
Surface, "Charging" at the Surfaces of the Oscillistors 10,489
Hartree-Fock Equation in Terms of Localized Orbitals, 10,371
Hearing Aids 10,555, 10,616
High Frequency Application of Parametric Diodes 10,475
High Voltage Diodes, Field Effect Pinch Off of Leakage Current in 10,476
Hole Interaction with Acoustic Waves in Intrinsic Semiconductors 10,378
Host Crystals for Electroluminescence, Survey of 10,449
Hot Electrons in:
Metal Films, Injection and Collection of 10,395
Semiconductors 10,389
Hyperfine Field in Ferromagnetic Alloys 10,423
Hyperfine Structure in FeF_2, Mössbauer Effect 10,421

I

IF Transistor Amplifiers 10,532
Impact Ionization Electroluminescence, Theory of 10,449
Impurities,
Electron Scattering by 10,394
in In, Spectrochemical Method for Determination of 10,323
in Se, Determination of Trace 10,328
in Semiconductors,
Change in Absorption Coefficient Due to 10,329
Determination of Ultratrace 10,324
Spectrographic Procedures of Detection 10,325
in Si, Spin Resonance of Acceptor 10,436
Impurity:
Level Model for Au-Doped Ge, Noise Prediction Using 10,390
Segregation in Crystal Growth from Melt 10,340
Studies in Compound Semiconductors Using Electron Spin Resonance 10,443
Indium Antimonide,
Anisotropic Segregation of Se in 10,316
Coherent Excitation of Plasma Oscillations in 10,417
Hall Effect Influence on Transverse Magnetoresistance in 10,409
Influence of Magnetoconductivity Discontinuities on Galvanomagnetic Effects in 10,408
Interband Magneto-Reflection in 10,374
Low Surface Recombination Velocity on <111> Faces of 10,392
Noise in 10,411
Indium Arsenide, Single Crystals of 10,604
Indium, Spectrochemical Method for Trace Impurity Determination in 10,323
Industrial Control Systems 10,592
Injection:
and Collection of Hot Electrons in Metal Films 10,395
Electroluminescence, Theory of 10,449
of Hot Electrons in Metal Films 10,395
Integrating Circuits 10,584
Interferometer Studies of Iron Whiskers 10,339
Intermetallic Diffusion in Large Temperature Gradients 10,332
Interstitial Li on the Density of Si, Effect of 10,467
Intrinsic Semiconductors, Interaction of Electrons and Holes with Acoustic Waves in 10,378
Inverters,
DC for Fluorescent Lamps 10,590
Power 10,589
Ions in Crystals, Effect of Pressure on the Spectra of Rare Earth 10,446
Iron, Smooth Spalls and Polymorphism of 10,470
Iron-Cobalt Alloys, Nuclear Magnetic Specific Heat in 10,422
Iron-Doped Silicon, Passage Effect in the Electron Spin Resonance of 10,445
Iron-Ni, Intermetallic Diffusion in the System Alpha- 10,332
Iron-Pd, Intermetallic Diffusion in the System Alpha- 10,332
Iron-Silicon Alloys, Magnetocrystalline Anisotropy Constants of Some 10,427
Iron-Vanadium Alloys,
Effect of Magnetic Clusters on Specific Heat of 10,462
Nuclear Magnetic Specific Heat in 10,422
Iron:
Whiskers, Interferometer Studies of 10,339
Wire, Internal Friction in Lightly Deformed Pure 10,471
Isotope Shift in Superconducting Ru, Absence of 10,402

J

Junction:
Diodes, Leakage and Breakdown Voltage of 10,476
Transistors, Characteristics of 10,561
Junctions,
Avalanche Breakdown in 10,477
Fast-Neutron Induced Damage in 10,599
Generation of Power by Irradiation of 10,482
Graded, Transition Layer Characteristics of 10,474
Radiation Detecting 10,590, 10,599
Reverse Voltage Breakdown in 10,477
Signal-to-Noise Ratio in 10,597
Zener Breakdown in 10,477

K

Kerr Effect in Ferromagnetic Films, Measurement of Parameters for 10,461

L

Lasers - See also Masers
Lasers,
Beam Characteristics of Ruby 10,504
Characteristics of Modes in Ruby 10,503
Lattice Parameters of GeTe-SnTe 10,318
Lead Ions in KCl, Diffusion of 10,336
Lead-Manganese Activated $CaCdSiO_3$ Phosphors 10,353
Lead Oxide Layers, Electrical and Photoconductivity of S, Se and Te Treated 10,396
Lead Selenide, Furnace for the Growth of 10,348
Light Source and Amplifier, Electroluminescent 10,493
Lithium Ferrite, Single Crystals of 10,605

Lithium Fluoride,
Paramagnetic Resonance of F Centers in 10,437
X-Ray Induced Defects in Plastically Deformed 10,319
Lithium Hydride, Electron Spin Resonance of Color Centers in 10,438
Lithium on the Density of Si, Effect of Interstitial 10,467
Logic, Impulse Selection for Core 10,580
Logic:
Circuits,
Esaki Diode 10,571
High Speed Diode 10,570
Magnetic 10,568, 10,569
Devices, Magnetic Film 10,578
Logical Design of Magnetic Core Circuits 10,567
Losses in $SrTiO_3$, Microwave 10,385
Luminescence of:
Calcium Fluorophosphate 10,455
Tl Activated Alkali Halides 10,372

M

Magnesium, Fermi Surface Area of 10,377
Magnetic:
Cluster, Effects on Specific Heat of Ni-Cu and Fe-V Alloys on 10,462
Core:
Amplifier 10,572
Circuits, Logical Design of 10,567
Memories 10,579, 10,581
Oscillator 10,542
Cores,
Analysis of Characteristics of 10,499
Flux Distribution in 10,497
Testing of 10,498
Devices 10,612
Effective Field in Co-Fe and V-Fe Alloys 10,422
Excitation in Thin Film Ferromagnets 10,496
Field:
Device, Superconducting Solenoid for Producing 15 Kilogauss Fields 10,512
Measurement by Hall Probes 10,593
Fields, Esaki Tunneling in Presence of 10,419
Films,
Coercive Force of Thin 10,424
Preparation and Properties of 10,359, 10,360
Storage and Logic Devices for 10,578
Logic Circuits 10,568, 10,569
Properties of Au-Mn System 10,428
Reed Relay, Characteristics of 10,500
Refrigerators at Temperatures Below 1°K 10,510
Specific Heat in Ferromagnetic Co-Fe and V-Fe Alloys 10,422
Tape, Digital Recording on 10,577
Magneto:
-Optical Absorption 10,447
-Reflection in InSb 10,374
Magnetoconductivity Discontinuities on Galvanomagnetic Effects in InSb 10,408
Magnetocrystalline Anisotropy Constants of Some Fe-Si Alloys 10,427
Magnetoplasma Effects in Solids 10,416
Magnetoresistance,
Influence of Carrier Concentration Gradients on 10,407
in InSb, Hall Effect Influence on 10,409
Magnetoresistance of Moderately Doped Te 10,410
Manganese-Gold System, Magnetic Properties of 10,428
Manganese Impurity in Brucite, Electron Spin Resonance Study of 10,444
Manganese-Lead Activated $CaCdSiO_3$ Phosphors 10,353
Manganous Oxide, Deviations from Stoichiometry in 10,337
Maser:
Amplifier, Design of 10,529
Radiometer 10,554
Ultra-Low-Noise Receiver 10,559
Masers,
Adiabatic Rapid Passage in 10,502
CaF_2:
Fluorescence in 10,454
Oscillations of U^{3+} and Sm^{2+} in 10,508
Dielectric Cavity Design for 10,509
Fabry-Perot Interferometer Resonator for Optical 10,506, 10,507
Millimeter and Submillimeter Resonator for 10,507
Multimode Resonators for Optical 10,505
Ruby:
Fluorescence in 10,452, 10,453
Relaxation Time of 10,452
Masking for Chemical Etch of Mesas 10,483
Measurement Devices, Application of Hall Generators in 10,488
Measurement of:
Absorption Coefficient 10,329
Elastic Constants of Crystals, Diffusely Reflected X-Ray Method for 10,468
Epitaxial Layer Thickness 10,350
Internal Friction in Pure Fe Wires 10,471
Kerr Effect in Ferromagnetic Films 10,461
Optical Constants of Ge 10,460
Superconducting Energy Gap 10,404
Surface Dependence of Thermoelectric Power in Ge at Room Temperature 10,465
Temperature Dependence of Scintillation Detectors 10,601
Y_e Parameter Frequency Dependence 10,480
Memory, Content Based Associative 10,576
Memory Systems, Magnetic 10,579
Mesas, Method for Producing 10,483
Metal Films, Energy and Angular Distribution of Electrons Scattered by 10,370
Microwave:
Absorption in Crystalline $SrTiO_3$ 10,384
Application of Ferrites 10,495
Losses in $SrTiO_3$ 10,385
Modulation by CdS Thin Films 10,494
Switches, Low-Loss Diode 10,544
Mode Characteristics of Ruby Lasers 10,503
Modulation of Microwaves by Photoconductive CdS Thin Films 10,494
Möllenstedt Interferometers, Iron Whiskers Studied with 10,339
Monitor System, 30 Channel DC 10,556
Mössbauer Effect:
in Gamma-Ray Fluorescence 10,450
Hyperfine Structure in FeF_2 10,421
Multi-Port Networks,
Synthesis of 10,518
Tree Graph Matrix of 10,517
Multistage Amplifier, Design of 10,529
Multivibrators, Tunnel Diode 10,545

N

Negative Resistance:
Amplifier, Design of 10,529
Circuit 10,514
Networks,
Communication Net Analysis of 10,518
Darlington's Synthesis of Two Terminal-Pair 10,523
Flowgraph Theory of 10,519, 10,520
Graph Theory Analysis of 10,521
Polytype-Port 10,524
Synthesis of:
Communication Nets in 10,522
Linear 10,527
Multi-Port Tree Graph Matrix 10,517
N-Port Resistive 10,525, 10,526
Topology, Tree Expansion in 10,515
Tree Graph:
Matrix Analysis of Multi-Port 10,517
Theory of 10,516
Neutrons,
Activation Methods for Impurity Determination in Se by 10,328
Diffraction:
Investigation of Antiferromagnetism by 10,430
Observations on Single Crystal $CrCl_3$ by 10,430
Monoenergetic Irradiation of Ge by 10,368
Nickel-Copper Alloys, Effect of Magnetic Clusters on Specific Heat of 10,462
Nickel-Pd, Intermetallic Diffusion in the System of 10,332
Noise:
Corner Frequency of Transistors, Equations for 10,481
in InSb, Generation-Recombination 10,411
Nonlinear Systems, Flowgraphs for 10,519
Nonreciprocal Systems, Transmission in 10,530
N-Port Resistive Networks, Synthesis of 10,525, 10,526
Nuclear Magnetic:
Specific Heat in Ferromagnetic Co-Fe and V-Fe Alloys 10,422
Spectrometer 10,594

O

Optical:
Constants of Ge 10,460
Masers,
Fabry-Perot Interferometer Resonator for 10,506
Multimode Resonators for 10,505
Ruby Masers 10,453
Orbitals, Solution of Hartree-Fock Equation in Terms of 10,371
Organic Solids, Highly Conductive 10,398
Oscillations:
in the Longitudinal Tunnel Current of Tunnel Diodes 10,418
in Superconductors, Transverse Collective 10,403
of U^{3+} and Sm^{2+} in CaF_2 Masers 10,508
Oscillators,
1 cps to 100 kc Temperature Stabilized 10,615
Saturating Core 10,542
Oscillistor, Surface Charging 10,489
Oxidation Kinetics of Platinum 10,364
Oxide Growth at Room Temperature on Cu Crystals in Water 10,363
Oxygen:
Ions from Dispenser Cathodes, Emission of 10,414
Vacancies on the Dielectric Properties of TiO_2, Effects of 10,380

P

Paramagnetic:
Behavior, Phenomenological Classification of Substances by 10,431
Excited State in P-Doped Si 10,435
Resonance, Role of Phonons in 10,432
Resonance:
in LiF, F Center 10,437
- See also Electron Spin Resonance
Paramagnetism in Chemical Bonding Theory 10,431
Parametric:
Amplifiers 10,535, 10,536, 10,539
Amplifiers,
S-Band 10,614
Stability of Traveling Wave 10,537
Diodes,

Characteristics and Parameters of 10,475
High Frequency Application of 10,475
Phase Feedback Filters, Analysis of 10,553
Phonons:
in Intrinsic Semiconductors, Electron and Hole Interaction with 10,378
in Paramagnetic Resonance, Role of 10,432
Phosphors, Emission of (Pb + Mn)-Activated $CaCdSiO_3$ 10,353
Phosphorus-Doped Si,
Electron Spin Relaxation in 10,434
Infrared Pumped Excited State in 10,435
in Ge, Diffusion of 10,334
Phosphorus, Ultra Pure 10,604
Photocells,
Gallium Arsenide 10,610
Positional 10,595
Series Resistance Effects in 10,492
Silicon "Photran" 10,611
Spectral Response of Si and GaAs 10,491
Photoconductive ZnS Crystals, Growth of 10,354
Photoconductivity:
of CdS, Low Temperature Low Field 10,406
of S, Se and Te Treated PbO Layers 10,396
Spectra of CdS 10,458
Photocurrents, Analyses of Drift and Diffusion Contributions to 10,457
Photodiodes, Reduction of Surface Recombination in 10,391
Photomagnetothermal (PMT) Effect in Semiconductors 10,464
Photothermal Effect (PT) in Semiconductors 10,464
Photovoltages in Si and Ge 10,459
Photovoltaic Device,
Resistance Effects in 10,492
Spectral Response of 10,491
Piezoelectric Ceramic Resonators 10,550
Plasma:
Effects in Solids Magneto- 10,416
Oscillations in Solids, Coherent Excitation of 10,417
Plasmas and Semiconductors, Complex Conductivity of 10,397
Platinum Oxidation, Kinetics of 10,364
Polarized Luminescence of Calcium Fluorophosphate 10,455
Polishing:
of Copper Crystals 10,365
and Grinding Machine 10,606
Polyethylene, Electron Spin Resonance Spectrum of Stretched 10,441
Polymorphism of Fe 10,470
Positron, Lifetime Measurement of 10,602
Potassium Chloride, Diffusion of Thallous and Lead Ions in 10,336
Potassium Didenterium Phosphate, Electron Spin Resonance in Irradiated 10,440
Potassium Dihydrogen Phosphate, Electron Spin Resonance in Irradiated 10,440
Power:
Generation by Irradiated Junctions 10,482
Inverters, Transistor 10,589
Supplies, Satellite Beacon 10,558, 10,588
Supply 10,617
Precipitation from Supersaturated Solid Solutions 10,317
Pressure Effects on the Spectra of Rare Earth Ions in Crystals 10,446
Properties and Applications of Si Rectifiers 10,473
Properties of:
Au-Mn System, Magnetic 10,428
Hamiltonian Independent Susceptibility Tensor 10,429
Semiconducting Diamond, Optical and Electrical 10,456
Superconductive Thin Tin Films 10,405
Pulse:
Filters, Analysis of 10,552
Generators, Time Code 10,582
Height Discriminator, Tunnel Diode 10,546
Selector, DME 48 Channel 10,562

Q

Quartz Clock 10,603
Quartz, Vacuum Ultraviolet Absorption Studies of Irradiated 10,448

R

Radiated NaCl, Thermoluminescence of 10,367
Radiation, Transient Production of F Centers in NaCl by 10,320
Radiation:
Counter, Diode 10,597
Detector 10,598
Detector,
Cosmic 10,600
Positional 10,595
Surface Barrier 10,596
of Ge, Neutron 10,368
Induced Color Centers and Defects in Al_2O_3, Annealing of 10,321
Radiometer Maser 10,554
Radiotelephone Relay, Satellite Station for 10,560
Random Dilution, Lowering of Curie Temperature of Ferromagnetics by 10,425
Rare Earth:
Garnet Ferrites 10,426
Ions in Crystals, Effect of Pressure on the Spectra of 10,446
Reaction Kinetics of YIG 10,361
Readout Device for Computers 10,575
Receiver,
224 McAirborne 10,564
Ultra-Low-Noise Maser 10,559
Recombination, Reduction of Surface 10,391
Recombination:
-Generation in Au-Doped Ge 10,390
Velocity on <111> Faces of n-Type InSb 10,392
Recording:
on Magnetic Tape, Digital 10,577
System, Aircraft 10,557
Reduction of Surface Recombination in:
Junction Transistors 10,391
Photodiodes 10,391
Reed Relays, Characteristics of 10,500
Refrigerators at Temperatures Below 1°K, Magnetic 10,510
Relaxation:
in n-Type Silicon, Compensation Dependent Electron Spin 10,433
in P-Doped Si, Electron Spin 10,434
Time of Masers 10,452
Times of Excess Carriers in InSb 10,411
Relays,
Magnetic Reed 10,500
Solid State 10,591
Resistivity of:
Inorganic Amorphous Semiconductors 10,400
Moderately Doped Te 10,410
Rare-Earth Doped Barium Titanate 10,383
Resonance,
General Theory of Ferromagnetic 10,429
Role of Phonons in 10,432
Resonance:
of F Centers in LiF 10,437
in Irradiated KH_2PO_4 and KD_2PO_4 10,440
of Mn Impurity in Brucite 10,444
Spectrum of Stretched Polyethylene 10,441
Resonator for Millimeter and Submillimeter Masers 10,507
Resonators for Optical Masers 10,505, 10,506
Ruby Laser, Mode Characteristics of 10,503
Ruby Maser, Relaxation Time of 10,452
Ruby Maser:
Millimeter Amplifier 10,502
Millimeter Oscillator 10,502
Operation as an Amplifier of Oscillator 10,502
Ruthenium, Absence of Isotope Shift in Superconducting 10,402
Rutile, Effects of Oxygen Vacancies on the Dielectric Properties of 10,380

S

S-Band Parametric Amplifier 10,614
Sapphire Microcrystals, Growth of 10,362
Satellite,
Power Supply for 10,588
Relay for Radiotelephone Communication 10,560
Tracking Transmitter for 10,558
Satellite-Borne:
Cosmic Radiation Counter 10,600
Radiation Detector 10,600
Satellite Instrumentation for Observing Cosmic Radiation 10,600
Sawtooth-DC Comparator 10,547
Scattering by:
Metal Films, Energy and Angular Distribution of 10,370
Phonons and Impurities 10,394
Thin Foils 10,369
Scintillation Counters, 10,602
Temperature Dependence of 10,601
Seebeck Coefficients of Inorganic Amorphous Semiconductors 10,400
Segregation:
in Crystal Growth from Melt 10,340
of Se in InSb, Anisotropic 10,316
Selenium,
Determination of Impurities in 10,328
in InSb, Anisotropic Segregation of 10,316
Treated PbO Layers, Electrical and Photoconductivity of 10,396
Self-Powered Transistors 10,482
Semiconductors,
Absorption Coefficient of 10,329
Complex Conductivity of Plasmas and 10,397
Determination of Ultratrace Impurities in 10,324
Hot Electrons in 10,389
Photothermal (PT) and Photomagnetothermal (PMT) Effects in 10,464
Spectrographic Determination of 10,325
Sequential Logic Circuits, Magnetic 10,569
Shift Register, Solid State 10,524
Shock Front in Barium Titanate, Ratio of Dielectric Constant Across 10,387
Shot Noise in Tunnal Diode Amplifiers 10,538
Signal:
-To-Noise Ratio of Diode 10,597
Transmission in Transistor Amplifiers 10,530
Silica, Vacuum Ultraviolet Absorption Studies of Irradiated 10,448
Silicides of Transition Elements, Electrical Conductivity of 10,399
Silicon,
Compensation Dependent Electron Relaxation in n-Type 10,433
Effect of Interstitial Li on the Density of 10,467
Electron Spin Relaxation in P-Doped 10,434
Emission, Desorption and Surface Migration in 10,413
Hall Effect Analysis of Ultrapure 10,327
Infrared Pumped Paramagnetic Excited State in P-Doped 10,435
Passage Effect in the Electron Spin Resonance of Fe-Doped 10,445
Photovoltages in 10,459
Saturation in Chemical Etching Solutions of n-Type 10,366

Spin Resonance of Acceptor Impurities in 10,436
Silicon:
Crystals,
Comparison of Properties of Floating Zone Produced Crystals with Pulled 10,344
Floating Zone Preparation of 10,344
Photocells 10,491
Wafers, Residual Thermoelastic Stresses in 10,484
Silicon-Iron Alloys, Magnetocrystalline Anisotropy Constants of 10,427
Silicon Tetraiodide, Removal of Boron by Zone Melting 10,330
Silver Films, Helium Flush in Vacuum Deposition of 10,355
Silver Iodide Crystals, Diffusion Paths and Activation Energies in 10,331
Sintering in Crystalline Solids 10,341, 10,342
Sintering, Theory of 10,317
Sodium Chloride Single Crystals, Transient Production of F Centers in 10,320
Sodium Chloride, Thermoluminescence of Irradiated 10,367
Solar-Cell Power Supply for Satellite 10,588
Solid:
Solutions, Precipitation from Supersaturated 10,317
State:
Devices, Construction Survey of 10,472
Relays 10,591
Space Charge of Semiconductors, Curves of Surface 10,412
Spalls and Polymorphism of Fe 10,470
Specific Heat:
in Ferromagnetic Co-Fe and V-Fe Alloys 10,422
of Ni-Cu and Fe-V Alloys, Effect of Magnetic Clusters on 10,462
Spectra of:
Rare Earth Ions in Crystals, Effect of Pressure on 10,446
Trivalent Thulium 10,451
Spectrochemical Method for Trace Impurity Determination in In 10,323
Spectrographic Analysis of:
GaAs, Electron Gun Excitation Source for 10,326
Impurities in Semiconductors 10,325
Spectrometer,
Design and Characteristics of a Nuclear Magnetic Resonance 10,594
Differential Absorption Infrared 10,329
Spin Relaxation in:
n-Type Si, Compensation Dependent Electron 10,433
P-Doped Si 10,434
Spin Resonance:
of Acceptor Impurities in Si 10,436
in Irradiated KH_2PO_4 and KD_2PO_4 10,440
- See also Electron Spin Resonance
Spectrum of Stretched Polyethylene 10,441
Study of Mn Impurity in Brucite 10,444
Stability of:
Molten Zones in Horizontal Sheets 10,343
Tunnel Current in the Presence of a Magnetic Field 10,419
Stabilization of Parametric Amplifiers 10,537
Stoichiometry in MnO and FeO, Deviations from 10,337
Storage:
Devices,
Magnetic Film 10,578
Thin Film 10,496
Tube, Direct View Halftone 10,587
Stresses in Bonded Silicon Wafers, Residual Thermoelastic 10,484
Strontium Titanate,
Interpretation of Measurements of Microwave Absorption in Crystalline 10,384
Microwave Losses in 10,385
Structural Changes in GeTe-SnTe 10,318
Sulfur Treated PbO Layers, Electrical and Photoconductivity of 10,396
Superconducting:
Energy Gap, Direct Measurement of 10,404
Ru, Absence of Isotope Shift in 10,402
Solenoid for Producing 15 Kilogauss Fields 10,512
Superconductive Properties of Thin Tin Films 10,405
Superconductors,
Critical Fluctuations in 10,401
Transverse Collective Oscillations in 10,403
Supersaturated Solid Solutions, Precipitation from 10,317
Surface:
Conductance of Mg, Zn and Cd 10,377
Conductivity of Germanium 10,415
Dependence of Thermoelectric Power in Ge at Room Temperature 10,465, 10,466
Energy of Alkali Halide Crystals, Distortion Correction to the 10,373
Migration in Si and Ge 10,413
Properties of Semiconductors 10,412
Recombination, Reduction of 10,391
Recombination Velocity on <111> Faces of n-Type InSb 10,392
Susceptibility Tensor, Hamiltonian Independent Properties of 10,429
Switch, Matrix Magnetic Core 10,573
Switches, Microwave, Use of Diodes in 10,544
Switching:
Circuit,
Coupling Network for 10,548
Design of Multi-Level 10,543
Functions, Design of 10,543
Speed of Magnetic Cores, Testing of 10,498
Synthesis of:
Communication Nets 10,522
Linear Networks 10,527
Multi-Port Networks 10,517, 10,518
N-Port Resistive Networks 10,525, 10,526
Two Terminal-Pair Networks 10,523

T

Tecnetron, Analysis of the Operation of 10,485
Television:
Image Tube, Electroluminescent 10,493
Receivers, HF and Rise Time Circuits for 10,561
Tellurium, Measurement of Galvanomagnetic Effects in Moderately Doped 10,410
Tellurium Treated PbO Layers, Electrical and Photoconductivity of 10,396
Temperature:
Compensated Audio Amplifiers 10,531
Dependence of Coercive Force in Garnet Ferrites, Anomalies in 10,426
Stability of High Impedance Amplifiers 10,541
Stabilization of Transistor During Testing 10,478
Stabilized 1 cps to 100 kc Oscillators 10,615
Temperatures Below 1°K, Theory of Magnetic Refrigerators at 10,510
Tetracyanoguinodimethan as Highly Conductive Organic Solid 10,398
Thallous Ions in KCl, Diffusion of 10,336
Thermal:
Conductivity, Normal Phonon Scattering in 10,463
Radiation Dielectric Bolometer 10,511
Thermoelectric:
Figure of Merit of $CdSnAs_2$ 10,420
Power in Ge at Room Temperature,
Measurement of Surface Dependence of 10,465
Theory of Surface Dependence of 10,466
Properties of Inorganic Amorphous Semiconductors 10,400
Thermoluminescence of Irradiated NaCl 10,367
Thickness of Epitaxially Grown Films, Measurement of 10,350
Thin Film Ferromagnets, Magnetic Excitation in 10,496
Thin Films, Hall Effect in 10,487
Thin Films:
CdS 10,494
Photoconductive Modulation of Microwaves 10,494
Thulium, Emission Spectra of Trivalent 10,451
Time Code Generator 10,582
Tin:
Films, Superconductive Properties of Thin 10,405
in GaAs, Diffusion of 10,335
Titanium Dioxide, Effects of Oxygen Vacancies on the Dielectric Properties of 10,380
Transistor:
Amplifiers - See Amplifiers
Applications in TV Circuits 10,561
Clock 10,603
Integrating and Differentiating Circuits 10,584
Parameters,
Analysis of 10,479
Y_e Frequency Dependence of 10,480
Power Inverters 10,589
Transistors,
Avalanche: Electron Heating Phenomena in 10,389
Design of High Frequency 10,479
Junction:
Miniaturized 10,609
Reduction of Surface Recombination 10,391
Noise Frequency Equations for 10,481
Self-Powered 10,482
Temperature Stabilization Device Used in Testing 10,478
Transition:
Elements, Electrical Conductivity of Silicides of 10,399
Layer Characteristics of Linearly Graded Junctions 10,474
Transmitters, Satellite Beacon 10,558
Transport Theory of Semiconductors 10,393
Traveling-Wave Amplifier, Analysis of 10,536
Tree Graphs 10,515, 10,516
Tri-Glycine Sulfate, Electron Spin Resonance of Irradiated Ferroelectric 10,439
Tunnel Diode:
Amplifier,
Design of 10,529
Nonreciprocal 10,539
Unidirectional 10,533
Amplifiers, Shot Noise in 10,538
Analog-To-Digital Converters 10,586
Circuit with Four Stable States 10,574
Flip-Flop 10,545
Pulse Height Discriminator 10,546
Univibrator 10,546
Tunnel Diodes,
Calculation of Elastic Tunneling Current in 10,375
Oscillation of Longitudinal Tunnel Current 10,418
Tunneling in Presence of Magnetic Fields 10,419
Twistor Bits, Demagnetization of 10,513
Two Terminal-Pair Network, Darlington's Synthesis of 10,523

U

Ultra Pure Elements 10,604
Ultrasonic Absorption in Intrinsic Semiconductors 10,378
Ultraviolet Absorption Studies of Irradiated Silica and Quartz 10,448
Unidirectional Tunnel Diode Amplifier 10,533
Univibrator, Tunnel Diode 10,546
Up-Converter, X-Band 10,614

V

Vacancies on the Dielectric Properties of TiO_2, Effects of Oxygen 10,380
Vacancy Clusters in Solid Solutions 10,317
Vacuum:
Deposition of Thin Films, Helium Flush in 10,355
Ultraviolet Absorption Studies of Irradiated Silica and Quartz 10,448
Valence Band Splittings in Zincblende and Wurtzite Structures, Theory of 10,376
Vanadium-Iron Alloys,
Effect of Magnetic Clusters on Specific Heat of 10,462
Nuclear Magnetic Specific Heat in 10,422
Vapor Phase Preparation of GaP 10,349
Varley Mechanism, Production of F Centers in NaCl Single Crystals by 10,320

W

Wafers, Residual Thermoelastic Stresses in Bonded Silicon 10,484
Waveguides, Analysis of Ferrite Filled 10,501
Whiskers, Interferometer Studies of Iron 10,339
Wurtzite Structures, Theory of Valence Band Splittings in 10,376

X

X-Band Up-Converter 10,614
X-Ray:
Induced Defects in Plastically Deformed LiF 10,319
Scattering, Theory of Crystal 10,468

Y

Y_e Transistor Parameters, Measurement of Frequency Dependence of 10,480
Yttrium Gallium Garnet, Hydrothermal Crystallization of 10,356
Yttrium Iron Garnet,
Flux-Grown Crystals of 10,338
Hydrothermal Crystallization of 10,356
Reaction Kinetics of 10,361
Single Crystals of 10,605

Z

Zener:
Breakdown in Junctions 10,477
Diode Coupling Networks 10,548
Zinc, Fermi Surface Area of 10,377
Zinc Oxide Crystals, Diffusion Paths and Activation Energies in 10,331
Zinc Selenide, Zone Melting of 10,346
Zinc Sulfide,
Preparation of Single Crystals of 10,354
Zone Melting of 10,346
Zinc Telluride, Zone Melting of 10,346
Zincblende Structures, Theory of Valence Band Splittings in 10,376
Zone Melting:
of CdS, ZnS, ZnSe, and ZnTe 10,346
Removal of Boron from SiI_4 by 10,330
Zones in Horizontal Sheets, Stability of Molten 10,343

AUTHOR INDEX

Adams, E. N. 10,419
Adams, W. H. 10,371
Adler, S. 10,376
Aitchison, R. E. 10,475
Albers, W. 10,333
Allen, C. A. 10,579
Allen, F. G. 10,413
Allen, G. 10,367
Allred, W. P. 10,316
Anderman, A. I. 10,394
Andrews, J. D. 10,498
Andrychuk, D. 10,326
Arajs, S. 10,427
Azároff, L. V. 10,331

Baily, N. A. 10,598
Balk, P. 10,373
Ballman, A.A. 10,356
Banks, E. 10,359
Barkemeyer, H. 10,459
Barrett, W. A. 10,513
Bartlett, B. E. 10,340
Bate, R. T. 10,316, 10,407, 10,408
Beck, P. A. 10,422
Beckman, O. 10,318
Beer, A. C. 10,407, 10,408
Bell, J. C. 10,408
Bell, R. O. 10,385
Belov, K. P. 10,426
Benjamin, H. 10,600
Benson, G. C. 10,373
Bernard, W. 10,390
Betts, R. 10,499
Bickart, T. A. 10,519
Bierly, J. N. 10,318
Bierstedt, P. E. 10,398
Billings, A. R. 10,487
Binder, D. 10,368
Biorci, G. 10,525
Birman, J. L. 10,376
Bishop, G. 10,499
Blinc, R. 10,439
Blok, J. 10,411
Blum, H. 10,437
Bogert, B. P. 10,343
Booker, G. R. 10,351
Bowen, L. O. 10,594
Boyd, G. D. 10,505
Braid, T. H. 10,596
Brant, P. J. 10,347
Braun, E. A. 10,372
Brezina, B. 10,388
Brody, P. S. 10,387
Brown, D. P. 10,517
Bruce, G. D. 10,579
Buehler, E. 10,512
Buford, J. T. 10,330
Bulman, W. E. 10,494
Bushor, W. E. 10,555
Butler, S. A. 10,571

Cable, J. W. 10,430
Callaway, J. 10,463
Castner, T. 10,434
Castro, P. L. 10,380
Cederbaum, I. 10,526
Chase, A. B. 10,338
Cheng, C. H. 10,422
Cherry, E. M. 10,477
Chessin, H. 10,427
Chien, R. T. 10,518, 10,522
Christopherson, W. A. 10,573
Civalleri, P. P. 10,525
Coble, R. L. 10,341, 10,342
Cook, R. L. 10,383
Cooke, H. F. 10,481
Cooper, J. N. 10,405
Corenzwit, E. 10,402
Councill, E. D. 10,579
Cowen, J. A. 10,440
Cranshaw, T. E. 10,423
Crittenden, Jr., E. C. 10,405
Crocket, J. H. 10,356
Croft, W. J. 10,360
Culshaw, W. 10,507

Daly, R. T. 10,453
Daughton, J. M. 10,578
Davies, L. W. 10,389, 10,595
Davis, J. L. 10,392
Davis, R. G. 10,591
DeGrasse, R. W. 10,559
de Hoog, F. J. 10,411
Dempsey, E. 10,373
Denda, S. 10,483
Derick, L. 10,345
Detoni, S. 10,439
Drickamer, H. G. 10,446
Duke, J. F. 10,323

Eckertová, L. 10,379
Erikson, A. 10,560
Erkman, J. O. 10,470

Fang, P. H. 10,397
Farazmand, B. 10,382
Fast, J. D. 10,471
Faughnan, B. W. 10,432
Fawcett, E. 10,377
Ferrell, R. A. 10,403
Ferretti, A. 10,357
Fischer, A. G. 10,346, 10,449
Folweiler, R. C. 10,469
Fousek, J. 10,388
Fowler, H. A. 10,339
Fox, A. G. 10,506
Free, P. B. 10,473
Frisch, H. L. 10,393
Frosch, C. J. 10,345
Fryburg, G. C. 10,364
Fuller, C. S. 10,322

Gambino, R. J. 10,358
Garrett, C. G. B. 10,454
Gärtner, W. W. 10,464
Geballe, T. H. 10,402
Gersherzon, M. 10,349
Ghausi, M. S. 10,534
Giamati, C. 10,367
Gianola, U. F. 10,569
Giddy, J. H. 10,541
Giordmaine, J. A. 10,554
Glasner, A. 10,336
Goldberg, H. B. 10,558
Goldstein, B. 10,335
Goldthorp, J. R. 10,561
Gordon, J. E. 10,510
Gordon, J. P. 10,505
Goss, A. J. 10,344
Gottfried, K. 10,401
Green, J. H. 10,602
Green, R. B. 10,494
Greene, R. F. 10,466
Grosvalet, J. 10,486
Grubbs, W. J. 10,533

Hacskaylo, M. 10,367
Huering, R. R. 10,418, 10,419
Hagelbarger, D. W. 10,343
Haidemenakis, E. 10,459
Hakimi, S. L. 10,516
Hall, F. R. 10,563
Halperin, A. 10,456
Hancock, D. J. 10,592
Hanel, R. A. 10,511
Hanson, H. 10,600
Hargreaves, C. M. 10,362
Harper, H. T. 10,410
Harris, P. O. 10,472
Hart, J. P. 10,556
Harwood, J. L. 10,582
Hashi, T. 10,442
Haynes, J. L. 10,568
Hazoni, Y. 10,546, 10,574
Headford, P. W. 10,562
Healy, J. H. 10,400
Heijn, H. J. 10,565
Heinrich, J. T. 10,596
Hellkvist, N. 10,472
Hewitt, D. F. 10,495
Hinc, F. A. 10,582
Hogg, D. C. 10,559
Hollander, Jr., L. E. 10,380
Holmquist, W. R. 10,361
Holton, W. C. 10,437
Honig, A. 10,433, 10,435
Honnold, V. R. 10,320
Hooper, D. E. 10,479
Hsu, F. S. L. 10,512
Hull, Jr., G. W. 10,402

Igo, T. 10,445

James, R. H. 10,497
Jeffers, F. 10,440
Johnson, B. R. 10,563
Johnson, C. E. 10,423
Johnson, P. D. 10,455
Johnston, W. R. 10,575
Jones, C. E. 10,326
Jones, D. L. 10,532

Kadanoff, L. P. 10,401
Kaenel, R. A. 10,545, 10,586
Kaiser, W. 10,454
Kallmann, H. 10,459
Kan, T. 10,476
Kane, W. M. 10,395
Kanter, H. 10,369
Karel, F. 10,354
Keating, K. B. 10,446
Keller, H. P. 10,335
Kepler, R. G. 10,398
Khodakov, A. L. 10,386
Kim, W. H. 10,521
King, E. F. 10,478
Kiseda, J. R. 10,576
Klaassen, F. M. 10,411
Klein, C. A. 10,327
Klein, M. L. 10,556
Kobuke, Y. 10,353
Kok, H. 10,572
Konorov, P. P. 10,396
Kool, C. F. 10,361
Kramer, B. 10,459
Kramer, H. P. 10,343
Kruger, J. 10,363
Kunzler, J. E. 10,512
Kushida, T. 10,353

Laisk, E. 10,488, 10,594
Lancaster, B. J. 10,514
Laudise, R. A. 10,356
Lax, B. 10,374, 10,416
Lebowitz, J. L. 10,393
Lee, J. W. 10,602
Lefever, R. A. 10,338
Lehovec, K. 10,334, 10,391
Lehrer, N. H. 10,587
Lemaire, H. P. 10,360
Le Mée, J. 10,485
Leonhard, F. 10,358
Levstek, L. 10,439
Levy, S. L. 10,347

Levy, W. 10,321
Lewis, W. B. 10,438
Li, T. 10,506
Libby, D. 10,441
Lifshitz, I. M. 10,317
Lindeberg, G. K. 10,457
Lindgren, W. A. 10,599
Löcherer, K-H. 10,539
Loebner, E. E. 10,524
Loferski, J. J. 10,491
Loscoe, C. 10,464
Ludwig, G. W. 10,443, 10,436
Lundberg, C. W. 10,497
Lustig, H. 10,450

Macario, R. C. V. 10,550
Madsen, P. E. 10,423
Mansey, R. 10,557
Marsden, K. H. 10,594
Martin, A. V. J. 10,485
Martin, R. L. 10,503, 10,504
Marton, L. 10,339
Masuda, I. 10,353
Matthias, B. T. 10,402, 10,512
Maurer, R. 10,539
Mayer, J. W. 10,598
McAleer, W. J. 10,459
McCubbin, J. G. 10,558
McLay, A. B. 10,444
McMillan, J. A. 10,431
Meechan, C. J. 10,332
Melngailis, I. 10,490
Mengali, O. J. 10,599
Merrifield, R. E. 10,398
Merz, G. 10,581
Mette, H. 10,464
Mikoshiba, N. 10,378
Mikulyak, R. M. 10,349
Miles, R. J. 10,548, 10,570
Miller, D. S. 10,427
Miller, P. B. 10,418
Mina, K. V. 10,583
Minnick, R. C. 10,567
Mitsuhashi, H. 10,458
Molnar, R. J. 10,540
Morgan, D. J. 10,425
Morrison, G. H. 10,324
Moss, R. W. 10,361
Mudgway, D. J. 10,535
Mukhopadhyay, A. 10,543
Muldawer, L. 10,318
Mulligan, Jr., J. H. 10,530
Myers, W. C. 10,325

Nahum, J. 10,456
Nelson, C. M. 10,448
Neshpor, V. S. 10,399
Neuringer, L. J. 10,390
Newhall, E. E. 10,583
Nicol, J. 10,404
Nodvik, J. S. 10,460
Nolta, J. P. 10,320
Nowicki, J. R. 10,590

O'Dell, T. H. 10,496
Offenbacher, E. 10,381
Ohm, E. A. 10,559
Okazaki, M. 10,447
Olson, F. A. 10,537
Oono, Y. 10,527
Ormerod, M. G. 10,441
Overn, W. M. 10,497

Pace, J. H. 10,502
Pajgrt, M. 10,480
Papoulis, A. 10,523
Pederson, D. O. 10,534
Petersen, H. E. 10,576
Ped'ko, A. V. 10,426
Peek, Jr., R. L. 10,500
Pell, E. M. 10,467
Perkins, Jr., J. F. 10,528
Petch, H. E. 10,444
Petrus, H. M. 10,364
Pieczonka, W. A. 10,444
Pihl, C. 10,334
Pines, D. 10,417
Pintar, M. 10,439
Poberaj, S. 10,439
Pohm, A. V. 10,578
Pollak, P. I. 10,459
Pomerantz, M. A. 10,600
Potts, B. C. 10,494
Prior, A. C. 10,348
Prener, J. S. 10,467
Pretzel, F. E. 10,438

Rappaport, P. 10,482
Read, A. A. 10,578
Rebsch, D. L. 10,544
Reed, M. B. 10,520
Reisfeld, R. 10,336
Reiss, H. 10,394
Richards, W. A. 10,566
Ridout, M. S. 10,423
Riederman, N. H. 10,359
Riney, T. D. 10,484
Robinson, C. C. 10,461
Robinson, D. A. 10,553
Rogers, K. T. 10,489
Roshon, Jr., D. D. 10,593
Roth, H. 10,410
Rupprecht, G. 10,385
Rushbrooke, G. S. 10,425
Rustgi, O. P. 10,460

Sah, C. T. 10,474
Sampson, D. F. 10,502
Samsonov, G. V. 10,399
Sandler, S. S. 10,501
Sarles, L. R. 10,452
Sato, H. 10,428
Schara, M. 10,439
Schleuning, H. W. 10,359
Schlosser, H. 10,375
Schmidlin, F. W. 10,405
Scholten, J. W. 10,551
Schools, R. S. 10,577
Schröder, K. 10,462
Schultz, H. E. 10,589
Schwarz, R. F. 10,395
Schwed, P. 10,600
Scott, G. D. 10,355
Scovil, H. E. D. 10,559
Seelbach, W. C. 10,576
Selman, J. C. 10,565
Shapiro, S. 10,404
Shenker, H. 10,406
Silber, L. M. 10,359
Silberbach, R. 10,531
Silsbee, H. B. 10,510
Silverman, B. D. 10,384
Simmons, C. A. 10,409
Simpson, J. A. 10,339
Skotnicky, J. 10,603
Skrivánek, J. 10,601
Slyozov, V. V. 10,317
Smay, T. A. 10,578
Smith, D. H. 10,493
Smith, P. H. 10,404
Smith, R. C. 10,352
Smoluchowski, R. 10,319
Smyth, D. M. 10,337
Soden, R. R. 10,451
Sokolov, A. N. 10,396
Sorokin, P. P. 10,508
Spany, V. 10,584
Sparnaay, M. J. 10,415
Spaulding, S. W. 10,381
Spitzer, W. G. 10,350, 10,420
Spratt, J. P. 10,395
Srivastava, G. N. 10,355
Starks, R. J. 10,330
Stein, I. 10,588
Stevenson, M. J. 10,508
Strandberg, M. W. P. 10,432
Strohm, W. G. 10,571
Sturge, M. D. 10,329
Suddeth, J. A. 10,339
Surplice, N. A. 10,414

Tancrell, R. H. 10,580
Tanenbaum, M. 10,350
Tang, D. T. 10,518
Teig, M. 10,576
Tennery, V. J. 10,383
Teutsch, W. B. 10,410
Thornhill, A. F. 10,566
Thorp, J. S. 10,502
Tieman, J. J. 10,538
Tokad, Y. 10,517
Torpy, J. W. 10,338
Trainor, A. 10,340
Troup, G. J. 10,509
Turnbull, A. R. T. 10,479
Turner, D. R. 10,366
Tyablikov, S. V. 10,429

Uehara, Y. 10,353
Uhl, K. 10,552
Uphoff, H. L. 10,400

Valentine, R. D. 10,547
van der Does de Bye, J. A. W. 10,597
Van Ruler, J. 10,415
Van Uitert, L. G. 10,451
Verrijp, M. B. 10,471
Veselá, M. 10,601
Vojtásek, S. 10,549
Wahl, C. 10,512
Walker, F. L. 10,478
Walters, J. S. B. 10,585
Ward, J. 10,564
Watanabe, H. 10,370, 10,515
Weeks, R. A. 10,448
Wei, C. T. 10,422
Weinberg, L. 10,529
Weiss, W. L. 10,599
Weissler, G. L. 10,4
Wernick, J. H. 10,42
Wertheim, G. K. 10,
Wickham, D. G. 10,
Wieder, I. 10,452
Wiegand, D. A. 10,3
Wiener, P. 10,588
Wigen, P. E. 10,440
Wilkinson, M. K. 10,
Williams, A. I. 10,32
Williams, F. E. 10,4
Williams, M. F. 10,5
Wilson, T. R. 10,365
Wing, O. 10,522
Winkler, S. H. 10,58
Winterbottom, N. 10,
Wittekindt, R. H. 10,3
Wohlfarth, E. P. 10,4
Wold, A. 10,357
Wolfe, R. 10,420
Wollan, E. O. 10,43
Woodbury, H. H. 10,4 10,443
Wooster, W. A. 10,4
Wragge, H. S. 10,54
Wright, G. B. 10,374
Wysocki, J. J. 10,491 10,492

Yang, G. 10,433
Young, C. E. 10,412
Young, Jr., F. W. 10,365
Yourke, H. S. 10,571

Zarowin, C. 10,503
Zemel, J. N. 10,465
Zucker, H. 10,536
Zuleeg, R. 10,391

CONFERENCES

1961

Dec. 12-14

Eastern Joint Computer Conference
Sheraton Park Hotel, Washington, D.C.

Dec. 18-19

Materials Research Conference
Rensselear Polytechnic Institute, Troy, N.Y.

Dec. 27-29

American Physical Society
University of California, Los Angeles, Calif.

1962

Jan. 9-11

8th National Symposium on Reliability and Quality Control
Statler Hilton Hotel, Washington, D.C.

Feb. 7-9

3rd Winter Convention on Military Electronics
Ambassador Hotel, Los Angeles, Calif.

Feb. 14-16

International Solid State Circuits Conference
Sheraton Hotel and University of Pennsylvania, Philadelphia, Pa.

CAPSULE
CLASSIFICATION OUTLINE
for
COMPUTER ABSTRACTS ON CARDS

C0 ELECTRONIC COMPUTERS — GENERAL

- C0.1 History and Prediction
- C0.2 Surveys and Visits; State of the Art
- C0.3 Summaries of Technical Conferences
- C0.4 Bibliographies, Abstracts, and Reviews
- C0.5 Texts
- C0.6 Standards and Suggested Standards
- C0.8 Personnel
- C0.9 Education

C1 LOGIC AND SWITCHING THEORY

- C1.0 General
- C1.1 Basic Theory and Principles
- C1.2 Truth Functions (Switching or Boolean Functions)
- C1.3 Combinational Switching Networks
- C1.4 Non-Deterministic and Unreliable Switching Networks
- C1.6 Iterative Switching Networks
- C1.7 Theory of Automata
- C1.8 Sequential Switching Theory and Networks

C2 DIGITAL COMPUTERS AND SYSTEMS

- C2.0 General
- C2.1 System Design and Machine Organization
- C2.2 Applied Logic Design
- C2.3 Digital Arithmetic Methods and Systems
- C2.4 Error Detection and Correction in Computing Systems
- C2.5 Reliability, Maintenance, Mechanical Construction, and Production of Computers
- C2.6 General-Purpose and Special-Purpose Digital Computers (Alphabetically)
- C2.7 General-Purpose Digital Computers (by Country and Type)
- C2.8 Special-Purpose Digital Computers (For Real-time Control and Data Acquisition Systems see Section C12.)

C3 DEVICES AND BASIC LOGIC AND WAVEFORMING CIRCUITS

- C3.0 General
- C3.1 Electromechanical and Passive Linear Electrical Components
- C3.2 Electron Devices and Electronic Logic Circuits (including Microwave)
- C3.3 Semiconductor Devices and Logic Circuits
- C3.5 Parametrons and their Logic Circuits; Parametric Amplifiers
- C3.6 Nonlinear Magnetic Devices and Logic Circuits
- C3.7 Cryogenic (Superconductive) Devices and Logic Circuits
- C3.8 Other Devices for Logic and Their Circuits
- C3.9 Basic Sequential and Waveforming Circuits

C4 STORAGE AND INPUT-OUTPUT

- C4.0 General
- C4.1 Principles and Theory of Storage Organization
- C4.2 Static Magnetic Random-Access Storage
- C4.3 Static Non-Magnetic Random-Access Storage
- C4.4 Dynamic (Volatile) Random-Access Storage
- C4.5 Reference Storage (Contents Not Changeable by the Machine)
- C4.7 Sequential-Access Storage in Fixed Media or Elements (Usually Dynamic)
- C4.8 Storage on Moving Media
- C4.9 Input-Output

C5 PROGRAMMING AND CODING

- C5.0 General
- C5.1 Basic Principles and Techniques of Programming
- C5.2 Machine Programming and Coding Techniques
- C5.3 Programming Languages
- C5.4 Automatic Programming
- C5.6 Concurrent Programming; Multi-Problem Handling
- C5.8 Program Monitoring and Debugging
- C5.9 Non-Mathematical Algorithms; Data-Handling Algorithms

C6 FORMAL AND NATURAL LANGUAGES, INFORMATION RETRIEVAL, AND HUMANITIES

- C6.0 General
- C6.1 Formal Languages and Systems
- C6.2 Symbol Manipulation
- C6.4 Natural Languages, Linguistics, and Mechanical Translation
- C6.6 Information Retrieval
- C6.8 Humanities and Social Sciences

C7 BEHAVIORAL SCIENCE AND ARTIFICIAL INTELLIGENCE

- C7.1 Pattern and Character Recognition and Detection
- C7.2 Speech Recognition and Production
- C7.3 Psychology and Behavioral Science
- C7.5 Probabilistic and Self-Organizing or Adaptive Systems
- C7.7 Learning, Problem Solving, and Game Playing
- C7.8 Man and the Machine

C8 MATHEMATICS

- C8.0 General
- C8.1 Number Representation and Arithmetic; Number Theory
- C8.2 Functional Approximation to Data
- C8.3 Computation of Functions
- C8.4 Algebra and Analysis
- C8.6 Calculus and Differential Equations
- C8.8 Combinatorial Mathematics

C9 PROBABILITY, INFORMATION THEORY, AND COMMUNICATION SYSTEMS

- C9.1 Probability
- C9.2 Statistics
- C9.3 Operations Research and Game Theory
- C9.4 Simulation
- C9.5 Information Theory and Noise (Interference)
- C9.7 Communication and Broadcast Systems and Radar

C10 SCIENCE, ENGINEERING, AND MEDICINE

- C10.0 General
- C10.1 Electrical Science and Engineering
- C10.2 Mechanics; Mechanical and Civil Engineering
- C10.3 Aeronautical Engineering and Design
- C10.4 Astronomy, Space, and Geophysics
- C10.6 Chemistry and Chemical Engineering
- C10.7 Classical and Atomic Physics
- C10.8 Nuclear Physics
- C10.9 Medicine and Biology

C11 ANALOG AND HYBRID COMPUTERS

- C11.1 Direct Analogs
- C11.2 Analog Computer Techniques and Systems
- C11.3 Analog Computer Components (Subassemblies)
- C11.5 Analog Computer Mathematical Methods and Programming
- C11.7 Hybrid (Analog-Digital) Computers
- C11.9 Analog-Digital Conversion

C12 REAL-TIME SYSTEMS AND AUTOMATIC CONTROL; INDUSTRIAL APPLICATIONS

- C12.0 General
- C12.1 Control System Theory
- C12.2 Sampled-Data System Theory
- C12.4 Data Acquisition and Transmission Systems
- C12.5 General-Purpose Real-Time Systems
- C12.6 Real-Time Control Computers (on-line)
- C12.8 Industrial Engineering and Production Techniques; Automation

C13 GOVERNMENT, MILITARY, AND TRANSPORTATION APPLICATIONS

- C13.1 Government and Politics
- C13.3 Military Applications
- C13.6 Transportation Operations
- C13.7 Aviation
- C13.8 Railroads

C14 BUSINESS APPLICATIONS

- C14.0 General
- C14.1 Business Data Processing Techniques
- C14.3 Management Science
- C14.5 Application of Computing (Data-Processing) Machines in Specific Businesses

CAPSULE
CLASSIFICATION OUTLINE
for
SOLID STATE ABSTRACTS ON CARDS

(For an extended version of this outline see pp. 13-76 in Instructions-Outline-Pre-Index)

M METALLURGY AND CHEMISTRY OF SOLIDS

- M0 General
- M1 Chemical Compounds and Reactions
- M2 Thermodynamic Properties of Elements and Alloys
- M3 Crystal Structure
- M4 Crystal Growth
- M5 Crystal Surfaces
- M6 Environmental Effects

P SOLID STATE PHYSICS

- P0 General
- P1 Crystal Physics
- P2 Electrical Properties
- P3 Magnetic Properties
- P4 Optical Properties
- P5 Thermal Properties
- P6 Mechanical Properties

D SOLID STATE DEVICES

- R CONDUCTIVE DEVICES
  - a Diodes and Rectifiers
  - b Transistors
  - c Functional Units
  - d Magnetoelectric Devices
  - e Other Conductive Devices
- L PHOTODEVICES
  - f Photoelectronic Devices
  - g Luminescent Devices
  - h Other Photodevices
- T THERMAL DEVICES
  - k Thermistors
  - m Thermoelectric Devices
  - n Other Thermal Devices
- H MAGNETIC DEVICES
  - p Ferromagnetic and Ferrite Devices
  - q Paramagnetic Devices
  - r Other Magnetic Devices
- E DIELECTRIC DEVICES
  - s Ferroelectric Devices
  - t Other Dielectric Devices
- G OTHER SOLID STATE DEVICES
  - u Superconductive Devices
  - v Electromechanical Devices
  - w Magnetomechanical Devices
  - z Miscellaneous Devices

B SOLID STATE DEVICE CIRCUITS

- B0 General
- B1 Amplifiers
- B2 Oscillators
- B3 Switching Circuits
- B4 Signal Converters
- B5 Wave Generators
- B6 Pulse Circuits
- B9 Other Solid State Device Circuits

A APPLICATIONS OF SOLID STATE DEVICES

- A1 Communications and Related Applications
- A2 Computers and Other Data Handling Systems
- A3 Power Applications
- A4 Control Applications
- A5 Instrumentation
- A9 Other Applications

(SEE BACK COVER)

FOR SURFACE STUDIES

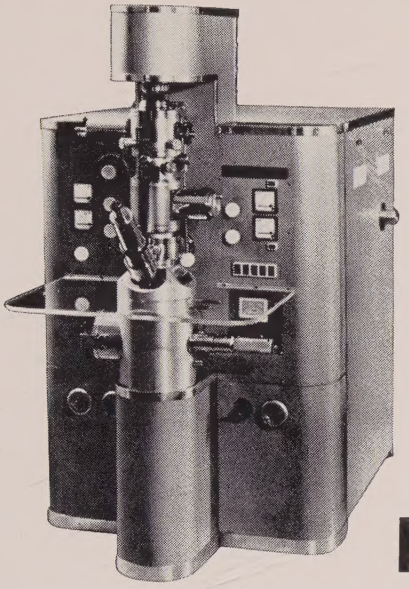

KE1

Trüb, Täuber Secondary Electron Emission Microscope

for direct viewing of metallic and semiconducting specimens by means of secondary electrons released from ion bombardment of the surface — featuring . . .

- Images free of distortion and deformation
- Enlargement up to 1500 X electronoptically
- Resolution 500–600Å
- Object temperature 150°–800° C
- Observable surface of the object 25 mm square
- Differentiation of the material

The Instrument Includes . . .

Electrostatic immersion objective
Ion beam system
Revolving contrast diaphragms
2 electromagnetic projectors
Observation chamber with fluorescent image screen
Recording chamber with plate cassette
High-intensity optical microscope
All-metal housing with vacuum equipment including diffusion pump
High-voltage equipment for 45 kV
Measuring instruments and control equipment

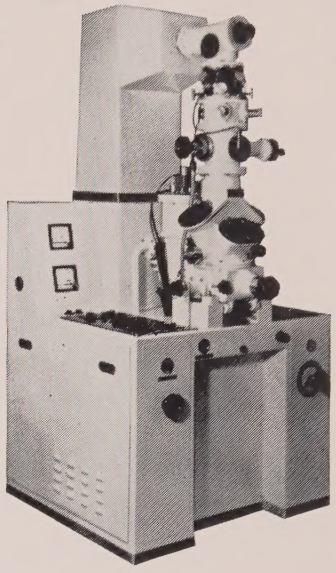

KD3

Trüb, Täuber Electron Diffractograph

for determining the crystalline structure of surfaces, thin layers, and extremely small quantities of material, including dynamic processes — featuring . . .

- Cold-cathode electron gun with practically unlimited life
- Simple design — dependable operation, extreme flexibility
- Balanced optical system
- High resolving power
- Large variety of specimen holders for various methods of investigation
- Devices for heating and cooling the test specimens (from liquid nitrogen to 1000°C)
- Devices for discharging, etching, surface evaporating
- Various cameras for photographic recording on plates and films
- Unique kinematic recorder

Specifications

Acceleration Voltage —	
continuously adjustable:	10 to 50 kV
ripple (fractional):	$\approx 10^{-4}$
stability:	$\pm 0.1\%$
Final vacuum:	approx. 2 x 10^{-5} mm Hg
Magnification with electronic lens:	75X
Minimum line width:	0.001 mm
Minimum diameter of beam for focussing on specimen, without additional diaphragms:	4μ

Distributed by:

NEW ENGLAND SCIENTIFIC INSTRUMENTS CO.

238 MAIN STREET · CAMBRIDGE 42, MASSACHUSETTS · KIrkland 7-2932

Electron Microscopes • Nuclear Induction Spectrographs • High Voltage Oscillographs • Precision Laboratory Instruments • Nuclear Track Microscopes

in'for·ma'tion re·triev'al, *n.* **1.** rapid location of technical information on specific topics.

information retrieval system for the solid state:

SOLID STATE ABSTRACTS ON CARDS

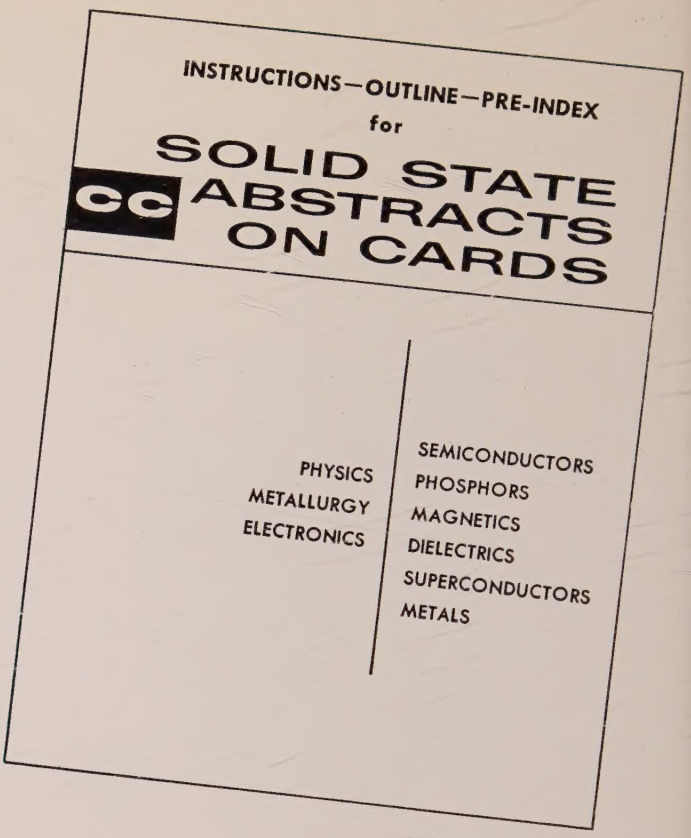

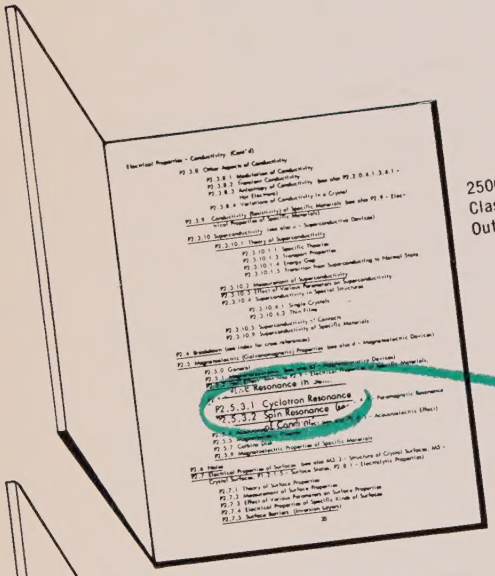

2500-Topic Classification Outline

Send for your free copy of our new 120 page book describing this unique system which is now being used in more than 300 solid state laboratories throughout the world.

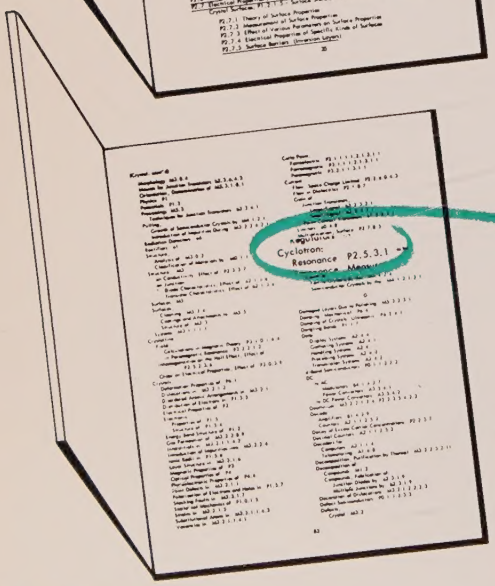

4000-Entry Alphabetical Pre-Index

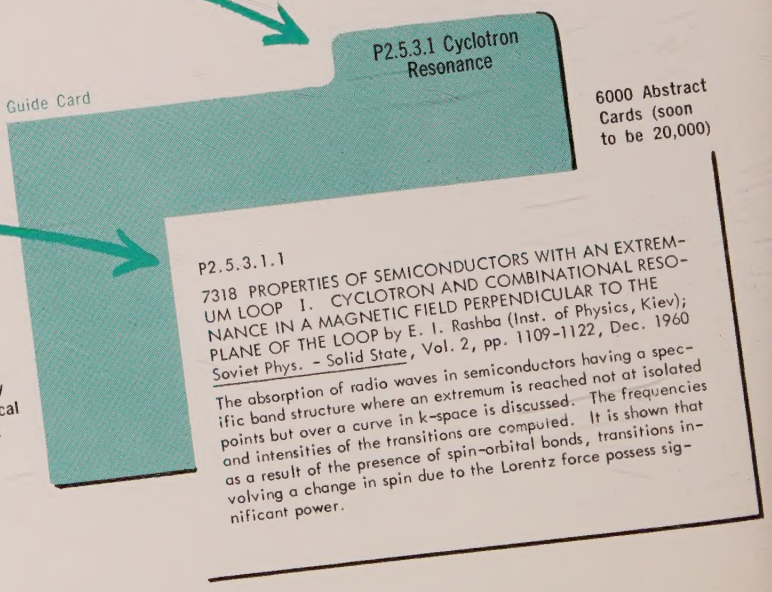
P2.5.3.1 Cyclotron Resonance
Guide Card
6000 Abstract Cards (soon to be 20,000)
P2.5.3.1.1
7318 PROPERTIES OF SEMICONDUCTORS WITH AN EXTREMUM LOOP I. CYCLOTRON AND COMBINATIONAL RESONANCE IN A MAGNETIC FIELD PERPENDICULAR TO THE PLANE OF THE LOOP by E. I. Rashba (Inst. of Physics, Kiev); Soviet Phys. - Solid State, Vol. 2, pp. 1109-1122, Dec. 1960
The absorption of radio waves in semiconductors having a specific band structure where an extremum is reached not at isolated points but over a curve in k-space is discussed. The frequencies and intensities of the transitions are computed. It is shown that as a result of the presence of spin-orbital bonds, transitions involving a change in spin due to the Lorentz force possess significant power.

CAMBRIDGE COMMUNICATIONS CORPORATION

236 MAIN STREET • CAMBRIDGE 42, MASSACHUSETTS • **Tel. 491-0710**